TNO Environment, Energy and Process Innovation

Laan van Westenenk 501
Postbus 342
7300 AH Apeldoorn
The Netherlands

www.mep.tno.nl

T +31 55 549 34 93
F +31 55 541 98 37
info@mep.tno.nl

TNO-report

R 1997/363b

IGCC Power Plant: CO_2 removal with high temperature adsorbents Part II: Zeolite adsorbents

Date	October 1997
Authors	Ir. J.C.P.L. Saeijs Ir. L.B.M. van Kessel Dr.Ir. A.B.M. Heesink Ir. H.M.G. Temmink
Order no.	27084
Keywords	Carbon dioxide removal High temperature absorbents IGCC Zeolite
Intended for	ECSC attn. Mr. J.K. Wilkinson Rue de la Loi Bruxelles

Abstract

Carbon dioxide (CO_2) is the main contributor to the enhanced greenhouse effect that is disturbing the environment and that is generally believed to cause global warming.

A substantial reduction of the CO_2 emissions, as agreed upon internationally, is inevitable. In the Netherlands, 25 % of the emission is produced by power plants. This contribution could increase even further when, as a result of the limited resources of oil and natural gas, the amount of coal used for power generation increases.

One option for an emission reduction is the removal of CO_2 from the flue gases produced by power plants and the subsequential storage of the CO_2 in depleted gas fields. The separation of the CO_2 could for instance be done by adsorption.

This project aims at the development of a Temperature Swing Adsorption (TSA) unit that uses a zeolite as adsorbent and that can be applied in an Integrated Coal Gasification Combined Cycle (IGCC) power plant.

In comparison with conventional techniques of removing CO_2 in IGCC power plants, the use of a TSA process with zeolite adsorbents can be advantageous if it is operated at high pressure and high temperature:

a) A regeneration at high pressure (~20 bar) can reduce the compression work needed for the injection in the gas fields.

b) An adsorption at high temperature (~ 325 °C) makes it possible to use the adsorption heat for the generation of electricity, so that the loss in plant efficiency due to the CO_2 removal can be kept small.

Both, the regeneration at high pressure and the adsorption at high temperature require that the zeolite adsorbent has good thermal stability and a sufficient capacity.

Several zeolites have a stability that allows regeneration at temperatures between 500 °C and 800 °C that are needed for complete desorption at 20 bar. The reduction of the compression work can, therefore, be realized easily by using a TSA process operating with adsorption at a moderate temperature (~125 °C).

To operate a TSA process with adsorption at high temperature (~325 °C), the zeolite should have an adsorption heat of 70 kJ/mole CO_2 or more. For the few zeolites of which an adsorption heat is mentioned in the literature, the reported value is less than 70 kJ/mole. By carefully selecting the zeolite type and its modifications, it might however be possible to find an adsorbent that meets the criterium.

The selection of the zeolite type and its modifications cannot be made on the basis of the theory on zeolite. The theory describes a great many parameters that influence the adsorption behavior and the stability. Unfortunately, most of these parameters are mutual dependent, by that preventing the optimization of the adsorption properties needed for the selection.

Consequently, the selection has to be based on the limited amount of experimental data concerning CO_2 adsorption that have been published. The highest adsorption capacities are mentioned for Zeolite A, Zeolite X, and Chabazite. Their heat of adsorption is, however, only 40-60 kJ/mole. For Mordenite, a heat of adsorption of 60-70 kJ/mole is reported.

Considering the specific demands of an IGCC power plant and the objectives of this study, five zeolite types have been selected: Zeolite A, Zeolite X, Zeolite P, Mordenite, and Zeolite β. The stability and the adsorption behavior of these zeolites, in particular of the alkaline earth metal forms, have been studied with the use of EDS, XRD and TGA. The results are summarized in table 1.

Table 1 *The main results of the zeolite characterization*

Zeolite type	*CO_2 adsorption (25 °C and 1 bara)*	*Thermal stability between 500 °C and 800 °C*
Zeolite A	Ca-A > Na-A > Sr-A > Mg-A	Ca-A > Mg-A > Sr-A > Na-A; Ba-A was unstable
Zeolite X	Na-X > Ca-X > Ba-X > Sr-X	Na-X, Ca-X > Sr-X, Ba-X
Zeolite P	no adsorption due to instability	all samples became unstable at low temperatures
Mordenite	Ca-Mor > Ba-Mor > H-Mor, (Mg-Mor)*	all samples were stable up to at least 800 °C **
Zeolite β	Ca-β > Mg-β, Na-β, H-β	all samples were stable up to at least 800 °C **

*) unreliable: there are indications that the ion-exchange of the Mg-Mor sample has been unsuccessful
**) meaning that no indications were found that instability occurred.

Based on these results, the feasibility of a TSA process with one of these zeolite adsorbents can be evaluated. For most of the samples, the adsorption capacity at 325 C is too low to be interesting for a high-temperature TSA process. Mordenite is the only zeolite type that offer some perspective. The capacity measured for Ca-Mordenite is still somewhat low, but Mg-Mordenite is expected to be a good option. Although a confirmation could not be given by the measurements in this study, as there were indications that the ion-exchange of the Mg-Mordenite sample has been unsuccessful, data in the literature suggest that Mg-Mordenite has a higher capacity then Ca-Mordenite.

Table 2 *Temperature Swing Adsorption (TSA) process*

TSA process:

	pressure (bara CO_2)	temperature (°C)	moderate temperature TSA Na-X	Ca-A	Na-A	Ca-X	high temperature TSA Mg-Mor	Ca-Mor
adsorption (mg/mg)	1.0	25	0.24	0.22	0.18	0.18	... (>0.12)	0.12
	7.5 ***	125	0.21	0.19	0.15	0.12	... (>0.10)	0.10
	7.5 ***	325	0.05	0.04	0.03	0.03	... (>0.05)	0.05
heat of adsorption at 0.025 mg/mg (kJ/mole) **			35 (36-51)	39 (37-52)	58 (39-54)	44 (48-48)	... (75-85)*	56 (70-80)*

*) estimated values based on data for other gases from references in the literature
**) the values given between brackets: data from references in the literature.
***) the partial pressure of CO_2 during adsorption in an IGCC power plant

Because the use of Mg-mordenite as an absorbent for the high-temperature TSA process is still uncertain, the process design has been based on a moderate temperature TSA process. A zeolite with a capacity of 0.15 mg CO_2/ mg sorbent at 125 °C, 7.5 bar CO_2 pressure, and an adsorption heat of 42 kJ/mole is used in these calculations.

Table of Contents

Chapter 1

Introduction

1.1 The enhanced greenhouse effect

In the last decades, the possible changes in the Earth's climate, known as the global warming phenomenon, have become one of the most discussed environmental issues on the political agenda. [Alders (1992), Ministry of VROM (1993)]

Although the exact mechanism of these changes is still unclear, it is generally recognized that it partly involves the absorption of infrared radiation. [Baird (1995)] The Earth's surface and the atmosphere are kept warm primarily by radiation of the Sun, consisting of ultraviolet, visible and infrared light.

The ultraviolet light is filtered out in the stratosphere by ozone, while the small fraction of infrared light is absorbed by gases in lower atmospheric layers. Of the remaining visible light, 35 % is directly reflected by clouds, ice, snow, sand and other reflecting bodies. This results in only 50 % of the total radiation reaching the Earth's surface, where its energy is transformed into heat. Like any other warm body, the Earth emits this energy again as thermal infrared radiation.

On its way out through the atmosphere part of this radiation is absorbed by gases and re-emitted to the Earth's surface. Consequently, both the surface and the air are further heated by this mechanism. So, by forming an atmospheric blanket around the Earth, these gases cause a greenhouse effect, resulting in an increase of the average global temperature. [Cox (1995), Williams (1994)]

Most of the absorption can be related to the atmospheric concentrations of water (H_2O) and carbon dioxide (CO_2). Both gases are present there by nature and the natural absorption they cause is in itself not a problem. On the contrary, without this absorption the temperature on Earth would probably too low for human habitation. So, a natural occurrence of the greenhouse effect is indispensable.

Lately, the concentrations in the atmosphere are, however, increasing due to human activity. The higher concentrations result in intensified adsorption and in a temperature above the natural level. This intensification is known as the enhanced greenhouse effect, although often simply referred to as greenhouse effect.

Water, although being the major greenhouse gas, is generally left out of consideration in discussions on global warming, as its atmospheric concentration is outside direct human control. Whereas the water vapor concentration is influenced by the temperature and vice versa, under

normal conditions, a climatologic equilibrium is preserved. When the equilibrium is, however, disturbed as a result of any global warming by other greenhouse gases, the amount of infrared redirected by water vapor will rise. In that case, the temperature increase is amplified by the water vapor. Since it comes about as an indirect effect, the increment is usually incorporated in the warming effects of the other gases. [Cox (1995), Williams (1994)]

Of the remaining greenhouse gases, carbon dioxide is believed to contribute to the enhanced greenhouse effect by 61 %. Since the introduction of industry around 1750, its concentration is increased by one-quarter, to 356 ppm, by 1992. Measurements over the last 50 years show an average increase in its concentration of 0.4 % annually. [Cox (1995), Mot (1992), RIVM (1991)]

As carbon dioxide participates in the carbon cycle in the environment, its atmospheric concentration is related to the carbon distribution over the other four ecological compartments, i.e., the biosphere, the Earth crust, the ocean surface, and the deep ocean waters. Without any human activities, only small fluctuations, instead of the increase in its concentration, are to be expected, as perturbations would be leveled out by the other compartments. Therefore, the reported increase has to be explained by human activities.

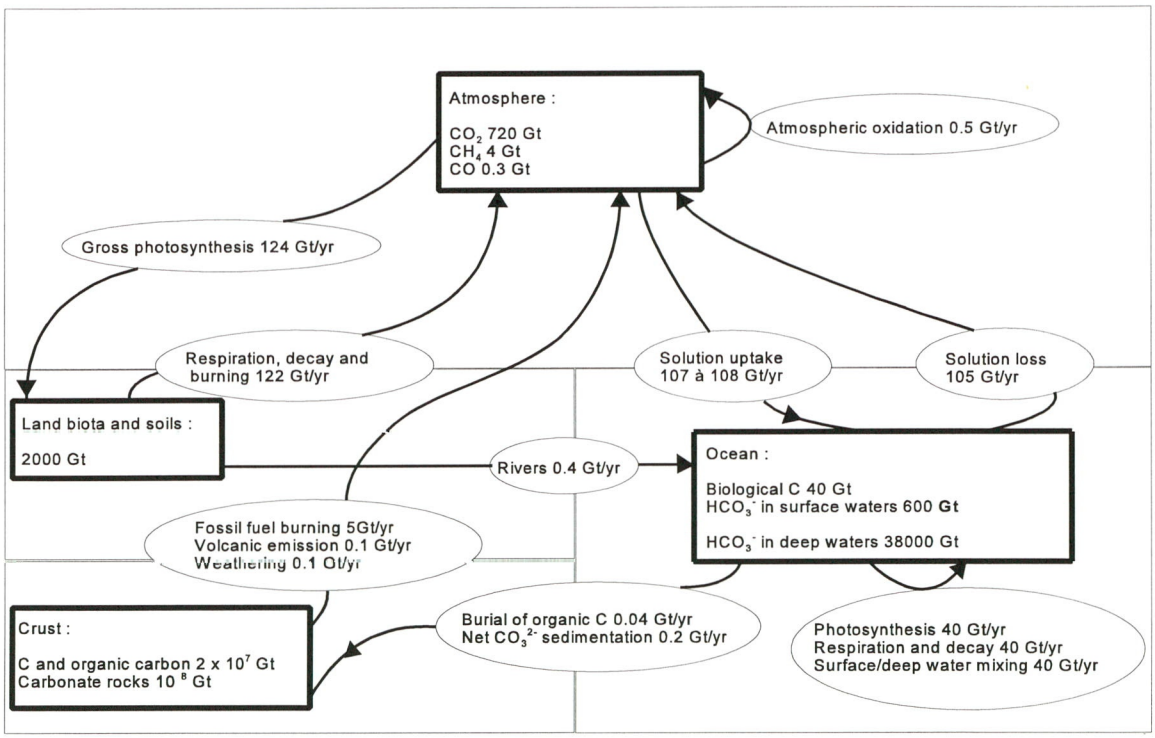

Figure 1.1 *The carbon cycle*

- *Atmospheric oxidation : reaction of methane with hydroxyl radicals and carbon monoxide to carbon dioxide*
- *units : Gt = gigatons of carbon*

[Cox (1995), Mot (1992), Williams (1994)]

The current anthropogenic emission is 26 gigatons CO_2 annually, of which 18 gigatons are the result of fossil fuel burning and the remainder is caused by deforestation. This is only about 4 % of the amount produced by nature. Nevertheless, a third of this emission accounts for the observed increase of the atmospheric CO_2-concentration. The other two third are consumed by newly formed biomass or dissolved in the oceans. [Cox (1995), Williams (1992)]

Because of the different time-scales of the processes involved in the distribution between the different compartments, the perturbation cannot be compensated further by other compartments, i.e., the Earth crust or the deep ocean waters. Therefore, a net transport of carbon from the Earth crust to the atmosphere and the ocean surface is established. It is this clear change in the equilibrium position of the environment that affects the climate and causes great concern. [Cox (1995), Mot (1992), Steinberg (1992)]

To prevent a serious global climate change, the worldwide emission of carbon dioxide will have to be reduced by as much as 60 %. [Alders (1992), VDI (1992)] Assuming that the developing countries must be allowed further development and therefore an increase in CO_2 emissions, the industrialized countries will have to reduce their emissions by 80 %.

At the international conference in Toronto (1988), a 20 % reduction scheme for the year 2005 has been set as an intermediate goal. The European Union Member States have agreed on reaching at least a stabilization of the emission at the level of 1989 in the year 2000. Meanwhile, the Dutch government aims at a reduction of the CO_2 emission by 3-5% (compared with 1989) in 2000, in combination with a 20-25 % reduction of the total emission of greenhouse gases, i.e., carbon dioxide (CO_2), methane (CH_4), nitrous oxide (N_2O), tropospheric ozone (O_3) and chlorofluorocarbons (CFC). [Alders (1992), Ministry of VROM (1993). Mot (1992)]

Studies on the feasibility and the implementation of the Dutch target have come up with a policy that concentrates mainly on the minimization of the effects caused by fossil fuel burning. As 20 % of the CO_2 emission is produced by the electricity production sector and most of the 42 % emission from industry is produced by energy conversions, it is not surprising that 75 % of the target has to be met by the energy sector. [Alders (1992), RIVM (1991)] Therefore, the current policy consists of five strategies: [Alders (1992), van Hilten (1994), Jack (1992), Ministry of VROM (1993), RIVM (1991), Steinberg (1992)]

(1) The reduction of the CO_2 concentration by reforestation:
On a long term, reforestation might contribute to a reduction. However, its potential is limited and any substantial capacity can only be realized outside the Netherlands.

(2) The reduction of energy consumption and the improvement of efficiency:
In general, looking at efficient energy consumption, there are three different points of views. First, by conscious use and the implementation of better technology, the unnecessary consumption of energy by the consumer himself can be reduced.

Secondly, as energy is often only needed in small quantities and in a specific form, the capacity of the energy generated by the combustion of fossil fuels is partly left unused. For instance, if in industry a high reaction-temperature is needed, a direct combustion of fossil fuels in a furnace is used. However, when the remaining heat of the combustion gases is not used to generate steam, as there is no application for steam on site, part of the capacity is lost. To use this capacity, the remaining energy has to be transported to other locations. As electricity can be easily converted into other forms of energy and is relatively easy to handle, it is more and more used as a universal transport medium in an effort to improve the

efficiency by using the full capacity. The importance of electricity in the energy provision is thereby growing.

The third view is the improvement of the energy conversion process itself. Besides the fact that conversion processes normally become more efficient when operated on a large scale, it is also possible to increase efficiency by improving the technology used. An example of an area with ongoing efficiency improvements is represented by the integrated combined cycles power plants, with or without the use of coal gasification. [Hendriks (1994), VDI (1992)]

The strategy of reduction of consumption and improvement of efficiency has been especially effective on a short term. It has so far been used to stabilize and slightly reduce the emission level. As electricity fulfils, on the one hand, a key role in the improvement of efficiency, but, on the other hand, is responsible for substantial CO_2 production, it is worthwhile searching for better power generation technologies.

(3) The substitution of CO_2-rich fossil fuels by CO_2-lean fossil fuels:
As fossil fuels differ in composition and heating values, different amounts of CO_2 are produced per equivalent of electricity:

Table 1.1 *Lower Heating Value (LHV) of fossil fuels per mole CO_2 produced*

fossil fuel	*combustion reaction*	*LHV (kJ/mole CO_2)*
Coal	$CH_x + (1+¼x)\ O_2 \rightarrow CO_2 + ½x\ H_2O$ $\quad x = 0.36 \ldots 0.64$	435 … 470
Oil	$CH_2 + 1.5\ O_2 \rightarrow CO_2 + H_2O$	610
Natural Gas	$CH_4 + 2\ O_2 \rightarrow CO_2 + 2\ H_2O$	790

So, by using natural gas, instead of coal or oil, less CO_2 is produced per equivalent of electricity. However, as incomplete combustion and leakage during transport results in an increase of the methane emission, the advantage with regard to the greenhouse effect is reduced from 42 % theoretically to 10 % in practice. Besides, the strategy is only of limited use, as 50 % of the Dutch power plants already use natural gas to generate electricity.

A more fundamental disadvantage of this strategy is related to the in time diminishing resources of natural gas. Both technologically and economically, it is easier to implement cleaning technology at a small number of large power plants than at a large number of small sources, like for instance households. Therefore, it is likely that natural gas will by use for these applications and no longer will be available for power generation. A good replacement seems to be the use of coal gasification for power generation, possibly in combination with hydrogen (H_2) as an energy carrier. [Alders (1992), VDI (1992)]

(4) The substitution of fossil fuels by renewable or alternative CO_2-free energy sources:
The use of sources like wind, nuclear, or biomass energy is restricted by their capacity or by their present technological status. [VDI (1992), Mot (1992)]

(5) The removal of CO_2 caused by fossil fuels:
This strategy is in itself not a solution; it nearly prevents the carbon dioxide of getting into the atmosphere. By doing so, it immediately raises the question of what to do with the carbon dioxide that is removed.

One option is using it as a feedstock in industry. However, estimations show that only as much as 5 % (1 gigaton CO_2) could be recycled in this way. [van Ree (1993)] The other option is storage until it can be reintegrated in the carbon cycle without causing a disturbance:

(a) Storage by injection into the deep ocean waters:
Although storage in the deep ocean waters has the advantage of a large capacity, it is uncertain whether it will be sufficiently effective and whether there are any negative effects on marine life. [Cox (1995), van Ree (1993)]

(b) Storage in underground caves or depleted gas fields:
In this option the carbon dioxide is injected with a pressure of 110 bars in underground caves. [van der Burgt (1993), van Hilten (1994), Mot (1992)] In this way the storage can be controlled easily and is not connected with any negative effects. Simulations show that it is technically possible against relatively small costs. Therefore, as depleted natural gas fields are available, the Dutch government prefers this solution. [Hendriks (1990, 1994), van Ree (1993)]

To meet the target of 20-25 % CO_2 reduction in 2005, agreed upon internationally, the strategy of removal and storage will have to be used substantially.

In conclusion, with on the one hand 20 % of the CO_2 emission being produced by a small number of power plants, while on the other hand a growing demand for electricity, the need for the development of a new clean technology for the power generation is clear. So far, the results of several studies point toward the use of an integrated gasifier combined cycles (IGCC) plant based on coal gasification in combination with CO_2 removal as a possible solution: [TNO (1995)]

(1) Coal gasification will become an important technique of power generation in the future, as natural gas and oil resources are smaller than those of coal.

(2) Gasification is a clean technology compared with the conventional processes using coal for power generation.

(3) The coal gas produced with an IGCC plant consists mainly of H_2 and CO, which can be shifted to CO_2 and H_2 using the water gas shift reaction. By producing hydrogen as a commercial side product the IGCC plant can continuously be operated at full capacity, even in times of low electricity demand. Hydrogen is not only a clean energy carrier; it also is a valuable commodity. In this way, the efficiency and profitability of the IGCC plant is greatly increased. [TNO (1995)]

1.2 IGCC power plant with CO_2 removal

In a conventional IGCC plant with an entrained flow gasifier, coal is gasified to coal gas, a mixture of mainly H_2 and CO, which is then completely burned to CO_2 and H_2O in a gas turbine. In the gas turbine, electricity is generated with the mechanical power released by the decompression of the gas stream from 10-15 bara to atmospheric pressure. The gas steam that is leaving the gas turbine has still a temperature of 550 °C. With the remaining heat content, high pressure steam is produced, which by using steam turbine adds to the generation of electricity. In figure 1.2, this conventional process is represented by the base case.

Over the years, several processes to remove carbon dioxide have been developed in other industrial areas. Most of them are based on gas-liquid absorption using physical or chemical bonding and operating at a low temperature and a low final CO_2 pressure. Their application

Table 1.2 *Gas-liquid absorption processes commonly used in industry for CO_2 removal*

classification	*solvent*	*process name*	*T (°C)*	*p_{out}-CO_2 (bar)*
Chemical scrubbing processes				
Amine washes	monoethanolamine (MEA)	MEA, UCAR	25 - 150	~ 1-3
	diethanolamine (DEA)	DEA, SNEA-DEA		
	diisopropanolamine (DIPA)	DIPA		
	methyldiethanolamine (MDEA)	MDEA		
	2-(2-aminoethoxy)-ethanol (DGA)	DGA, Econamine		
	hindered amine	Flexsorb		
Hot potash washes	potassium carbonate	Catacarb, Benfield	40 - 110	~ 1-3
Physical-chemical processes				
	sulfolane/DIPA, sulfolane/MDEA	Sulfinol	25 - 150	~ 1
	methanol/amine	Amisol	25 - 65	~ 1
Physical processes				
	methanol	Rectisol	-30 - -10	~ 1
	dimethyl ether of polyethylene glycol	Selexol	0 - 40	~ 1
	n-oligoethylene glycol methyl isopropyl ethers	Sepasolv	0 - 40	~ 1
	n-methyl-2-pyrrolidone	Purisol	-15 - 30	~ 1
	propylene carbonate	Fluor	0 - 30	~ 1

[Elvers (1989-A12, 1989-A13), Grayson (1983-V2, 1983-V4 1983-V22), Jack (1992), Kessler (1992), Oudhuis (1992)]

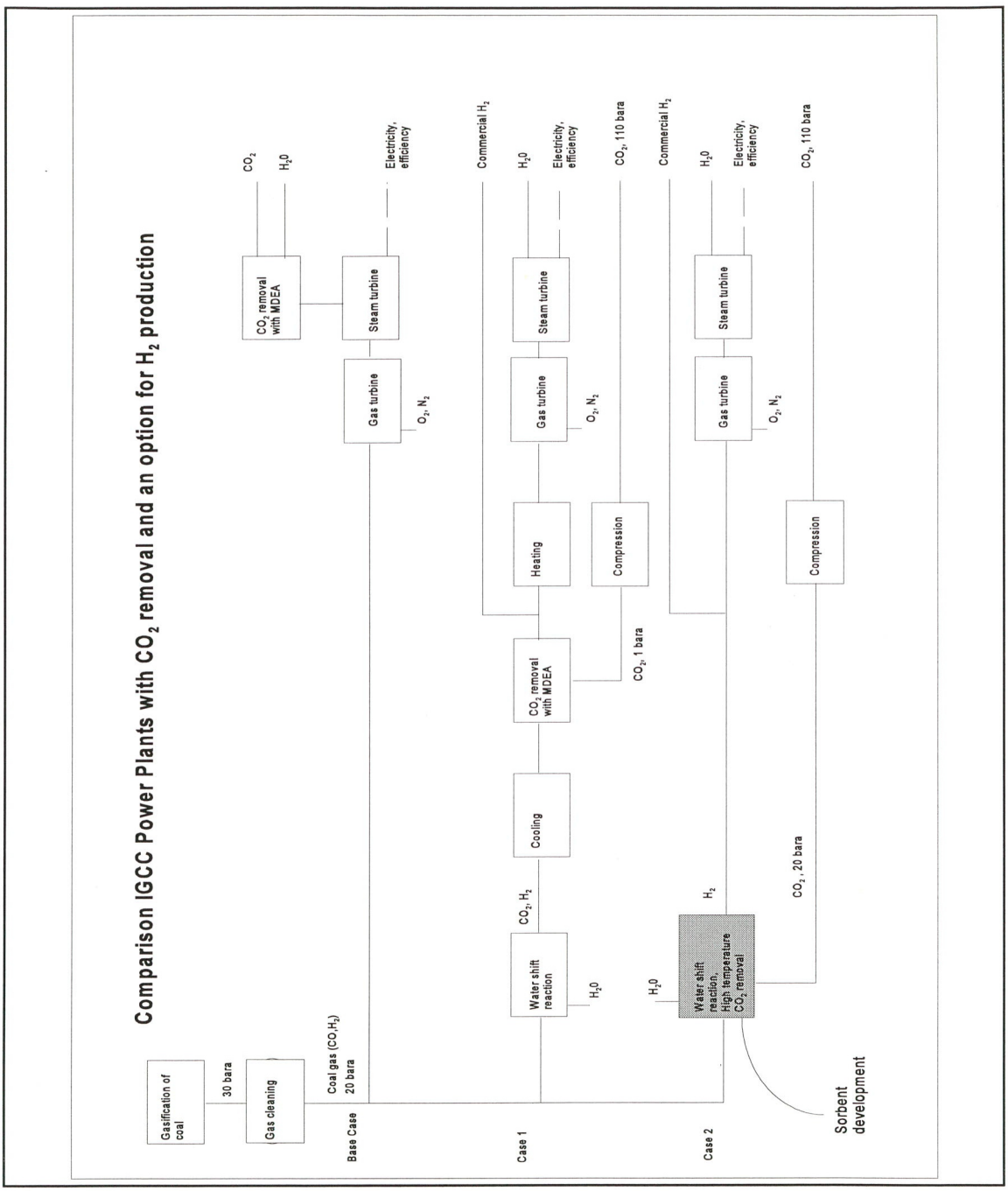

Figure 1.2 *Research concept :*
A comparison of IGCC plant with and without high pressure CO_2 removal

[TNO (1995)]

on the flue gases of a conventional IGCC power plant is, although technically feasible, not an interesting option. With the partial pressure of CO_2 being 0.07 bar or less at the outlet of the turbines, the use of an absorption solvent with physical bonding is out of the question, as it would require recompression of the gas stream. What remains is the use of a solvent with chemical bonding (e.g., MDEA: monodiethanolamine), but even then a large amount of solvent is needed for sufficient absorption. The heat lost in the regeneration of these large amounts would no longer be available for steam generation. So, the plant efficiency would decrease considerably.

Table 1.3 *Composition (vol.%) of coal gas from Drayton coal for the Shell-IGCC process (first water gas shift reaction: 350-500 °C, second reaction: 200-350 °C)*

	after gasification	*before shift reaction*	*after first shift reaction*	*after sec. shift reaction*
H_2	30.1	13.1	35.8	39.8
CO	62.9	27.4	4.7	0.8
CO_2	1.5	0.6	23.3	27.3
H_2S	0.3	0.1	0.1	0.1
N_2	3.8	1.6	1.6	1.6
Ar	1.1	0.5	0.5	0.5
H_2O	0.3	56.5	33.8	29.8

[Hendriks (1994)]

When low carbon fuel gas or hydrogen is produced, the coal gas is shifted with steam at high temperature (200-500 °C) and high pressure (20-25 bara) in the presence of a catalyst:

$$CO + H_2O \rightleftarrows CO_2 + H_2 \qquad \textbf{(1.1)}$$

The CO_2 removal can now be integrated in an earlier stage of the process. This opens the possibility of a CO_2 gas-cleaning step that operates at high pressure and at a moderate or high temperature. This step is integrated with the shift reactor or is directly following it.

Using the conventional way of removal with MDEA would require cooling of the gas mixture to 50-100 °C, followed by the separation of CO_2 and the reheating of the remaining H_2 to 300 °C, the inlet temperature of the turbine (figure 1.2: case 1). The major disadvantages of this separation process are the large consumption and release of heat at such a low temperature and the losses of heat that come with the cooling and reheating.

In addition, a considerable amount of compression work is required to bring carbon dioxide from the desorption pressure of 1 bara at the pressure of 80-120 bara, needed for storage in the depleted gas fields. [van der Burgt (1993), Hendriks (1990, 1994), Oudhuis (1992)]

As a result, the overall power generation efficiency decreases by 10 to 20 %-points compared with the efficiency of the conventional plant without CO_2 removal. [Heesink (1996), Hendriks (1994), VDI (1992), Silaban (1995)]

Table 1.4 *Calculated net work needed for the compression of CO_2 to 110 bara as a function of the desorption pressure*

inlet pressure (bara)	*single stage compression without cooling*		*5-stage compression with interstage cooling*	
	net work (MW/kg)	*outlet temperature (°C)*	*net work (MW/kg)*	*outlet temperature (°C)*
1	0.64	625	0.34	35
11	0.20	262	0.14	35
21	0.12	190	0.08	35
31	0.08	149	0.06	35
41	0.06	121	0.04	35

Calculated with AspenPlus™ release 9.2-1 of Aspen Technology Inc.

Blocks Compr and Mcompr: polytropic efficiency 0.84, mechanical efficiency 0.98
Conditions: Peng-Robinson equation of state, inlet temperature 35 °C

[Aspen (1994)]

A decrease in efficiency of such a magnitude is hardly acceptable as it would mean an increase in the amount of fuel that has to be burned to produce the same amount of electricity. This would be a magnification of the CO_2 problems. Therefore, new processes are developed which optimize the efficiency by further integrating the CO_2 removal and the power generation. [Heesink (1996), Jack (1992), Oudhuis (1992)]

This work aims at the development of a regenerative sorbent for CO_2 that can delivering CO_2 at a high pressure in order to reduce the compression work needed. With the data from table 1.4, it can be calculated that approximately 2-5 %-points could be gained if the desorption is operated at the adsorption pressure of 20 bara. [Heesink (1996), TNO (1995)]

Preferably, the sorption is also performed at high temperature (350 °C or more), thereby avoiding, on the one hand, the reheating of the hydrogen stream and, on the other hand, the energy consumption of the separation by using the exergy of the high temperature combustion heat which otherwise would have been lost. (figure 1.2: case 2)

Preliminary calculations have shown that the decrease in overall power plant efficiency can be limited to 4-14 %-points when such a process at high pressure and high temperature is used. [van Kessel (1993, 1994), Heesink (1996)]

In three previous studies [van Kessel (1993, 1994), Saeijs (1997)], the use of metal oxides as sorbent has been proposed. In theory, they reversibly react with carbon dioxide to form carbonates:

$$MeO\ (s)\ +\ CO_2\ (g)\ \rightleftarrows\ MeCO_3\ (s) \qquad \textbf{(1.2)}$$

At low temperatures the equilibrium favors the carbonate, resulting in a small equilibrium pressure of CO_2. With increasing temperature, the carbonate decomposes and the equilibrium pressure becomes also higher. So, by changing the temperature during the adsorption-desorption cycle (TSA: Temperature Swing Adsorption), the position of the equilibrium is influenced and the carbon dioxide that is adsorbed at low temperature, can be released at a higher pressure.

Calcium oxide has been proven to be a suitable sorbent. [Carty (1990), Han (1994), Siliban (1995)] However, disadvantages of this system are the high temperature needed for regeneration (900-1000 °C) and the high heat of adsorption (i.e., 160 kJ/mole CO_2). Experiments with theoretically more suitable sorbents, like magnesium oxide, dolomite (calcium magnesium oxide), and manganese oxide, have been unsuccessful so far. Although, the decomposition of the carbonates was proven to be fast, no substantial reaction was seen between these oxides and carbon dioxide.

A literature survey on these metal oxide-carbonate systems and their reaction mechanism, covering 101 articles and 14 patents, showed that the inactivity of these oxides is caused by the formation of a non-porous carbonate layer that kinetically limits the reaction with CO_2. It was concluded that the newly to develop sorbent should have an open structure that is preserved during reaction. As a solution, it was recommended to look either at supported metal oxides, coprecipitates of a metal oxide and other salts, and complex metal oxide-carbonate compounds with more than one kind of cation, or at the application of ion-exchanged zeolites. [Saeijs (1997)]

In this report, the use of ion-exchanged zeolites is further examined. Zeolites are crystalline, hydrated aluminosilicates with a framework build of AlO_4 and SiO_4 tetrahedra and holding a negative charge that is compensated by non-framework cations. After dehydration, they show the ability of adsorbing molecules in the pores of their framework:

$$M_{x/n}.[(AlO_2)_x(SiO_2)_y]\ (s)\ +\ CO_2\ (g)\ \rightleftarrows\ CO_2\,(ads)\,.\,M_{x/n}.[(AlO_2)_x(SiO_2)_y]\ (s) \qquad \textbf{(1.3)}$$

with:

CO_2 (ads)	= a molecule CO_2 adsorbed in the pores of the zeolite
y/x	= Si/Al ratio
M	= non-framework cations
n	= the valency of the cation

In comparison with other types of adsorbents, zeolites have three features that make them attractive for a high pressure TSA process: [Breck (1974), van Bekkum (1991), Jasra (1988)]

(1) Zeolites have high adsorption capacity, which is reasonably well maintained at moderately elevated temperatures.

(2) The three-dimensional crystalline micro porous structure has an unusual high thermal and hydrothermal stability.

(3) There are a large variety of framework types that all have their own adsorption properties, so that a zeolite type can be chosen that matches the separation. By changing the Si/Al ratio, the character of the internal surface can be adjusted from highly polar to non-polar. They can be modified by ion-exchange to improve the properties further.

Zeolites have already been used for the adsorption of carbon dioxide. Zeolite A and X are, for example, used in air-separation plants to remove the few percent of carbon dioxide from the air feed. In the production of hydrogen and of ammonia, zeolite adsorbers are use to remove bulk carbon dioxide. [Breck (1974), Elvers (1996-A28)] These applications are, however, operated at ambient or slightly elevated temperatures, while here the interest is focussed on higher temperatures.

In the energy sector, zeolites have recently been tested to remove carbon dioxide from the flue gases in conventional coal-fired thermal power plants. In these tests, like the ones by Tohoku Electrics, carbon dioxide is separated from nitrogen with a PSA (Pressure Swing Adsorption) process which is operated between 0.1 and 1.2 bara at slightly elevated temperatures. The main disadvantage of such a process is the need of large vacuum pumps and of special constructed valves. [Ministry of Economic Affairs (1991)] A TSA process avoids this disadvantage and may, therefore, be a better option.

Although, much research is done to understand and improve the adsorption properties of zeolites, these industrial data are not available in the open literature. [Breck (1974)] For carbon dioxide adsorption, the published data are mainly restricted to a few experiments for the well-known zeolite types (i.e., Zeolite A, X, Y, Chabazite and Mordenite). Data on the behavior at high temperatures are not directly available. The information on the effects of ion-exchange is incomplete as well: for the well-known types, the effects of alkali metal ions are more or less known, but the effects of alkaline earth metal ions are hardly described, while for the other types, information is rare.

This report gives the results of a feasibility study on the use of zeolites as a high temperature adsorbent that can be regenerated at high pressure. In chapter 2, the objectives are described in detail. In chapter 3, the background on the selection of a zeolite type is explained. In chapter 4, the experimental set-up of the adsorption measurements is shortly summarized. In chapter 5, the results of adsorption measurement with five different zeolite types (Zeolite A, X, P, β and Mordenite) are given. These measurements have been set up to examine the effects of ion-exchange on the CO_2 adsorption using alkaline earth metal ions. As alkaline earth metals are known for their strong interaction with CO_2 in carbonates, it was expected that the adsorption could be improved by ion-exchange. In chapter 6, the conclusions are presented.

Chapter 2

Objectives

2.1 Objectives: the original research proposal

Objective of the research project: [TNO (1995)]

- The objective of this research project is the development of a sorbent with which carbon dioxide can be adsorbed at a temperature of 400-700 °C and from which it can be desorbed in pure form at a temperature of 600-800 °C. The sorbent should be able to be regenerated at high pressure (approximately 60 bara and more) and to operate with sufficient capacity.

CO_2 sorbent: [TNO (1995)]

I a high sorption capacity for CO_2 at temperatures of 400-700 °C: preferably more than 50 wt.%,

II a steep increase of the equilibrium CO_2 pressure with temperature,

III a low heat of adsorption: preferably less than 100 kJ/mole,

IV fast intrinsic sorption and desorption kinetics; if the kinetics is limited due to insufficient surface area, the use of a support with a high surface area will be considered,

V chemical stability of the sorbing material in a reducing atmosphere during adsorption at temperatures up to 600 °C,

VI chemical stability of the sorbing material in an oxidizing atmosphere during desorption at temperatures up to 700 °C,

VII sufficient mechanical strength to allow for long operation times in packed, moving, or fluidized bed reactors: at least 2 years,

VIII preferably catalytic behavior with respect to the water gas shift reaction allowing for the simultaneous shift of CO and sorption of the produced CO_2.

Coal gasification process: [TNO (1995), Saeijs (1997)]

- the coal gas leaving the gasifier has a pressure of 30 bara.
- coal gas composition: 63 vol.% CO, 31 vol.% H_2, 1 vol.% CO_2, 5 vol.% others.
- a high temperature water shift reaction with 1:1 (mole ratio) coal gas/steam feed .
- the integration of this shift reaction with the new sorption process is optional

CO_2-removal process: [TNO (1995), Saeijs (1997)]
- adsorption: 400-700 °C, 30 bara, 7.5 bars partial CO_2 pressure
- desorption: 600-800 °C, 30 bara, 30 bars partial CO_2 pressure
- CO_2 pressure for transport and storage: 110 bara

2.2 Discussion

The objectives mentioned in the original research proposal, were initially written with a distinct solution in mind: the use of a metal oxide-carbonate system as the adsorbent. A first exploratory examination of zeolites has made it clear that with zeolites several of these objectives are no longer realistic [Saeijs (1997)]. At this stage of the project, a reevaluation of the objectives is in order:

For a metal oxide-carbonate system, the expected gain that should result in the efficiency improvement of 6-16 %-points was based on two separate ideas: [Heesink (1996)]

(a) The CO_2 desorption at high pressure with less compression work:
As already mentioned, it is necessary to compress the CO_2 that is release during the desorption, to a pressure of 110 bara before transportation and storage in the depleted gas fields. By desorbing at a higher pressure than ~ 1 bara, the usual pressure in conventional absorption processes, the compression work can be reduced.

(b) The separation of CO_2 with practically no net consumption of energy:
In the steam cycle of a power plant, the high pressure steam circuit is operated at 140 bara with a maximum temperature of approximately 540 °C. For 140 bara, the phase transition temperature, which at the same time is the pinch temperature in the heat integration, is ~ 330 °C. Most of the heat that is released during the combustion is needed for this phase transition.

The combustion heat is, however, available at a much higher temperature (900-1500 °C), and by employing it at 330 °C, much of its exergy is lost without being used. When a CO_2-adsorption process can be designed that operates between 350-900 °C, it can use this exergy for its separation without negatively influencing the efficiency; the adsorption heat is released at 350 °C, where it is needed for the phase transition, while the regeneration heat is consumed at high temperatures, where it is available. So, the separation would cost no net energy.

In order to operate the such adsorption at 350 °C, it was estimated that for a metal oxide-carbonate system, the heat of adsorption should be at least ~ 80 kJ/mole. [Saeijs (1997)] On the other hand, an adsorption heat of ~ 120 kJ/mole or more could lead to a regeneration heat that is larger than the amount produced in the combustion.

For metal oxide-carbonate systems, the adsorption of carbon dioxide is a chemical reaction for which the adsorption heat of ~ 70-120 kJ/mole can, in principal, be realized just by choosing the right cation. [Saeijs (1997)] Such a chemical reaction which is mainly governed by thermo-dynamics, makes it even possible to operate the adsorber as a combined TSA-PSA process: adsorbing at 400-700 °C and 7.5 bars CO_2, while desorbing at 600-800 °C and 60 bara. When not

hindered by mass transfer limitations, high conversions are not unusual, so that an adsorption capacity of more than 50 wt.% is in itself not impossible.

For zeolites, on the other hand, the adsorption is not a chemical reaction, but simply a bonding of carbon dioxide at the surface. Adsorption capacities as high as 50 wt.% are in these cases rather rare. According to the values, mentioned in literature and summarized in chapter 3, the heat of adsorption is 66 kJ/mole at most. So, the interaction between CO_2 and the zeolite should rather be characterized as physical instead of chemical bonding. With such a weak interaction, the adsorption at 300 °C is probably not much more than a few weight-percents. This is not enough to operate a process as mentioned under (b). Only, if by ion-exchange of the zeolite the interaction can be strengthened, which most likely is done by introducing alkaline earth metal ions, the expected gain is not reduced to the contribution of (a): the reduction of the compression work.

2.3 Objectives: the zeolite adsorbent

Objective for the development of a zeolitic adsorbent:

- The objective of this research project is the development of an adsorbent with which carbon dioxide can be adsorbed at 20-30 bara, 25-350 °C and from which it can be desorbed in pure form at a higher temperature. The sorbent should be able to be regenerated at high pressure (approximately 20-30 bara) and to operate with sufficient capacity.

CO_2 adsorbent:

I a high adsorption capacity for CO_2 at temperatures of 25-350 °C, but preferable at temperatures of 300-350 °C.
II a relatively high heat of adsorption: preferably between 70 and 100 kJ/mole, which might allow an adsorption temperature of approximately 300 °C or more,
III fast adsorption and desorption kinetics,
IV a high thermal stability: preferably resistant to temperatures up to 500-800 °C,
V a high hydrothermal stability: at least resistant to temperatures up to 350 °C,
VI sufficient mechanical strength to allow for long operation times in packed, moving, or fluidized bed reactors: at least 2 years,
VII preferably catalytic behavior with respect to the water gas shift reaction allowing for the simultaneous shift of CO and sorption of the produced CO_2.

Coal gasification process:

- the coal gas leaving the gasifier has a pressure of 30 bara.
- coal gas composition: 63 vol.% CO, 31 vol.% H_2, 1 vol.% CO_2, 5 vol.% others.
- a high temperature water shift reaction with 1:1 (mole ratio) coal gas/steam feed.

CO_2-removal process:

- adsorption: 25-350 °C, 30 bara, 7.5 bars partial CO_2 pressure
- desorption: 25-800 °C, 30 bara, 30 bars partial CO_2 pressure
- CO_2 pressure for transport and storage: 110 bara

Chapter 3

Zeolites

3.1 Introduction

Zeolites are crystalline, hydrated aluminosilicates with a framework structure. This framework is constructed of SiO_4 and AlO_4 tetrahedra linked through oxygen atoms. It forms an infinitely extending three-dimensional structure that bears a net negative charge as a result of the AlO_4 tetrahedra. It contains a network of regular channels and interconnected voids, which is occupied by water molecules and by cations. The cations, which are necessary to balance the negative charge, are mobile and ordinarily undergo exchange. [Breck (1974), Barrer (1978), Dyer (1988)]

On heating, the water molecules may be removed reversibly from the channels and voids without major alternations of the structure. This leaves crystalline dehydrated zeolites with a large free pore volume and a large interior surface, which can be used for the adsorption of other molecules such as carbon dioxide. As the channels and voids have the size of molecular dimensions (3-20 Å), these zeolites are referred to as molecular sieves. [Elvers (1996-A28)]

Compared with other inorganic oxide materials that are used as adsorbents, zeolites have a number of unique properties that will be discussed in detail in the following sections of this chapter [van Bekkum (1991)]:

(1) A high microporosity with uniform pores dimensions:
As the pores are a part of the crystal structure, their dimensions are uniform and can be controlled by choosing the type of zeolite structure that is used.

(2) A large internal surface and a full accessibility of the metal-oxygen atoms:
As the pores have molecular dimensions and the pore volume can get as high as 50% of the total volume, almost every metal oxygen atom is a part of the internal surface. Consequently, all sorbent material is fully accessible and can be used effectively. Moreover, this means that it is possible to have a large specific surface area without having to reduce the particle size.

(3) A high thermal stability:
As the surface is not formed by breakage of bonds but instead the local coordination of the atoms at the surface is kept unchanged, the stability is determined by the crystalline framework structure and therefore relatively high.

(4) An ability of controlling the adsorption properties by modifying the structure
As the zeolite structure is retained when small modifications in the composition are made, it

is possible, to some extent, to tailor the chemical and physical properties for the application as a sorbent.

First, modifications can be made by changing the amount of aluminum in the framework. For instance when the aluminum content is decreased, the number of non-framework cations also decreases. Consequently, the free pore volume will increase but the number of active sites for chemical adsorption will decrease. Therefore, the capacity will probably increase but the interaction will change from a chemical bonding to a physical bonding.

Secondly, modifications can be made by exchanging the non-framework cations. For instance, replacing sodium ions by magnesium will reduce the number of ions and increase the free pore volume. However, this increase in volume will be smaller than expected as the bivalent magnesium ion has to compensate two negative charges that are not close to each other. The magnesium ion, therefore, will be less closely bond to the framework. This may result in a partial blockage of the aperture to the voids and, although the volume increased, in a decrease in capacity. In addition, the character of the interaction with the sorbate will be affect by the change of the cation. Here also, predicting the exact effect is hard. On the one hand, the polarity and the charge of the cation are changed, while, on the other hand, the interaction is influenced by the looser bonding of the cation to the framework.

Finally, modification can be made by changing the acidity or by introducing traces of other elements than Al and Si in the framework. Furthermore, it is possible to introduce metal particles on the internal surface which might assist in the adsorption process.

3.1.1 Structure

Composition

The composition of zeolites can be represented by the formula:

$$M_{x/n} \left[(AlO_2)_x \, (SiO_2)_y \right] \cdot z \, H_2O \qquad \textbf{(3.1)}$$

with: M = non-framework metal cation
n = valency of the cation
y/x = Si/Al ratio
z = number of water molecules

The cations are mainly alkali metal and alkaline earth metal ions, in particular sodium, potassium, calcium, strontium and barium. In most zeolites that occur naturally as minerals, a combination of these cations is present. In the synthetic zeolites, the synthesis often dictates the presence of one particular cation. However, as the cations are mobile, other ions can be introduced after the synthesis of the framework by ion exchange. Therefore, it is possible to make zeolites with practically any cation present.

The physical and chemical properties of the zeolites are essentially determined by the

aluminum content which is usually expressed by the Si/Al ratio. According to the Loewenstein Rule, Al-O-Al groups cannot occur in crystalline aluminosilicates. Hence, the Si/Al ratio is always equal to or greater than 1.

A distinction can be made between low-silica ($1 \leq Si/Al < 2$), intermediate-silica ($2 \leq Si/Al < 10$), and high-silica ($10 \leq Si/Al < 100$) zeolites. Zeosils, a group of zeolites that contain only a trace of aluminum, and Silicalite, a related structure consisting of only SiO_4, are left out of consideration in this report. In table 3.1 is shown how the main properties change when going from low-silica to high-silica zeolites.

Table 3.1 *The general influence of the Si/Al ratio on the main properties of zeolites*

property	*Si/Al* = 1	*Si/Al* = ∞
Cation concentration	High	Low
Acidity	Low	High
Surface selectivity	Hydrophilic / Polair	Hydrophobic *)
Thermal stability	≤ 700 °C	~ 1300 °C
Structure	4-, 6-, 8- rings	5- rings

*) The transition between hydrophilic and hydrophobic occurs at a Si/Al ratio of ca. 10 [Elvers (1996-A28)]

[van Bekkum (1991)]

The term zeolite is sometimes used for a group of materials that have a similar framework of tetrahedra but in which the aluminum or silicon is partially or completely replaced by other elements. For instance, a large variety of metalsilicates can be formed when aluminum is replaced by tri- or tetravalent atoms such as B, Fe, Ti or Ga. In the same way, alumino- and gallophosphates can be formed when silicon is replaced by phosphor. [van Bekkum (1991), Elvers (1996-A28)] Although these materials have interesting properties, they are not further examined here.

Nomenclature

So far, there is no systematic nomenclature for zeolites that describes both the composition and the structure. Although formula (3.1) gives information about the composition, it does not tell anything about the framework structure. In fact, it is possible to have the same composition but different structures, or the same structure but different compositions.

The naming and classification of zeolites are mainly based on structural similarity alone. If a natural zeolite with the same structure exists, the synthetic zeolite is often named after this mineral (e.g., Faujasite or Mordenite). Frequently, however, the original names given by the discoverers are still used. Back then, they gave the synthetic zeolites names using letters of the

Latin and Greek alphabets (e.g., A, X, or Y, and β, ρ, or ώ), or using acronyms (e.g., ZSM-5). Zeolites with identical structures can, therefore, appear in the literature under different names. [Szostak (1992), Elvers (1996-A28)]

Some order has been imposed by the introduction of an IUPAC nomenclature [Barrer (1979), Dyer (1988)] and by the classification system of the International Zeolite Association as described in the *Atlas of Zeolite Structure Types* [Meier (1996)].

This atlas gives an overview of the 100 different structure types that, so far, have been found and sufficiently investigated. The structure types are denoted by a combination of three capital letters (e.g., LTA, or FAU) They can be used to classify different materials which belong to the same type.

On the basis of similarities in the topology of their framework, the structure types are often divided in 5 or 6 main categories. This kind of division can offer some support in the selection of zeolites for an application such as adsorption. However, it considers only one aspect that is important in this application. [Breck (1974), Barrer (1978), Dyer (1988)]

Topology of the framework

The basic elements of the framework are Al and Si tetrahedra. The topology of the framework, however, is better described by the concept of larger units known as secondary building units (SBUs) and structural subunits (SSUs).

The SBUs are structural units of 4 to 12 linked tetrahedra. They are arranged as simple rings, complex rings, or prisms of various sizes. The different shapes are shown in figure 3.1.

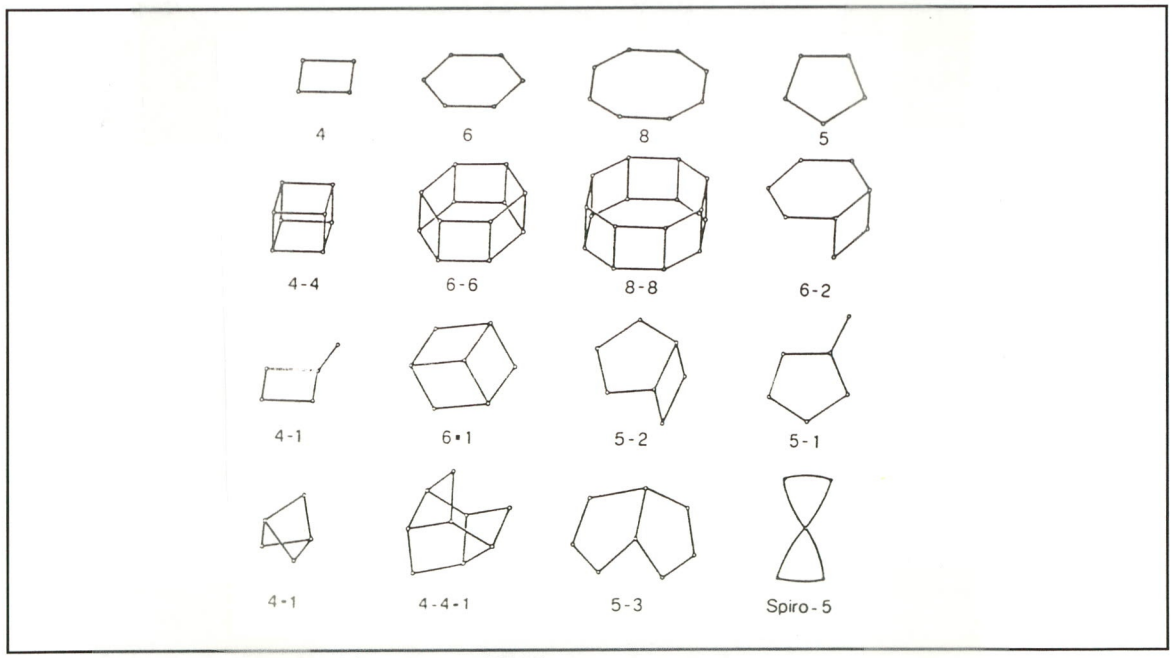

Figure 3.1 *Secondary Building Units (SBU)*

[van Bekkum (1991)]

In the original concept, a SBU represents a relatively stable intermediate that plays a key role in the synthesis of the framework. They were invented with the idea that a framework could be generated from one SBU only. As more and more structure types were discovered, their number rose from 8 to 16. Although, the occurrence of SBUs as stable intermediates in the synthesis of silicas have been demonstrated [van Bekkum (1991), Wijnen (1989, 1990)], their use in the description of zeolite synthesis is questionable. There are still structure types that need two SBUs to make up their framework, while others can be described by more than one type of SBU.

In the nomenclature, the SBUs are used as a criterion in a division of structure types in main categories. Based on the presence of single rings (S4R or S6R), double rings (D4R or D6R), or more complex SBUs (4-1 (T_5O_{10}), 5-1 (T_8O_{16}), or 4-4-1 ($T_{10}O_{20}$)) a division in 5, 6, or even 7 categories is made. An example of such a division will be discussed later in table 3.4. A more detailed description of these categories can be found in the publications of Barrer [(1978)], Breck [(1974)] and Dyer [(1988)].

For the selection of adsorbents, this kind of division is of some interest as these ring shape SBUs (4-, 5-, 6-, and 8-rings) form the apertures to the channels and voids in the structure. Their sizes give information on whether or not ion exchange and adsorption are possible.

Table 3.2 *The average diameter of the ring shaped apertures*

ring type	*no. of oxygen atoms or tetrahedra*	*average free diameter (Å)*	
4-ring	4	1.4	(1.2 - 1.6)
5-ring	5	1.7	(1.5 - 2.0)
6-ring	6	2.8	(2.3 - 2.8)
8-ring	8	4.3	(2.6 - 4.5)
10-ring	10	6.3	(5.1 - 7.2)
12-ring	12	8.0	(6.5 - 8.0)

[Barrer (1978), van Bekkum (1991), Breck (1974), Dyer (1988), Elvers (1996-A28)]

The exact free diameter will be different for each framework type. The values given in table 3.2 can only be used as a first estimate. The framework is not a rigid structure. The angles and the distances between the individual atoms in a ring will depend on the total stress in the framework structure. By altering the angles and the distances, the total free energy of the structure is minimized. [Barrer (1978), Elvers (1996-A28)]

The diameter is a function of temperature, as thermal vibrations that lead to fluctuations around the position of minimum free energy will increase with temperature. Normally, these changes will be of the order of 0.4 Å. Consequently, the effective free diameter is larger than the crystallographic diameter and adsorptive molecules with a larger diameter than expected are able to pass. [Dyer (1988)]

Additionally, the diameter is influenced by the character of the non-framework cations and by the presence of adsorbed molecules such as water. Not only can they change the coordination of the framework atoms by their influence on the free energy, they can also cause a partial blockade of the aperture when their position of minimum free energy within the structure is unfavorably situated. [Barrer (1978), Elvers, (1996-A28)]

When selecting adsorbents, the Structural Subunits (SSU) form a better criterion for a division in main categories. The SSUs are more complex chains and layer structures and can be excellently used to describe the volume of the channels and of the voids [Barrer (1978)]. Their presence, therefore, gives an indication on the capacity of the adsorbent.

In determining the volume of the voids, the polyhedra form an important group of SSUs. The trunced octahedron (the β-cage or Sodalite cage), the trunced cubo-octahedron (the α-cage), and the regular cubo-octahedra are the most frequently encountered ones, but other shapes are observed as is shown in table 3.3.

Most frameworks can be constructed by stacking two or more types of polyhedron in simple coordinations. Sodalite is the only zeolite that is composed of only one type, namely the β-cage. As pointed out by Fedorov, there are only five polyhedra, which, stacked with others of the same kind can create a complete space-filling. Besides the β-cage, there are the cube (D4R SBU), the hexagonal prism (D6R SBU), and the two kinds of 12-hedrons.

Table 3.3 *The most common polyhedral Structural Subunits in zeolites*

polyhedron	*faces*	*approximate free dimension (Å)*
6-hedron	6 x 4-rings	--
8-hedron	2 x 6-rings, 6 x 4-rings	2.3 in plane 6-ring
10-hedron (δ-cage)	2 x 8-rings, 8 x 4-rings	4.5 in plane 8-ring
11-hedron (ϵ-cage)	5 x 6-rings, 6 x 4-rings	4.7 along the c-axis, 3.5 normal to c-axis
14-hedron I (β-cage)	8 x 6-rings, 6 x 4-rings	6.6
14-hedron II	3 x 8-rings, 2 x 6-rings, 9 x 4-rings	6.0 along the c-axis, 7.4 normal to c-axis
17-hedron I	3 x 8-rings, 5 x 6-rings, 9 x 4-rings	9.0 along the c-axis, 7-7.3 normal to c-axis
17-heron II	11 x 6-rings, 6 x 4-rings	7.7 along the c-axis, 6.4 normal to c-axis
18-hedron (γ-cage)	6 x 8-rings, 12 x 4-rings	10.8 x 6.6
20-hedron	6 x 8-rings, 2 x 6-rings, 12 x 4-rings	11 along the c-axis, 6.5 normal to c-axis
23-hedron	6 x 8-rings, 5 x 6-rings, 12 x 4-rings	15 along the c-axis, 6.3 normal to c-axis
26-hedron I (α-cage)	6 x 8-rings, 8 x 6-rings, 12 x 4-rings	11.4
26-hedron II	4 x 12-rings, 4 x 6-rings, 18 x 4-rings	11.8

[Barrer (1978), Breck (1974), Dyer (1988), Elvers (1996-A28)]

Besides describing the topology in terms of building units, it can be characterized by the type of network that the voids and channels form. If, starting from a given place in the structure, an adsorbate molecule may reach any other place in the structure through the channels, the network in termed three-dimensional. If the molecule can only reach places in the same plane, the network is two-dimensional, while, if the molecule's movement is restricted to one direction, the network is one-dimensional. For the selection of adsorbents, the type of network gives an indication on the accessibility of the active sides and, therefore, on the possibility of mass transfer limitations by either diffusion, steric hindrance, or channel blockage.

Whether a zeolite has an one-, a two- or a three-dimensional network for a certain adsorbate depends both on the size of the void's aperture and on the size of the adsorbate molecule. Water, with its small kinetic molecular diameter of 2.6 Å, can still pass a 6-ring aperture at normal temperatures. Most other molecules, among which carbon dioxide, having a kinetic diameter larger than 3 Å, can only pass 8-rings or larger [Barrer (1978), Elvers (1996-A28)]. Only the presence of 8-, 10-, and 12-rings, therefore, counts in the determination of the dimension. In table 3.4, the network type of most zeolites is listed.

A parameter more or less related to the dimension of the network is the void fraction. This fraction can vary from 0.18 to 0.50 . The highest fractions are seen for the three-dimensional network.

Table 3.4 *A classification of the most common zeolites*

Group 1: S4R - Secondary Building Unit

zeolite name *)		*Si/Al*	*channel network*	*void fraction*	*framework density (g/cc)*	*polyhedra* **)	*ring*	*aperture dimension (Å)* ***)
Analcime	(ANA)	2.00	1	0.18	1.85		6	4.2-1.6
Garronite	(GIS)	1.67	3	0.40	1.62		8	3.5
Gismondine	(GIS)	1.00	3	0.46	1.52		8, 8	3.1 x 4.4, 2.8 x 4.9
Harmotome	(PHI)	3.00	3	0.31	1.59		8, 8	4.2 x 4.4, 2.8 x 4.8
Laumontite	(LAU)	2.00	1	0.34	1.77		10	4.0-4.6 x 5.3-6.3
Paulingite	(PAU)	3.42	3	0.49	1.54	α,β,γ,δ	8	3.9
Phillipsite	(PHI)	2.20	3	0.31	1.58		8, 8	3.2-3.6, 2.9 x 4.3-4.8
Yugawaralite	(YUG)	3.00	2	0.27	1.81		8, 8	3.1 x 3.5-5.0, 2.8 x 3.6
Zeolite P	(GIS)	1.67	3	0.41	1.57		8	3.5
Zeolite W or K-M	(MER)	1.81	3	0.22	1.45		...	3.7 x 5.1, 3.6 x 2.7

*) Zeolites with the same framework, as indicated by the IZA-classification, may have different names depending on the Si/Al ratio and the non-framework cations present. For a full and up-to-date description see the publications by the IZA. [Meier (1996), IZA-SC (1997)]

**) If no polyhedra are mentioned, the framework has no specific cages as far as the description of the channel network is concerned.

***) The dimensions mentioned are based on the hydrated framework; the dimensions in the dehydrated framework may deviate.

Group 2: S6R - Secondary Building Unit

zeolite name		*Si/Al*	*channel network*	*void fraction*	*framework density (g/cc)*	*polyhedra*	*ring*	aperture dimension (Å)
Erionite	(ERI)	3.00	3	0.35	1.51	ϵ, 23	8	3.6 x 5.2
Levynite	(LEV)	3.50	2	0.40	1.54	17	8	3.2 x 4.8-5.2
Mazzite or Zeolite Ω	(MAZ)	3.50	1	0.38	1.65	14-II	12, 8	7.1-7.5, 5.6 x 3.4
Offretite	(OFF)	2.33	3	0.40	1.55	ϵ, 14-II	12, 8	6.4-6.7, 3.6 x 5.2
Sodalite	(SOD)	1.00	3	0.35	1.58	β	6	2.2
Zeolite L *)	(LTL)	3.00	1	0.32	1.61	ϵ	12	7.1
Zeolite Losod	(LOS)	1.00	3	0.33	1.58	ϵ, 17	6	2.2

*) In the classification by Breck, Zeolite L is placed in group 4 [Breck (1974)].

Group 3: D4R - Secondary Building Unit

zeolite name		*Si/Al*	*channel network*	*void fraction*	*framework density (g/cc)*	*polyhedra*	*ring*	*aperture dimension (Å)*
Zeolite A	(LTA)	1.00	3	0.47	1.27	α, β	8, 6	4.1-4.2, 2.3
Zeolite ZK-4	(LTA)	1.67	3	0.47	1.30	α, β	8, 6	4.2, 2.2

Group 4: D6R - Secondary Building Unit

zeolite name		*Si/Al*	*channel network*	*void fraction*	*framework density (g/cc)*	*polyhedra*	*ring*	*aperture dimension (Å)*
Chabazite	(CHA)	2.00	3	0.47	1.45	20	8	3.6 x 3.7-4.2
Faujasite	(FAU)	2.25	3	0.47	1.27	β, 26-II	12	7.4
Gmelinite	(GME)	2.00	3	0.44	1.46	14-II	12, 8	7.0, 3.6 x 3.9
Zeolite X	(FAU)	1.23	3	0.50	1.31	β, 26-II	12	7.4
Zeolite Y	(FAU)	2.43	3	0.48	1.25-1.29	β, 26-II	12	7.4
Zeolite ZK-5	(KFI)	2.20	3	0.44	1.46	α, γ	8	3.9

Group 5: 4-1 - Secondary Building Unit

zeolite name		*Si/Al*	*channel network*	*void fraction*	*framework density (g/cc)*	*polyhedra*	*ring*	*aperture dimension (Å)*
Edingtonite	(EDI)	1.50	2	0.36	1.68		8	2.8-3.5 x 3.9
Gonnardite	(THO)	1.50	2	0.31	1.74		8	2.6 x 3.9
Natrolite	(NAT)	1.50	2	0.23	1.76		8	2.6 x 3.9
Mesolite	(NAT)	1.50	2	0.30	1.75		8	2.6 x 3.9
Scolecite	(NAT)	1.50	2	0.31	1.75		8	2.6 x 3.9
Thomsonite	(THO)	1.00	2	0.32	1.76		8	2.2-2.6 x 3.9

Group 6: 5-1 - Secondary Building Unit

zeolite name		*Si/Al*	*channel network*	*void fraction*	*framework density (g/cc)*	*polyhedra*	*ring*	*aperture dimension (Å)*
Bikitaite	(BIK)	2.00	1	0.23	2.02		8	2.8-3.2 x 3.7-4.9
Dachiardite	(DAC)	3.80	2	0.32	1.72		10, 8	3.7 x 5.3-6.7, 3.6 x 4.8
Epistilbite	(EPI)	3.00	2	0.25	1.76		10, 8	3.2 x 5.3-5.6, 3.7 x 4.4
Ferrierite	(FER)	5.55	2	0.28	1.76		10, 8	4.3 x 5.5, 3.4 x 4.8
Mordenite	(MOR)	5.00	2	0.28	1.70		12, 8	6.7 x 7.0, 2.9 x 5.7
Zeolite ZSM-5	(MFI)	~ 30	3 *)	0.32	...		10	5.1 x 5.5, 5.3 x 5.6

*) In the classifications by Meier and by van Bekkum, the dimension of the channel network for ZSM-5 is 2; in *Ullmann's Encyclopedia of Industrial Chemistry* ZSM-5 has a dimension of 3. [van Bekkum (1991), Elvers (1996-A28), Meier (1987)]

Group 7: 4-4-1 - Secondary Building Unit

zeolite name		*Si/Al*	*channel network*	*void fraction*	*framework density (g/cc)*	*polyhedra*	*ring*	*aperture dimension (Å)*
Brewsterite	(BRE)	3.00	2	0.26	1.77		8, 8	2.3 x 5.0, 2.7 x 4.1
Clinoptilolite	(HEU)	5.00	3 *)	0.34	1.71		10, 8	3.0 x 7.2-7.6, 2.6 x 4.7
Heulandite	(HEU)	3.50	3 *)	0.39	1.69		10, 8	4.4 x 7.2-7.6, 4.0 x 5.5
Stilbite	(STI)	3.50	2	0.39	1.64		10, 8	4.1 x 6.2, 2.7 x 5.7

*) In the classifications by Breck and by van Bekkum, the dimension of the channel network for Heulandite is 2; in *Ullmann's Encyclopedia of Industrial Chemistry* both Heulandite and Clinoptolite have a dimension of 3. [van Bekkum (1991), Breck (1974), Elvers (1996-A28)]

[Barrer (1978), van Bekkum (1991), Breck (1974), Dyer (1988), Elvers (1996-A28), Meier (1987)]

Non-framework cations

The cations needed to balance the negative charge of the framework are introduced during the synthesis of the zeolite and are usually alkali metal and alkaline earth metal ions as the hydroxides of these ions are used to make the strong basic precursor solutions. In a few cases, the cations will be organic ions (e.g., alkyl ammonium salts, amines, alcohols, or esters), as some frameworks can only be synthesized in the presence of a specific functional group or need a spacious cation to aid in the stabilization of the framework. These organic ions are often referred to as templates. [van Bekkum (1991), Elvers (1996-A28)]

For both inorganic and organic ions, it is assumed that the cation exhibits a structure-directing effect. The hydrated ion creates a certain degree of order between the molecules in the precursor solution and thereby stabilizes the intermediate SBUs and SSUs. Several studies suggest that the properties of the cation present determine which intermediate is formed. It is, therefore, not astonishing that the cation composition of the precursor solution is of vital significance and that the cation species cannot be chosen freely during the synthesis. [van Bekkum (1991), Breck (1974), Elvers (1996-A28), Wijnen (1989)]

After synthesis, the cations occupy definite sites in the voids and channels, where they are surrounded by the partially negative charged oxygen atoms from the rings of the framework. The bond has a mainly ionic character which means that the cations are mobile and can be exchanged for other cation species. Their total number, however, is directly related to the amount of aluminum in the framework as dictated by the rule of electro-neutrality.

The number of sites in framework may be considerably larger than the number of cations. A framework usually provides different kinds of sites. There may be partial occupancy of some or all of these sites. The cations distribute themselves among the sites so as to minimize the total free energy of the system. The distribution equilibrium between the different sites is a function of temperature, of the cation species present, and of the adsorbate molecules present.

The preference of a particular cation for a particular available site can be due to energetic, steric, or coordinative considerations. This behavior is determined by an interaction between cation and framework. On the one hand, it is depending on the size, charge, the electronegativity, and the polarity of the cation species. On the other hand, it is depending on the total anionic charge, distribution of that charge, and the dimensions of the channels of the framework type. As shown in table 3.5, the size and the charge can change the effective pore size of a framework.

Table 3.5 *Some examples of effective aperture sizes for different cations*

zeolite type	*cation*	*charge*	*cation size (Å)*	*effective framework aperture size (Å)*
Li-Zeolite A, dehydrated (LTA)	Li	1+	0.68	3.6-3.8 *) (8-ring)
Na-Zeolite A, dehydrated (LTA)	Na	1+	0.97	3.8-4.0 (8-ring)
K-Zeolite A, dehydrated (LTA)	K	1+	1.33	3.0 (8-ring)
Ca-Zeolite A, dehydrated (LTA)	Ca	2+	0.99	4.3-4.8 (8-ring)
H-Mordenite, dehydrated (MOR)	H	1+	~0.3	8.0-9.0, ~3.8 (12-, 8-ring)
Na-Mordenite, dehydrated (MOR)	Na	1+	0.97	7.0-7.2, blocked (12-, 8-ring)
Ca-Mordenite, dehydrated (MOR)	Ca	2+	0.99	blocked, 3.8 (12-, 8-ring)
Ba-Mordenite, dehydrated (MOR)	Ba	2+	1.34	blocked, 3.8 (12-, 8-ring)
Na-Zeolite X, dehydrated (FAU)	Na	1+	0.97	7.4-7.8 **) (12-ring)
Ca-Zeolite X, dehydrated (FAU)	Ca	2+	0.99	7.8-10.0 **) (12-ring)

*) This value is based on the ring contraction mentioned by Breck [(1974)] and by Szostak [(1992)].

**) In his review, Breck is contradictory about these values. Referring to data on commercial molecular sieves by Union Carbide, he mentions values of 10 and 8 for Na and Ca, while in his discussion on experimental adsorption data he gives values that back up the figures given here by Dyer. Possibly, this discrepancy is caused by the temperature of the measurements. [Breck, pp. 638 and 748 (1974)]

[Breck (1974), Dyer (1988), Elvers (1996-A28), Szostak (1992), Weast (1981)]

In the case of Zeolite A, by replacing sodium with lithium, the framework is distorted which results in an aperture contraction of 0.17 Å [Breck (1974)]. The difference between sodium and potassium, however, is simply explained by a partial blocking of the aperture. Both ions occupy the same site, close to the 8-ring, but as the K^+ ion is larger than Na^+, the diameter of the passage is smaller. This phenomenon is often referred to as the 'sentinel effect'. Evaluating this effect for calcium, more or less the same size as for sodium would be expected. However, the Ca^{2+} ion prefers another site and the aperture size is equal to the theoretical ring dimension.

In the case of Mordenite, the cation charge and site preference explain the differences. The univalent Na^+ prefers a site in the 8-ring channels leaving the passage through the 12-ring channels unhindered. The divalent Ca^{2+} and Ba^{2+} occupy sites in the 12-ring channel and therefore reduce its effective size to less than 3.8 Å. [Dyer (1988)]

In the case of Zeolite X, the differences between sodium and calcium are less easily explained. Most likely, they are caused by the combination of a framework distortion, a shift in framework charge distribution, and a sentinel effect. [Breck (1974), Dyer (1988)]

In the presence of adsorptive molecules, especially polar molecules such as NH_3, SO_2, and H_2O, a redistribution of cations is possible that leads to similar changes in the aperture size. The interaction between the cation and the dipole of the molecule can, for instance, result in the formation of clusters or of complexes that block the channels. Also, the presence of an adsorbate may force the cation to occupy another site because of steric or of coordinative considerations. [Breck (1974), Dyer (1988)]

Zeolitic water: hydration and dehydration

Zeolites can only be synthesized in the presence of water. It is known that water aids in the formation of the framework. It has a pronounced stabilizing effect because it lowers the chemical potential of the zeolite crystal. [Breck (1974)] The water molecules are rather strongly bonded by H-bridges. These bonds are not only formed with other water molecules, but also with the bridged-oxygen and the hydroxyl groups of the framework. As H-bridges are easily formed and broken up again, water is very mobile and does not occupy specific sites. NMR studies show, for instance, that all water molecules are equally bonded in the α-cages of Zeolite A.

When differences in bonding appear, they are related to the non-framework cations. Because of the ion-dipole interactions, water is seen to take part in the coordination of these cations. The water molecules form clusters with the cation, but there is a rapid exchange of molecules. The situation is, therefore, best characterized by a kind of electrolyte solution.

Water has a small kinetic diameter of 2.6 Å. [Elvers (1996-A28)] It can easily penetrate in the channels and cages, even in the small ones that are inaccessible for other molecules. Most frameworks will, therefore, show a higher network dimension and a larger accessible void-volume for water.

So after synthesis, the channels and voids are filled with water. When the zeolite is to be used as an adsorbent, these water molecules have to be removed. Dehydration can be done by heating to 400-500 °C. Most zeolites may be dehydrated to a large extent without major alternations of their structure; they may, subsequently, be rehydrated by adsorbing water from a vapor or liquid phase. Many, however, undergo irreversible changes or suffer total structural collapse when completely dehydrated. [Breck (1974), Elvers (1996-A28)]

Table 3.6 *Some examples of small framework alternations in type (a) zeolites*

zeolite name	*effective aperture size of the 8-ring (Å)*		*effect of dehydration*
	hydrated	*dehydrated*	
Ca-Chabazite (CHA)	circular, 3.9	ellipsoidal, 3.7 x 4.2	ring distortion
Na-Zeolite A (LTA)	4.2	4.0	steric hindrance by the sentinel effect as a result of a change in the locations of cation sites

[Breck (1974), Dyer (1988)]

Based on their behavior upon dehydration, the zeolites can be classified as (a) those which do not show major structural changes and exhibit TGA-curves with a continuous weight loss as a function of temperature, and (b) those which undergo changes and show discontinuities in their curves. [Breck (1974)] This classification is given in table 3.7, together with some details on the structural changes.

Although the dehydration of type (a) zeolites does not lead to major alternations of the framework, small alternations are still seen. These alternations involve ring distortions and redistributions of cations, resulting in different effective aperture sizes. In table 3.6, some examples are given.

3.1.2 Stability

Thermal stability

Thermodynamically, dehydrated zeolites have the tendency to transform into more dense crystal structures. Their relatively high thermal stability is caused by the fact that for such transformations, it is necessary to break the covalent bonds of the framework. Nevertheless, if the temperature is high enough, the framework will either collapse forming an amorphous solid, or it will recrystallize forming a different zeolite or a non-zeolitic aluminosilicate.

The values given in table 3.7 can be used as an indication on the thermal stability of a certain framework type. An exact temperature for structural transformations cannot be given. This would require the definition of a time-scale on which the transformations should occur. Even at moderate temperatures transformation processes take place, though slowly.

The stability is a function of the framework type, the Si/Al ratio, and the character of the non-framework cations. Ab-initio calculations show that the influence of the framework structure itself is not that important. They show that, when different framework structures are constructed with an indefinite Si/Al ratio, so with only Si atoms, these structures all have more or less the same free energy. The framework type is only of importance as it is accompanied by a typical Si/Al ratio. So, not the fact that moderate- and high-silica zeolites have a more dense

Table 3.7 Thermal stability and dehydration behaviour

Group 1: S4R - Secondary Building Unit

zeolite name		*type*	*TGA behavior (°C) *)*	*DTA behavior (°C) *) **)*	*structure changes *)*
Analcime	(ANA)	1	continuous	endo, 200-400	stable to at least 700
Garronite	(GIS)	...			framework distortion
Gismondine	(GIS)	2	step 115-140	endo, 140, 160, 190, 270	new structures at 250-330
Harmotome	(PHI)	2	step 170-190		new structure at 150
Laumontite	(LAU)	2	step 200, 370, 500	endo, 71, 267, 430, 467	new structure at 500
Paulingite	(PAU)	...			stable to at least 250 ***)
Phillipsite	(PHI)	2	step 130	endo, 100, 200, 300	new structure at 160-200
Yugawaralite	(YUG)	2	step 200, 400	endo, 200-350; exo 540	new structure at 400
Zeolite P	(GIS)	2	step 83	endo, 190	change at 165 □), stable to 700
Zeolite W, K-M	(MER)	...			stable to at least 350

TGA thermogravic analysis
DTA differential thermal analysis

*) These data are only an indication, they may strongly depend on the actual cations present.
**) Endo = endothermic, exo = exothermic; Endothermic is associated with desorption of water, while exothermic is associated with structural changes.
***) Paulingite can be dehydrated, but its crystal will decrepitate on rehydration.
□) Zeolite P exists in three crystal structures: whether transitions between these structures occur, depends on the cation present.

Group 2: S6R - Secondary Building Unit

zeolite name		*type*	*TGA behavior (°C)*	*DTA behavior (°C)*	*structure changes*
Erionite	(ERI)	1	continuous	endo, 50-400; exo, 920	stable to 750
Levynite	(LEV)	1	continuous		stable to at least 340
Mazzite, Zeolite Ω	(MAZ)	1	continuous	endo, 180-255; exo, 410-675	stable to 700
Offretite	(OFF)	1	continuous	endo, 160, 410, 560; exo, 1092	stable to at least 965
Sodalite	(SOD)	1	continuous	endo, 100-300; exo, 805	stable to 900
Zeolite L	(LTL)	1	continuous		stable to at least 800

Group 3: D4R - Secondary Building Unit

zeolite name		*type*	*TGA behavior (°C)*	*DTA behavior (°C)*	*structure changes*
Zeolite A	(LTA)	1	continuous	endo, 25-300; exo 860, 910	stable to 700-800
Zeolite ZK-4	(LTA)	1	continuous		stable to 550

Group 4: D6R - Secondary Building Unit

zeolite name		*type*	*TGA behavior (°C)*	*DTA behavior (°C)*	*structure changes*
Chabazite	(CHA)	1	continuous	endo, 25-300; exo, 900	stable to at least 700
Faujasite	(FAU)	1	continuous		stable to 475
Gmelinite	(GME)	1	continuous		stable to ~300
Zeolite X	(FAU)	1	continuous	endo, 50-350; exo, 772, 933	stable to at least 700 *)
Zeolite Y	(FAU)	1	continuous	endo, 100-400; exo, 793	stable to at least 760-1000 *)

*) Stability varies with the cation.

Group 5: 4-1 - Secondary Building Unit

zeolite name		*type*	*TGA behavior (°C)*	*DTA behavior (°C)*	*structure changes*
Edingtonite	(EDI)	2	step 100, 250, 400	endo, 160-450; exo, 500	new structure 250, collapse 500
Gonnardite	(THO)	2	step 100, 200, 300	endo, 75-450	collapse 360-460
Natrolite	(NAT)	2	step 240	endo, 350	new structure 565, collapse 785
Mesolite	(NAT)	2	step 200, 350	endo, 225-380	collapse 440-490
Scolecite	(NAT)	2	step 200, 400	endo, 225-410	collapse 330-490
Thomsonite	(THO)	2	step 150, 300	endo, 175-520	collapse 370-520

Group 6: 5-1 - Secondary Building Unit

zeolite name		*type*	*TGA behavior (°C)*	*DTA behavior (°C)*	*structure changes*
Bikitaite	(BIK)	2	step	endo, 190-475	new structure at 750
Epistilbite	(EPI)	...			unstable
Ferrierite	(FER)	1	continuous		stable
Mordenite	(MOR)	1	continuous	endo, 25-300, exo, >1000	stable to at least 800

Group 7: 4-4-1 - Secondary Building Unit

zeolite name		*type*	*TGA behavior (°C)*	*DTA behavior (°C)*	*structure changes*
Brewsterite	(BRE)	...			stable to at least 300
Clinoptilolite	(HEU)	1	continuous	endo, 125-300; exo, >1000	stable to at least 750-1000
Heulandite	(HEU)	2	step 100, 250	endo, 25-300; exo, 300	new structure 250, collapse 360
Stilbite	(STI)	2	step 100, 200	endo, 191, 262; exo, 500	new structure 120, collapse 400

[Breck (1974), Dyer (1988)]

structure or 5-rings, but their low Al content makes them more stable. This does not mean that there are no differences between framework types. For a given Si/Al ratio, one type may be better in accommodating the charge than another. The charge has to be compensated by cations. In narrow channels, this will quickly result in steric stress as there is just not enough space. This is the explanation why these frameworks cannot exist with low Si/Al ratios. [Breck (1974), van Bekkum (1991), Elvers (1996-A28), van Santen (1989, 1990)]

The effect of the Si/Al ratio on stability is also seen in zeolites of the same framework type. Zeolite Y with a Si/Al ratio of 5 will, for instance, become amorphous above 700 °C. Dealuminated Zeolite Y, however, is structurally stable at 1000 °C.

In addition, there is the effect of the cations. By their size, charge, and polarizability, they may influence the stability. An example is seen in Zeolite A, where the Na form is losing structure at 660 °C, while the Ca form does not until 700 °C. [Elvers (1996-A28)]

Hydrothermal stability

When dehydrated zeolites are exposed to water vapor, at elevated temperature or at elevated pressure, they are experiencing conditions close to those under which they were formed. In the same way as water assists and stabilizes during their formation, it now assists in the transformation processes. With its H-bridges, it helps breaking the covalent bonds of the framework and is so speeding up the transformation processes.

In general, the hydrothermal stability is affected by the same factors that influence the thermal stability. The hydrothermal stability is normally less than the thermal stability. [Breck (1974), Elvers (1996-A28)]

3.1.3 Ion-exchange

In the production of adsorbents, ion exchange is an important way of making modifications that might improve the performance. Such an improvement can be the result of a minor structure alteration or of a different cation-adsorbate interaction.

Although ion exchange has a great potential and virtually every cationic element has been introduced in zeolites, not all frameworks undergo facile replacement. The equilibrium and kinetics for ion exchange are complex subjects in which several factors interact. A significant role is played by the process conditions and the properties of the cations involved. So, if modifications to improve an adsorbent are necessary, the combination of zeolite framework and cation should be chosen carefully. [Dyer (1988)]

For a detailed treatment of the theory on ion exchange, the publications by Breck [(1974)] and by Barrer [(1978)] are recommended. For references, a listing is given by Szostak [(1992)] and by Dorfner [(1991)].

Selectivity

Most ion-exchange reactions are performed with aqueous solutions and can be represented by

equation 3.2: [Barrer (1978), Breck (1974), Dyer (1988)]

$$b\ A^{a+}(aq) + B_a^{b+}[Zeolite]^{ab-} \leftrightharpoons A_b^{a+}[Zeolite]^{ab-} + a\ B^{b+}(aq) \qquad (3.2)$$

$$K_{eq} \doteq \frac{[A_z]^b\ [B^{b+}]^a}{[B_z]^a\ [A^{a+}]^b} \cdot f(activity\ coefficients) \sim f(T,\ framework\ type,\ Si/Al\ ratio) \qquad (3.3)$$

with: a, b = stoichiometric number or valencies
K_{eq} = equilibrium constant
$[A_z]$, $[B_z]$ = equivalent ion-fractions in the zeolite
$[A^{a+}]$, $[B^{b+}]$ = ion concentrations in the solution

In principal, the ion-exchange process is a reversible reaction. To what extent it is taking place, of course, depends on the cation concentrations and on the value of the equilibrium constant. This equilibrium constant is not only a function of temperature, but is also determined by the preference of the framework for each cation. This preference is expressed in a selectivity coefficient or a separation factor and graphically represented by the ion-exchange isotherm.

$$K_B^A \doteq \frac{[A_z]^b\ [B^{b+}]^a}{[B_z]^a\ [A^{a+}]^b} \qquad (3.4)$$

$$\alpha \doteq \frac{[A_z]\ [B^{b+}]}{[B_z]\ [A^{a+}]} \doteq \frac{[A_z]\ [B^{b+}]}{(1-[A_z])\ [A^{a+}]} \qquad (3.5)$$

with: K_B^A = selectivity coefficient
α = separation factor
$\alpha > a/b$ = zeolite is selective for cation A
$\alpha < a/b$ = zeolite is selective for cation B

The maximum theoretical ion-exchange capacity is determined by the Si/Al ratio. This ratio is directly related to the framework charge (*ab-*) and, as the cations *A* and *B* compensate this charge, the ratio fixes the maximum number of cation *A* or *B* that can be present in the zeolite. [Elvers (1996-A28)]

The maximum attainable ion-exchange capacity is limited by the five parameters that also govern the preference between the cation and the framework [Breck (1974), Dyer (1988)]:

(a) The nature of both the competing ions with respect to their relative sizes and to their state of solvation inside and outside the framework:
No exchange or incomplete exchange is observed when the new cation *B* is larger than the original one *A*. This is often the case for large organic cations such as quaternary alkyl-ammonium ions. These cations have an effective ion diameter that is so much larger that they cannot enter the channels of the zeolite at all. The accompanying selectivity is referred to as the molecular sieve properties of zeolites. [Breck (1974)]

Another example of this effect is seen for Na-Zeolite Y, where only 68 % of Na^+ can be substituted by Rb^+, since the remaining Na^+ ions are located in the small sodalite cages, where Rb^+ cannot penetrate. The Na^+ ions undergoing exchange are those located in the α-cages. [Dorfner (1991)]

A similar situation is observed for hydrated metal cations with a strongly bonded hydration shell, such as Li^+, Mg^{2+}, and La^{3+}. The effective diameter of these in itself small ions is more than doubled by this hydration shell and the ions, therefore, are no longer able to pass through the apertures of 6- and 8-rings. [Elvers (1996-A28)]

For cations with a less strongly bonded shell, slow ion exchange is possible when the ion can release some of the water molecules of its hydration shell during the passage of the aperture. But even then, this situation is not very favorable, as the partially unhydrated ion still has a size similar to the channel diameter. If the channel is not blocked by the ion, the mass transport through the channels will certainly be very slow. The free energy will be negatively influenced and the structure will probably collapse when the zeolite is dehydrated.

(b) The charge on the zeolite framework coupled with the framework geometry:
An example of the effect is given in table 3.8, where the overall cation-preferences for Zeolite X and Y are shown. Both zeolites have the same framework, but differ in their Si/Al ration: Zeolite X has a ratio of 1.0-1.5, while the ratio of Zeolite Y varies from 1.5-3.0. As already explained is the Si/Al ratio related to the framework charge. From table 3.8, it is seen that X prefers the alkali metals in the order of decreasing size, while Y prefers them in the order of increasing size. [Breck (1974), Dyer (1988)]

(c) The hetero-energetic nature of the cation sites available for occupation inside the framework:
When the cation-preference of Zeolite X is studied during the ion-exchange process, it is seen that initially the order of decreasing size is followed. Halfway, however, the order is changed and the cations are preferred with increasing size. [Breck (1974)]

(d) The temperature at which exchange is carried out, which influences both the removal of hydration-water and the accessibility of sites and improve exchange kinetics:
When a zeolite has channels or voids of different sizes, a sieve effect within the framework can occur if the original cations that are being exchanged, are located in small and inaccessible cages. For example, 30 % of the Na^+ ions in Zeolite X occupy a site that is located in the sodalite cages. At ambient temperatures, these ions cannot be replaced as the aperture is too small for larger hydrated cations such as La^{3+}. At 100 °C, however, the effective aperture diameter is some what larger and the dehydration of the La^{3+} ions is faster,

and so the ion exchange is completed after all. [Breck (1974)]

(e) The concentration of the external solution coupled with the presence of complexing agents other than water.

Table 3.8 *Ion-exchange selectivities of Zeolite A, X, Y and Chabazite for uni-, and divalent cations at ambient temperature*

zeolite name	*Si/Al ratio*	*overall cation-selectivity*	
Zeolite A (LTA)	1.0	1+ : Ag > Tl > Na > K > NH_4 > R b> Li > Cs 2+ : Zn > Sr > Ba > Ca > Co > Ni > Cd > Hg > Mg	Ca > Na
Zeolite X (FAU)	1.2	1+ : Ag >> Tl > Na > K> Rb > Cs > Li	Ca > Na
Zeolite Y (FAU)	2.4	1+ : Tl > Ag > Cs > Rb > NH_4 > K > Na > Li	Ca ≈ Na
Chabazite (CHA)	2.5	1+ : Tl > K > Ag > Rb > NH_4 > Pb > Na > Li 2+ : Ba > Sr > Ca	Na > Ca
zeolite name	*ion-exchange ratio*	*differential cation-selectivity*	
Zeolite X (FAU)	0.2	1+ : Ag >> Tl > Cs > Rb > K > Na > Li	
(Si/Al = 1.2)	0.5	1+ : Ag >> Tl > Na > K> Rb > Cs > Li	

[Breck (1974), Dyer (1988), Elvers (1996-A28)]

In general, the overall selectivity for uni-univalent ions, such as the alkali metal ions, depends on the Si/Al ratio. For low Si/Al ratios with their high charges, the contribution of the electric-field forces is decisive and a small cation size is, therefore, preferred. For high Si/Al ratios, the electric-field forces are less and the hydration energy of the cations is becoming important. Now, the larger, weakly hydrated cations are preferred:

$$uni\text{-}univalent: \quad \begin{matrix} Si/Al < 1.5 & Na > K > Rb > Cs > Li \\ Si/Al > 1.5 & Cs > Rb > K > Na > Li \end{matrix} \tag{3.6}$$

$$uni\text{-}divalent: \quad Ba > Sr > Ca > Mg \tag{3.7}$$

For the uni-divalent ions such as the alkaline earth metal ion, the hydration energy is decisive in all cases. The preference is ordered from large to small. Comparing the preference of sodium versus calcium, Ca is preferred by zeolites with a low Si/Al ratio and Na is preferred by zeolites with a high Si/Al ratio. [Breck (1974)]

These are, of course, only rough general trends and exceptions are not uncommon, as can be seen in table 3.8 for Zeolite A.

Kinetics

The kinetics of ion exchange is controlled by the mass transfer through the channels and voids of the zeolite. It is mainly a particle diffusion process and can be characterized by a self-diffusion coefficient that is written as an Arrhenius type of equation:

$$D = D_o \, e^{-\frac{E_a}{RT}} \tag{3.8}$$

with: D = self-diffusion coefficient
D_o = pre-exponential factor
E_a = activation energy for diffusion
R = gas constant
T = absolute temperature

The E_a value represents the energy barrier to ion movement and is influence by the same parameters as mentioned for the selectivity. The question of which of these parameters is the most important one, depends on the actual rate-determining step. This can, for instance, be a step involving the dehydration of the cation, the passage of an aperture, or the occupation of a site. [Dyer (1988)]

In the case of Zeolite A, the rate-determining step is the progress through the 8-ring of the α-cage and the activation energy E_a is mainly determined by the effective ion diameter. For the alkaline earth metal ions, the activation energy shows, therefore, a linear dependency on the ionic radius. An exception is formed by Mg^{2+}, which has a much higher E_a than expected, due to its strongly bonded hydration shell.

Unfortunately, for many other zeolites information on the rate-determining steps and the activation energies is not available [Dorfner (1991)].

Table 3.9 *Activation energies for cation diffusion in zeolite A*

cation	*dehydrated ionic radius (Å)*	*activation energy of diffusion E_a (kJ/mole)*
Mg^{2+}	0.66	79
Ca^{2+}	0.99	70
Sr^{2+}	1.12	82
Ba^{2+}	1.34	91

[Dyer (1988), Weast (1981)]

Ion exchange is a very slow process. In open zeolites (e.g., Zeolite A, X, and Y, with low framework densities), it takes about a week for uni-univalent exchanges to reach complete

equilibrium. With ions of a higher valency, it is not unusual for the period of time to be significantly longer. In the more dense zeolites, exchanges of even uni-univalent type can take months to reach completion. [Dyer (1988)]

3.1.4 Adsorption

Adsorption capacity

The usual concept in which adsorption is related to a specific surface area, is not applicable to zeolites. Although the adsorption isotherm is reasonable well described by a simple model isotherm equation like the one by Langmuir, the specific surface area that is calculated from this Langmuir isotherm has no direct physical meaning, and is depending on process conditions. The value that is calculated that way, may show large differences of the real internal area, which is approximately 800 m^2/gram. [Breck (1974), Barrer (1978)]

After dehydration, the zeolite has pores of a molecular dimension and the overlapping electrostatic fields of the opposite walls produce a rather extensive potential profile. As a consequence, the entire internal void volume acts as a space where an adsorption field exists and in which the adsorbate behaves more or less like a fluid. Adsorption in zeolites is, therefore, better described by the concept of pore filling as proposed by Gurvitsch and applied in the Dubinin-Polanyi adsorption theory. Only in a few cases, in which there is a strong interaction between the adsorbate and the zeolite framework or its cations, deviations of this concept are seen. [Breck (1974), Barrer (1978)]

Using the pore-filling concept, the adsorption capacity is proportional to the internal volume accessible to the adsorbate molecule. An analysis shows that the capacity is, therefore, influenced by five qualities of the zeolite and by two properties of the adsorbate:

(1a) The void fraction of the framework:
This void fraction represents the maximum internal volume that might be available and indicates the upper-limit for the capacity. As discussed earlier, the void fraction is depending on the framework type, but will, normally, be larger for zeolites with a low Si/Al ratio.

(1b) The molecular sieve effect of framework apertures:
To reach the cages and channels that make up the void fraction, the adsorbate molecule has to pass through the rings which form the entrances. If the effective ring diameter is smaller than the kinetic diameter of the molecule, part of the internal volume will be inaccessible. For example, the β-cage in Na-Zeolite A, which has a 6-ring as entrance, can be penetrated by water, but not by larger molecules such as carbon dioxide. The capacity for carbon dioxide is, therefore, only 0.39 cc/cc zeolite, while the capacity for water is nearly equal to the void fraction of 0.47 cc/cc zeolite.

(1c) The molecular sieve effect and the heterogeneity of the cation sites:
As is shown in table 3.5, the preference of cations for a particular site can tremendously

affect the effective aperture diameter of a framework. This influence causes either a sentinel effect or a total blockade of one of the channels, which might be accompanied by a reduction in network dimension.

There are no general guidelines on the effect of sites preference on the aperture diameter. The effect is different for each framework type. In Zeolite A divalent ion exchange opens the aperture to its full diameter whereas exchange with a larger univalent ion diminishes the diameter. In contrast, Zeolite X exhibits a reduction in diameter when exchanged with a divalent ion. [Breck (1974)]

(1d) The size, charge, and number of non framework cations:
Besides changing the effective diameter of the apertures, cations may diminish the void volume by changing the unit cell dimensions and by partially filling the void.

In general, the free void volume and thus the capacity, will increase with reducing size, except when strong hydration of the cation appears and the radius of the hydrated ion is decisive. With increasing valency, the number of cations is decreasing and the capacity is increasing (assuming a constant size). As shown in table 3.10, this increase is not caused by the cations volume alone, but is probably also determined by a shift in the location of the cation site.

Table 3.10 *Effect of the cation on the void volume of Zeolite A*

zeolite	*density (g/cc)*	*ion radius (Å)*	*unit cell length (Å)*	*cations' volume (Å ^{3})*	*void volume (Å ^{3}) *)*
$Li_8 Na_4$-Zeolite A . 24 H_2O	1.91	0.68 / 0.97	12.04	3.23	735
Na_{12}-Zeolite A . 27 H_2O	1.99	0.97	12.32	5.73	833
Ag_{12}-Zeolite A . 24 H_2O	2.76	1.26	12.38	12.57	733
$Tl_{9.6} Na_{2.4}$-Zeolite A . 24 H_2O	3.36	1.47 / 0.97	12.38	17.11	584
Ca_6-Zeolite A . 30 H_2O	2.05	0.99	12.26	3.05	883

*) Volume determined by water adsorption.

[Breck (1974), Weast (1981)]

(1e) The molecular sieve effect of mass transfer:
In several cases, the molecular effect mentioned under (1b) and (1c) is no absolute restriction of the capacity, but proves to be depending on the rate of mass transfer. The capacity, therefore, can be influenced by changing the time scale or the temperature of the measurement.

For an adsorbate molecule of the same size as the aperture, the diffusion process involved is too slow to give an adsorption of any significance at room temperature. By increasing the temperature, the adsorption may be improved as both the diffusion process accelerates and the aperture slightly expands.

(2a) The kinetic diameter of the adsorbate molecule:
The molecular sieve effect is, of course, depending on the size of the adsorbate molecule in comparison with the aperture diameter. In order to penetrate, the effective size might be approximately 0.3 Å larger than the aperture diameter.

(2b) The density of the adsorbate:
When the capacity is expressed in mass or volume, it changes with density. So, for a given void volume, the maximum capacity decreases with temperature and increases with pressure.

Heat of adsorption and bond strength

Like any other reaction, the adsorption can be described by the thermodynamical relation for Gibbs' free energy:

$$\Delta G \doteq \Delta H - T\Delta S \qquad \textbf{(3.9)}$$

with: G = Gibbs' free energy
H = enthalpy
S = entropy
T = absolute temperature

For adsorption to take place the free energy change must be negative. Since the change in entropy is negative when going from the chaotic gas phase to a more ordered semi-fluid phase, the change in enthalpy has to be negative also. So, adsorption is an exothermic process and change in enthalpy is known as the heat of adsorption. However, there are in fact three terms referring to the heat of adsorption. [Breck (1974), Barrer (1978)] These are:

(1) The isothermal integral heat of adsorption:
This is the total heat involved in the adsorption process from zero adsorbate loading to some final adsorbate loading at a constant temperature. In terms of equation 3.9, this heat is written as ΔH_T and expressed in energy per mole.

(2) The differential heat of adsorption:
This is the change in integral heat of adsorption with a small change in adsorbate loading. It is defined by the following equation:

$$\Delta h_{T,n} \doteq h_{adsorbate,ads} - H_{adsorbate,gas} \qquad \textbf{(3.10)}$$

$$\Delta h_{T,n} \doteq \Delta H_T + n\frac{\delta(\Delta H_T)}{\delta n} \tag{3.11}$$

with:
- $\Delta h_{T,n}$ = the differential heat of adsorption
- ΔH_T = the integral heat of adsorption
- $h_{adsorbate,ads}$ = the partial molar enthalpy of the adsorbed gas
- $H_{adsorbate,gas}$ = the molar enthalpy of the adsorbate gas in the gas phase
- n = the adsorbate amount

From its definition, the differential heat can be a function of pressure, of temperature and of the adsorbate loading θ.

(3) The isosteric heat of adsorption:
This is the heat of adsorption that is derived from measuring the adsorption isosteres. In fact, it is a differential heat of desorption that can be defined in the following way by using the Clausius-Clapeyron relation:

$$\phi_{isosteric}(\theta) \doteq RT^2\left(\frac{\delta \ln f_{adsorbate,gas}}{\delta T}\right)_{T,n} \approx RT^2\left(\frac{\delta \ln p_{adsorbate,gas}}{\delta T}\right)_{T,n} \tag{3.12}$$

$$\phi_{isosteric} \doteq -\Delta h_{T,n} \tag{3.13}$$

with:
- $\phi_{isosteric}$ = the isosteric heat of adsorption
- f = fugacity in gas phase
- p = pressure in gas phase
- R = gas constant
- T = absolute temperature
- θ = adsorbate loading or fraction

The isosteric heat can be calculated by plotting the logarithm of the pressure versus the reciprocal of the absolute temperature at a constant adsorbate loading. As the adsorption process is reversible, no hysterese occurs and both adsorption and desorption measurements can be used. [Breck (1974), Barrer (1978), Dyer (1988)]

Measurements of adsorption isotherms show that heat of adsorption is not a constant, but a function of the adsorbate loading:

(a) For small uptakes during the initial adsorption stage, $\phi_{isosteric}$ sometimes decreases strongly with the amount adsorbed. This indicates that in these systems instead of the uniform distribution of the homogeneous electrostatic field normally seen, there are some local positions where the adsorbate molecules are preferentially adsorbed and which have a higher bonding energy. Their number will be restricted to a few.

This behavior is, however, not always shown for a particular framework, but depends on the properties of the adsorbate. For large or non-polar molecules, the decrease is only small or completely absent.

(b) At intermediate uptake, the fall in $\phi_{isosteric}$ lessens and may actually change in an increase as the adsorbate-adsorbate interaction becomes perceptible. This is the adsorption stage in which the adsorbate forms first a monolayer at the internal surface and then fills the pore as a fluid.

(c) For uptakes approaching the maximum capacity, $\phi_{isosteric}$ declines again as multilayer adsorption and condensation on the external surface take over. Finally, the value of $\phi_{isosteric}$ will approach the $-\Delta H$ for liquefaction.

The energetic heterogeneity seen at the beginning, can be explained by seven general causes:

(1) The presence of pores with different dimensions and therefore different electrostatic fields.

(2) The relative size of the adsorbate molecule in comparison to the pore dimensions which determines whether different positions inside the pore can be taken in and the effect of the electrostatic field is not averaged out.

(3) The presence of residual water.

(4) The presence of different cations which cause different surroundings for the adsorbate.

(5) The presence of differences in the cation distribution caused by the differences in cation preference in the different pores present.

(6) The presence of lattice defects or framework modifications.

(7) The inhomogeneous distribution of Al over the framework causing a non-uniformic Si/Al ratio and differences in the anionic charge distribution.

The heat of adsorption is an indication for the bond strength between the adsorbate and the framework (with its cations and its zeolitic water). The heat of adsorption can therefore be written as the sum of the six interaction energies:

$$\phi_{isosteric} = \phi_D + \phi_R + \phi_P + \phi_{F\mu} + \phi_{FQ} + \phi_{SP} \qquad \textbf{(3.14)}$$

with:
- ϕ_D = dispersion energy
- ϕ_R = short range repulsion energy
- ϕ_P = polarization energy
- $\phi_{F\mu}$ = electrostatic field-dipole interaction energy
- ϕ_{FQ} = electrostatic field-quadrupole interaction energy
- ϕ_{SP} = adsorbate-adsorbate interaction energy or 'self-potential'

The dispersion, repulsion and the polarization contributions will always be present and are referred to as 'non-specific'. The contributions of $\phi_{F\mu}$ and ϕ_{FQ} depend on the presence of permanent dipoles and quadrupoles in the adsorbate molecule and are therefore called 'specific'.

When looking at the selection of a system in which the adsorbate with its properties is given and only the selection of the zeolite and its cations is open for discussion, $\phi_{isosteric}$ proves to depend on two parameters: (a) the charge density in the zeolite framework, which is related to the Si/Al ratio, and (b) the character of the cation present. The main features of this dependancy are explained in the following discussion of the individual contributions to $\phi_{isosteric}$.

The dispersion and repulsion contribution, which consist of non-oriented and induced dipole interactions, is given by:

$$\phi_D + \phi_R = -\frac{A_6}{r^6} - \frac{A_8}{r^8} - \frac{A_{10}}{r^{10}} + \frac{B}{r^{12}} \qquad \textbf{(3.15)}$$

with:
- r = distance between framework or cation and the adsorbate
- A_6, A_8, A_{10} = attractive constants which are a function of the polarizability, ionization energy, electron affinity and the diamagnetic susceptibility of both the adsorbate and the framework or cation.
- B = repulsive constant which is a function of the same properties.

The extent in which dipoles are induced in the adsorbate is depending on the adsorbate's polarizability and the electrostatic field it is experiencing. A change in Si/Al ratio that would lead to an increase in charge density and electrostatic field, may, therefore, result in a higher contribution. With the constants depending on the cation's polarizability and ionization energy, the value of this contribution increases also with the size of the cation.

The polarization energy is the contribution of monopole-induced dipole interactions and is given by:

$$\phi_P = -\frac{\alpha q^2}{2r^4(4\pi\varepsilon_o)^2} \qquad \textbf{(3.16)}$$

with: α = polarizability of the adsorbate
q = charge of the Si, Al, or O atoms in the framework or of the cations
ϵ_o = dielectric constant of vacuum

The contribution of this term to $\phi_{isosteric}$ is far less than would be expected and in fact smaller than the dispersion and repulsion term.

Table 3.11 *Experimental values of (ϕ_D +ϕ_R) and ϕ_P for Ar in Zeolite X compared with calculated values for the interaction between Ar and an isolated cation.*

cation	*experimental in Zeolite X*		*calculated for Ar-isolated cation*	
	-(ϕ_D+ϕ_R) (kJ/mole)	-ϕ_P (kJ/mole)	-(ϕ_D+ϕ_R) (kJ/mole)	-ϕ_P (kJ/mole)
Li^+	11.3	2.5	0.21	21.3
Na^+	11.7	0	0.67	16.0
K^+	12.5	0	1.80	10.2
Ca^{2+}	11.3	9.6	2.13	63.5
Sr^{2+}	13.2	2.7	3.26	52.7
Ba^{2+}	13.8	0	4.22	40.7

[Barrer (1978)]

The reason for the low value is a very strong screening of the cations by the much more numerous anionic oxygen of the framework, into which the cations tend to be recessed. The internal surface of the framework is formed by the negatively charged oxygen atoms as the positively charged Al and Si atoms are oriented to the inside and covered by the bulky oxygens. Meanwhile, the non-framework cations are located in the same plane as the oxygen atoms at their sites in the middle of the rings. Each cation has, therefore, 6 or more negatively charge neighbours. So, the adsorbate molecule that is experiencing the field of both these opposite charges is hardly polarized anymore. [Barrer (1978)]

Although the charge is present in equation 3.16, it is not clear whether an increase in charge

density would result in a higher ϕ_P contribution. The effect would probably be canceled completely by the screening. When comparing for example the initial $\phi_{isoteric}$ of krypton, which has no permanent electric moment, in Na-Zeolite X (Si/Al $\approx$1.2 and $\phi_{isoteric}(\theta=0) = 3.5$) and in Na-Zeolite Y (Si/Al $\approx$2.5 and $\phi_{isoteric}(\theta=0) = 3.6$), no essential change is seen. [Breck (1978)]

As shown in table 3.11, the q_P contribution increases with the valency of the cation and decreases with its size. [Dyer (1988)]

The contributions of monopole-permanent dipole and of monopole-permanent quadrupole interactions to $\phi_{isoteric}$ are given by:

$$\phi_{F\mu} \approx - \frac{q\,\mu}{r^2(4\pi\varepsilon_o)} .(\cos\vartheta) \qquad (r \gg l) \tag{3.17}$$

$$\phi_{FQ} = - \frac{q\,Q}{4r^3(4\pi\varepsilon_o)} .(-1+3\cos^2\vartheta) \tag{3.18}$$

with: μ = dipole moment of the adsorbate molecule
Q = quadrupole moment of the adsorbate molecule
l = charge distance in the dipole moment
ϑ = angle between r and the orientation of the dipole or quadrupole moment

Many adsorbates that are of commercial interest have a permanent dipole (e.g., H_2O, CO, and NH_3) or a quadrupole moment (e.g., H_2, N_2, O_2, CO, and CO_2). When either of these moments is present, the specific contribution will dominate in the value of $\phi_{isosteric}$.

Table 3.12 *Observed initial heats of adsorption and the calculated contributions of different interactions for CO_2 in Zeolite X*

energy (kJ/mole) *cation*	*Li*	*Na*	*K*	*Rb*	*Cs*
$-\phi_{isosteric}(\theta \approx 0)$	51.4	45.1	43.9	42.2	36.8
$-\phi_{D+R}$ (oxygens)	15.9	13.0	7.1	4.6	4.6
$-\phi_{D+R}$ (cations)	0.4	0.8	3.3	4.6	9.2
$-\phi_P$	9.6	5.0	2.1	0.8	0
$-\phi_{FQ}$	30.9	21.3	17.6	14.6	9.6
ϕ_o (zero point energy)	1.7	1.3	1.3	1.3	1.3

[Barrer (1964, 1978), Barthomeuf (1988)]

In contrast to the polarization interaction, the multipole interactions are not strongly influenced by the screening effect of the oxygen atoms. The molecules will orientate themselves in such a way that the multipole moment is accommodated. An increase in charge density is now resulting in a large increase in $\phi_{isoteric}$ as is demonstrated in table 3.13.

The influence of the cations is some what unpredictable, as it is depending on the zeolite type, the cation valency, the adsorbate loading and probably also on the adsorbate. Although, much research into the influence of cations has been done, these industrial data are unfortunately not available in the open literature. [Breck (1974)]

In table 3.14, the influence of cations on zeolite X and on Mordenite is given. For univalent ions in zeolite X, the $\phi_{isosteric}$ of the initial adsorption increases with decreasing cation size, while for higher adsorbate loading, $\phi_{isosteric}$ goes through a maximum. For divalent ions, $\phi_{isosteric}$ increases with increasing size. For divalent ions in Mordenite, however, $\phi_{isosteric}$ is decreasing with increasing size.

Table 3.13 *The effect of charge density on the isosteric heats of adsorption for CO_2*

zeolite type	*Na-Zeolite A*	*Na-Zeolite X*	*Na-Zeolite Y*
charge density	6.4 (10^{-21} Na^+/cm^3)	5.6 (10^{-21} Na^+/cm^3)	3.7 (10^{-21} Na^+/cm^3)
adsorbate loading (cm^3 CO_2 (stp) / cm^3 pore)	$-\phi_{isosteric}$ (kJ/mole)		
20	51.0	48.5	33.8
60	47.7	45.1	30.5
100	45.1	43.4	30.5
200	41.4	40.5	31.6
300	39.3	38.0	31.6

[Barrer (1978)]

Table 3.14 *The influence of univalent and divalent cations on $\phi_{isosteric}$ for polar adsorbates as a function of zeolite type, adsorbate loading, and cation valency*

$-\phi_{isosteric}$ *(kJ/mole)*

zeolite type / adsorbate / loading	*cation*	*Li*	*Na*	*K*	*Rb*	*Cs*
Zeolite X CO_2	θ=0.2	49.7	44.3	43.3	43.0	40.9
	θ=0.8	30.1	36.4	38.2		
H_2O	*) n=0.5	84	83	76	75	67
	n=6.0	63	66	70	69	64
Mordenite CO	θ=0.02	41.0	34.3	25.1		21.7

$-\phi_{isosteric}$ *(kJ/mole)*

zeolite type / adsorbate / loading	*cation*	*Mg*	*Ca*	*Sr*	*Ba*
Zeolite X CO_2	θ=0.2 θ=0.6		45.1 33.9	46.4 36.8	49.3 40.1
Mordenite CO	θ=0.02	66.0	50.6		38.9

*) n = number of molecules adsorbed in the large cavity of Zeolite X

[Barrer (1964, 1978), Furuyama (1982, 1984-1, 1984-2)]

3.2 Selection of systems

As has become clear from the previous discussion on zeolites, there is no obvious choice for a zeolite type.

The few general rules that could be given are not enough to make predictions on the quality of a zeolite type to act as a good adsorbent. For example, the general rule for thermal stability

Table 3.15 *Summary of properties relevant in the selection of a zeolite type for the adsorbent*

Group 1: S4R - Secondary Building Unit

zeolite name	*accessibility*		*stability*		*adsorption*			*remarks*
	ring	O_{ring}	S_{therm}	*Si/Al*	X_{void}	*x/m*	$-\phi_{iso}$	
Analcime (ANA)	6	- ; 2.9	+ , >700	2.00	0.18			
Garronite (GIS)	8	+/ ; 3.5	-	1.67	0.40			
Gismondine (GIS)	8, 8	+/- ; 3.8, 3.9	-	1.00	0.46			
Harmotome (PHI)	8, 8	+/- ; 3.8, 4.3	-	3.00	0.31			
Laumontite (LAU)	10	+ ; 5.0	+/-, 500	2.00	0.34	<0.01		
Paulingite (PAU)	8	+ ; 3.9	+/-, >250	3.42	0.49			
Phillipsite (PHI)	8, 8	+/- ; 3.4, 3.7	-	2.20	0.31			
Yugawaralite (YUG)	8, 8	+/- ; 3.7	+/-, 400	3.00	0.27			
Zeolite P (GIS)	8	+ ; 3.5	+ ?, 700	1.67	0.41			
Zeolite W, K-M (MER)	...	+/- ; 3.2, 4.4	+/-, >350	1.81	0.22	0.057		

ring : number of oxygen atoms in the ring that acts as the aperture of the pore
O_{ring} : an estimate on the accessibility of the pores for CO_2 ; the average diameter of the ring ($\AA$)
S_{therm} : an estimate on the thermal stability to high temperatures ; maximum temperature (°C)
Si/Al : Si/Al ratio of the zeolite
X_{void} : void fraction of the zeolite
x/m : the adsorption of CO_2 at 298 K and 700 torr (=0.93 bara) (wt.%)
$-\phi_{iso}$: the initial isosteric heat of adsorption (kJ/mole CO_2)
+, +/-, - : positive, maybe, negative

Group 2: S6R - Secondary Building Unit

zeolite name	*accessibility*		*stability*		*adsorption*			*remarks*
	ring	O_{ring}	S_{therm}	*Si/Al*	X_{void}	*x/m*	$-\phi_{iso}$	
Erionite (ERI)	8	+ ; 4.4		3.00	0.35	0.147		
Levynite (LEV)	8	+/- ; 4.1	+/-, >350	3.50	0.40	0.12		
Mazzite, Zeolite Ω (MAZ)	12, 8	+ ; 7.3, 4.5	+ , 700	3.50	0.38	0.167		at 760 torr
Offretite (OFF)	12, 8	+ ; 6.5, 4.4	+ , 965	2.33	0.40			**)
Sodalite (SOD)	6	- ; 2.2	+ , 900	1.00	0.35			
Zeolite L (LTL)	12	+ ; 7.1	+ , >800	3.00	0.32	0.11	33-42	at 750 torr

Group 3: D4R - Secondary Building Unit

zeolite name	*accessibility*		*stability*		*adsorption*			*remarks*
	ring	O_{ring}	S_{therm}	*Si/Al*	X_{void}	*x/m*	$-\phi_{iso}$	
Zeolite A (LTA) Na-Zeolite A Ca-Zeolite A	8, 6	+ ; 4.2	+ , 750	1.00	0.47	 0.30 0.24	 46-53 52	 *) *)
Zeolite ZK-4 (LTA)	8, 6	+ ; 4.2	+/-, 500	1.67	0.47			

Group 4: D6R - Secondary Building Unit

zeolite name	*accessibility*		*stability*		*adsorption*			*remarks*
	ring	O_{ring}	S_{therm}	*Si/Al*	X_{void}	*x/m*	$-\phi_{iso}$	
Chabazite (CHA)	8	+ ; 3.9	+ , >700	2.00	0.47	0.24	34-50	
Faujasite (FAU)	12	+ ; 7.4	+/-, 475	2.25	0.47			
Gmelinite (GME)	12, 8	+ ; 7.0, 3.8	+/-, 300	2.00	0.44	0.14		
Zeolite X (FAU) Na-Zeolite X Ca-Zeolite X	12	+ ; 7.4	+ , >700	1.23	0.50	 0.26 0.29	 51 48	 *)
Zeolite Y (FAU) Na-Zeolite Y Ca-Zeolite Y	12	+ ; 7.4	+ , >760	2.43	0.48	 0.23 0.15	 31-34 46	

Group 5: 4-1 - Secondary Building Unit

zeolite name	*accessibility*		*stability*		*adsorption*			*remarks*
	ring	O_{ring}	S_{therm}	*Si/Al*	X_{void}	*x/m*	$-\phi_{iso}$	
Edingtonite (EDI)	8	+/- ; 3.5	-	1.50	0.36			
Gonnardite (THO)	8	- ; 3.2	-	1.50	0.31			
Natrolite (NAT)	8	- ; 3.2	+/- , 565	1.50	0.23			
Mesolite (NAT)	8	- ; 3.2	-	1.50	0.30			
Scolecite (NAT)	8	- ; 3.2	-	1.50	0.31			
Thomsonite (THO)	8	- ; 3.2	-	1.00	0.32			

Group 6: 5-1 - Secondary Building Unit

zeolite name	*accessibility*		*stability*		*adsorption*			*remarks*
	ring	O_{ring}	S_{therm}	*Si/Al*	X_{void}	*x/m*	$-\phi_{iso}$	
Bikitaite (BIK)	8	+/- ; 3.6	+ , 750	2.00	0.23			
Epistilbite (EPI)	10, 8	+ ; 4.9, 4.2	-	3.80	0.32			
Ferrierite (FER)	10, 8	+ ; 4.3, 4.0	+/-	3.00	0.25			
Mordenite (MOR) H -Mordenite Na-Mordenite	10, 8	+ ; 4.9, 4.1	+ , >800	5.55	0.28	 0.070 0.12	 44-46 61-66	
ZSM-5 (MFI)	10	+ ; 5.4	+ , >650	~30	0.32		42	(Na-ZSM-5)

Group 7: 4-4-1 - Secondary Building Unit

zeolite name	*accessibility*		*stability*		*adsorption*			*remarks*
	ring	O_{ring}	S_{therm}	*Si/Al*	X_{void}	*x/m*	$-\phi_{iso}$	
Brewsterite (BRE)	8, 8	+/-; 3.7, 3.4	+/-, >300	3.00	0.26			
Clinoptilolite (HEU)	10, 8	+ ; 5.2, 3.7	+ , 750	5.00	0.34	0.082		
Heulandite (HEU)	10, 8	+ ; 5.9, 5.0	-	3.50	0.39			
Stellerite (STI)								
Stilbite (STI)	10, 8	+ ; 5.2, 4.2	-	3.50	0.39	0.097		

*) the adsorbate loading (θ) is 0.1 instead of nearly zero.
**) for Linde type T (ERI / OFF) : adsorption is 0.1-0.15 wt.%
remark: the values given in this table are the average values for these zeolites in their most common from. This means that ion-exchanged zeolites can have different values. Nevertheless, it is expected that larger differences are only seen for the adsorption capacity and the heat of adsorption.

[Breck (1974), Barrer (1978), Choudhary (1993), Dyer (1988),Elvers(1996-A28), Szostak (1992)]

predicts that the stability increases with the Si/Al ratio. This may be true for a changing ratio in one and the same zeolite type, but is certainly not always correct when comparing different ion-exchanged forms of one type, or when comparing different types. In table 3.15, several zeolite types are shown that have the same Si/Al ratio, but differ several hundred degrees in their stability.

Furthermore, using the general rules would means that the objectives given in chapter 2 are contradictory: they look for opposite qualities in a zeolite. For instance, a good adsorption capacity requires a high void fraction, but a high fraction is only seen for zeolites with low Si/Al ratios, which have a poor thermal stability.

So without general rules, the selection has to be based on the experimental information that is available. This information is summarized in table 3.15, which gives the properties that are important for the selection. For this study, the selection in done by choosing zeolites that are not excluded in advance and that fulfill at least one objective (mentioned in chapter 2) well. Five zeolite types have been selected and in their alkaline earth metal form tested as adsorbent:

Table 3.16 *The five zeolite types selected for this study*

zeolite type	advantages	disadvantages
Zeolite A	highest adsorption capacity high void fraction reasonable heat of adsorption reasonable thermal stability	difficult ion-exchange for Mg low stability for Ba-A
Zeolite X	highest void fraction high adsorption capacity reasonable heat of adsorption reasonable thermal stability	
Mordenite	highest heat of adsorption high thermal stability	low void fraction low adsorption capacity
Zeolite P	high void fraction good ion-exchange for Mg reasonable electron density (Si/Al) reasonable thermal stability	uncertainty on thermal stablity
Zeolite Beta	largest ring diameter (adsorption/ion-exchange) high Si/Al ratio (thermal stability)	unkown influence of the disordered framework no much information available

Zeolite P and Beta have been included mainly because for their lack of information and for their availability. Zeolite P is a thermodynamic form into which other zeolites (e.g, A) tend to transform. It is the best option in group 1 and has very good ion-exchange properties for magnesium. Zeolite Beta has not been studied much. It has the largest aperture diameter wich makes it quickly accessible for adsorbate molecules and ion-exchange cations, even for large ones like magnesium and barium. It probably has also a good thermal stability.

3.3 Zeolite A (LTA)

type material:	Linde Type A (LTA)
structure group:	3
composition:	(Na_{12} [$Al_{12}Si_{12}O_{48}$] . 27 H_2O)$_8$
variations:	Si/Al = 0.7-1.2
crystallographic data:	
symmetry:	cubic
space group:	pseudo cell: Pm3m, true cell: Fm-3c
cell constants:	pseudo cell: a = 11.19 Å, true cell: a = 24.6 Å,
cell volume:	pseudo cell: 1693-1870 Å^3
density:	1.99 g/cc
structural properties:	
SBU:	D4R
polyhedra:	α, β
void fraction:	0.47 cc/cc
framework density:	1.27 g/cc
network:	3-dimensional, 8-ring parallel to <100>
dehydration:	
free aperture:	4.1 Å, (2.2 Å into the β-cage)
stability:	no effects on framework
ion-exchange:	
alkaline earthe ions:	Mg^{2+} : slow ^{0} ; Ba^{2+} : instable product.*

[Adams^0 (1986), Barrer (1958), Breck (1974), Eberly* (1962), Sherry* (1966), Szostak (1992), IZA-SC (1997)]*

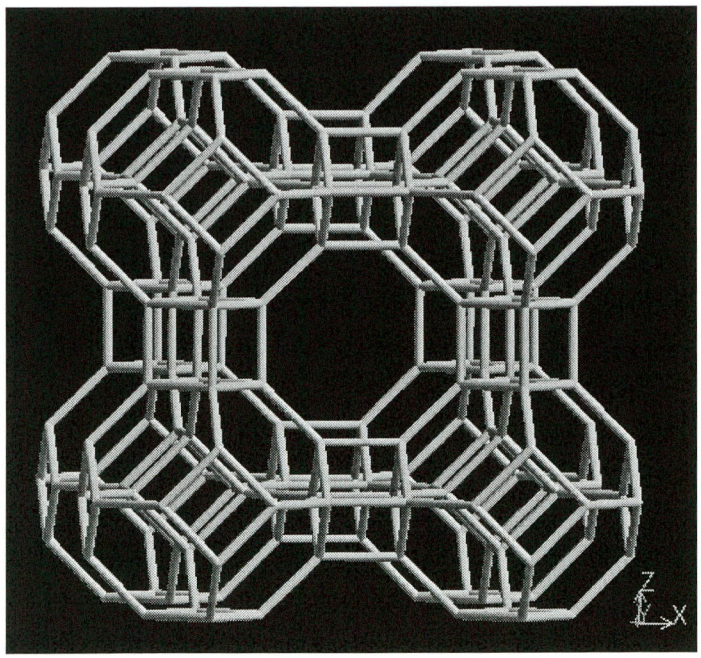

Figure 3.2 *Zeolite A (LTA)*

[IZA-SC (1997)]

3.4 Zeolite X (FAU)

type material:	Linde Type X/Faujasite (FAU)
structure group:	4
composition:	Na_{86} [$Al_{86}Si_{106}O_{384}$] . 264 H_2O
variations:	Si/Al = 1.0-1.5, Na/Al = 0.7-1.1
crystallographic data:	
symmetry:	cubic
space group:	Fd-3m
cell constants:	a = 24.8-25.0 Å,
cell volume:	15362-15670 Å^3
density:	1.93 g/cc
structural properties:	
SBU:	D6R
polyhedra:	β, 26-hedron (II)
void fraction:	0.50 cc/cc
framework density:	1.31 g/cc
network:	3-dimensional, 12-ring (<111>) parallel to [110]
dehydration:	
free aperture:	7.4 Å
stability:	no effects on framework
ion-exchange:	
alkaline earthe ions:	

[Breck (1974), Szostak (1992), IZA-SC (1997)]

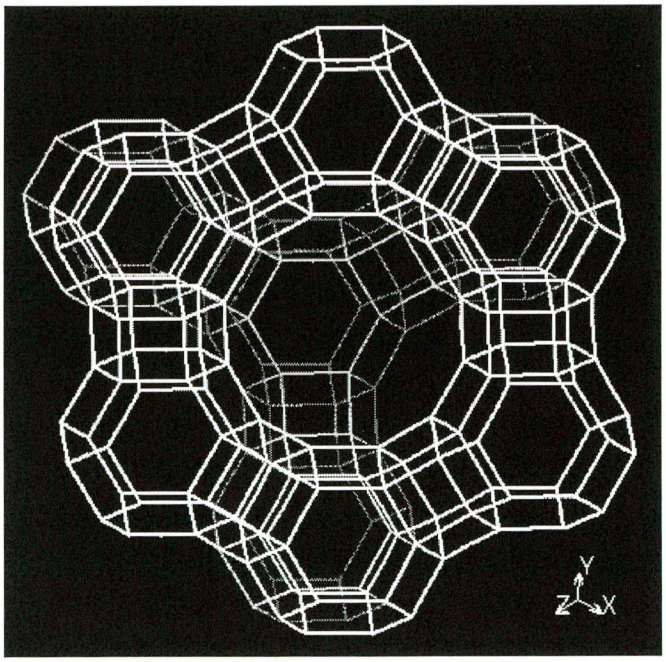

Figure 3.3 Zeolite X (FAU)

[IZA-SC (1997)]

3.5 Zeolite Mordenite (MOR)

type material:	Mordenite (MOR)
structure group:	6
composition:	Na_8 [$Al_8Si_{40}O_{94}$] . 27 H_2O
variations:	Si/Al = 4.5-5.0
crystallographic data:	
symmetry:	orthorhombic
space group:	CmCm
cell constants:	a = 18.1 Å, b = 20.5 Å, c = 7.5 Å
cell volume:	2794-2827 $Å^3$
density:	1.70 g/cc
structural properties:	
SBU:	5-1
polyhedra:	
void fraction:	0.28 cc/cc
framework density:	1.31 g/cc
network:	2-dimensional, 8-ring ([001]) and 12-rings ([010]) parallel to c
dehydration:	
free aperture:	6.5 x 7.0 and 2.6 x 5.7 Å
stability:	no effects on framework
ion-exchange:	
alkaline earthe ions:	

[Breck (1974), Szostak (1992), IZA-SC (1997)]

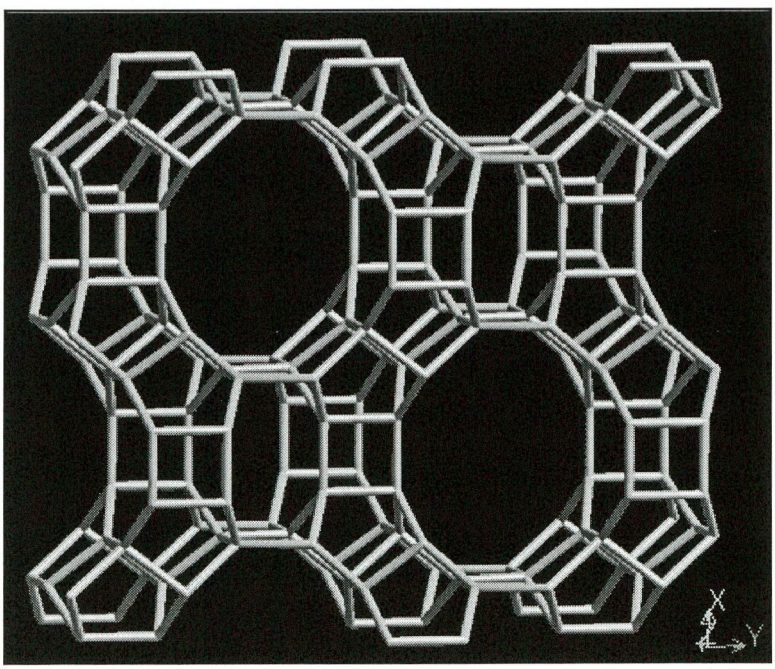

Figure 3.4 *Mordenite (MOR)*

[IZA-SC (1997)]

3.6 Zeolite P (GIS)

type material:	Gismonde (Gis)
structure group:	1
composition:	$Na_6 [Al_6Si_{10}O_{32}] . 15 H_2O$
variations:	Si/Al = 1.1-2.5
crystallographic data:	
symmetry:	near cubic
space group:	$I4_1/a$
cell constants:	a = c= 10.0 Å
cell volume:	1015 $Å^3$
density:	2.01 g/cc
structural properties:	
SBU:	S4R
polyhedra:	
void fraction:	0.41 cc/cc
framework density:	1.57 g/cc
network:	3-dimensional, 8-ring ([100] and [010]) parallel to a and b
dehydration:	
free aperture:	3.1 x 4.4 and 2.9 x 4.9 Å
stability:	framework sometimes shrinks (upto 30 vol.%)
ion-exchange:	
alkaline earthe ions:	Mg^{2+} : fast

[Breck (1974), Szostak (1992), IZA-SC (1997)]

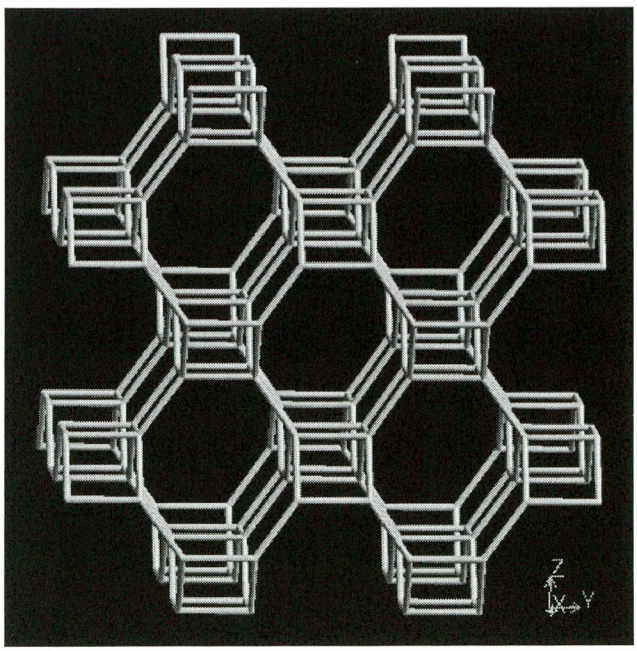

Figure 3.5 *Zeolite P (GIS)*

[IZA-SC (1997)]

3.7 Zeolite Beta (BEA)

type material:	Zeolite Beta (BEA)
structure group:	
composition:	$Na_7 [Al_7Si_{57}O_{128}] . ... H_2O$
variations:	
crystallographic data:	
symmetry:	tetragonal,
space group:	$P4_1$-22
cell constants:	a= 12.7Å, a= 26.4 Å
cell volume:	4178 $Å^3$
density:	
structural properties:	disordered framework
SBU:	
polyhedra:	
void fraction:	
framework density:	
network:	2-dimensional, 12-rings ([001] and <100>)
dehydration:	
free aperture:	5.5 x 5.5 and 7.6 x 6.4 Å
stability:	
ion-exchange:	
alkaline earthe ions:	

[Breck (1974), Szostak (1992), IZA-SC (1997)]

Chapter 4

Experimental

To determine the suitability of the selected zeolite types, zeolite samples in different alkaline earth metal forms were prepared by ion-exchange and subsequently tested on their stability and adsorption capacity.

The results of the ion-exchange process were audited by analyzing a selection of the samples with X-ray Energy-Dispersive Spectrometry (EDS) and X-ray Diffraction (XRD). XRD was also used to test the thermal stability. Spectra taking from samples before and after heating to 800 °C were therefore compared to find signs of structural decline. Thermogravimetric analysis (TGA) was used to measure the adsorption capacity.

Materials

The Zeocros CA-150 (LOT # 96.146) used as starting material for the preparation of the Zeolite A samples, was supplied by Crosfield (Crosfield B.V., Eijsden, NL). This Na-Zeolite A is a crystalline zeolite in powder form with the specified composition $Na_{12}[(AlO_2)_{12}(SiO_2)_{12}].27\ H_2O$, a Si/Al ratio of 1 and a relative density of 2.1. It is commercially available as a detergent builder. [Crosfield (1996)]

The Na-Zeolite X (LOT # 1665-56) for the Zeolite X samples was provided by The PQ Corporation (The PQ Corporation, Conshohocken (PA), USA). This zeolite powder which is normally used as a detergent builder, has a Si/Al ratio of approximately 1.5.

The H-Mordenite (JRC, JRC-Z-HM20) for the Mordenite samples was obtained from the Japanese Catalysis Society. A detailed analysis and characterization of this zeolite powder, which has a Si/Al ratio of 10, is given by Sawa et al. [(1990-1)].

For the Zeolite P samples, the Na-Zeolite P was supplied by Crosfield. This zeolite powder $Na_2[(AlO_2)_2(SiO_2)_2].nH_2O_{\ (n=1-5)}$, called Zeocros CG-180, is produced as a detergent builder. It has a Si/Al ratio of 1 and a relative density of 2.1. [Crosfield (1994, 1996), Edwards (1995)]

The Na-Zeolite Beta (Mol. sieve 806 B-25 LOT II B12) used to make the alkaline earth sample was provided by Shell (Shell, Amsterdam, NL). It is a powder and has a Si/Al ratio of 15. The H-Zeolite Beta that was used in the adsorption measurements was prepared from the same basic material by members of the Catalysis Group (University of Twente, Faculty of Chemical Technology).

Ion-exchange

Two gram of the zeolite (the sodium forms of the zeolite A, X, P, and Beta, and the hydrogen form of Mordenite) was added to 200 ml of a 1 N solution of $MeCl_2$ (Mercks, p.a. quality; Me = Mg, Ca, Sr, or Ba) and distilled water. While being stirred continuously, the mixture was heated to 90-100 °C in an erlenmeyer flask with a reflux cooler and left to react for a period of 4 days. Each day, the chloride solution was decanted and refreshed.

Subsequently, the zeolite was filtered off and washed with small amounts of water (5-10 ml) to remove the chloride solution. The washing was continued until an $AgNO_3$ solution no longer caused precipitation in the filtrate. Finally, the zeolite was dried for 24 hours at 110-120 °C. [Baker (1988), Barrer (1958), Eberly (1962), Franklin (1988), Furuyama (1982), Harjula (1992), Hathaway (1989), Sawa (1990-2), Sherry (1968)]

EDS analysis and XRD analysis

The X-ray Energy-Dispersive Spectrometry (EDS or EDX) analyses were performed on a HR-SEM Hitachi S800 field emission microscope with an Ultra-Thin Window EDX system by Kevex Delta Range. The build-in data analysis software of the system was used to assign the peaks to the different cations based on their characteristic energies. The intensity of the peaks was used to determine the relative quantity of each cation. [Joy (1986)]

The X-ray Diffraction (XRD) spectra were recorded with a Cu-$K\alpha_1$ (1.5406 Å) beam on a Philips PW1370 and a Philips X'Pert-MPD system.

TGA analysis

The atmospheric thermogravimetric analyses (TGA) were done with a PL Thermal Sciences Ltd TG-DTA STA 1500 system (Stanton Redcroft Ltd). (See figure 4.1)

A sample of approximately 10 mg was put in a Rh-Pt crucible placed on a sample holder which is connected to the microbalance. The holder was lowered into the furnace that was purged with the CO_2 gas stream (1 atm, 20 ml/min). While recording the changes in weight, the sample is dehydrated and activated by increasing the temperature from 25 °C to the initial temperature (in most cases: 600 or 800 °C) with 10 °C/min. Subsequently, the sample was cooled at a rate of 10 °C/min to measure the adsorption curve.

High-pressure (7.5 bar and 30 bar CO_2) adsorption experiments were carried out on a specially designed high-pressure TGA apparatus build by Deutsche-Montan Technologie für Rohstoff, Energie und Umwelt (DMT). (See figure 4.2)

An Al_2O_3 crucible (1) connected to the microbalance by a small chain is hanging in the furnace (3). The crucible can be lifted by a servo motor, so that it can be filled through a lock (2) with a sample of approximately 90 mg. Through the furnace a CO_2 gas stream is flowing upwards (for the 7.5 bar experiments: 600 ml/min; for the 30 bar experiments: 900 ml/min). Meanwhile, the annular space surrounding the furnace (4) and the balance chamber (5) are cooled by a He gas stream (for the 7.5 bar experiments: 800 ml/min; for the 30 bar experiments 1200 ml/min). The system can be pressurized by using the two pressure control valves that are place behind the furnace (G104/1 and /2).

Both the 7.5 bar experiments as the 30 bar experiments, the sample is heated from 25 °C to 800 °C (or in the case of Na-Zeolite A to 700 °C) at a rate of 10 °C/min. Then, the sample is hold at the temperature of 800 °C during 5 minutes before being cooled down again. Between 800 °C and 250 °C, the cooling is done with 10°C/min, while beyond 250 °C the cooling can no longer be controlled and therefore the cooling rate is less.

For all measurements, a sample of quartz glass with a apperent relative density of 2.1 was used to record a reference curve. By using pure CO_2 gas, external mass transfer limitation could be avoided, even with the large samples applied in the HP-TGA experiments. [Wendlandt (1986), Wunderlich (1990)]

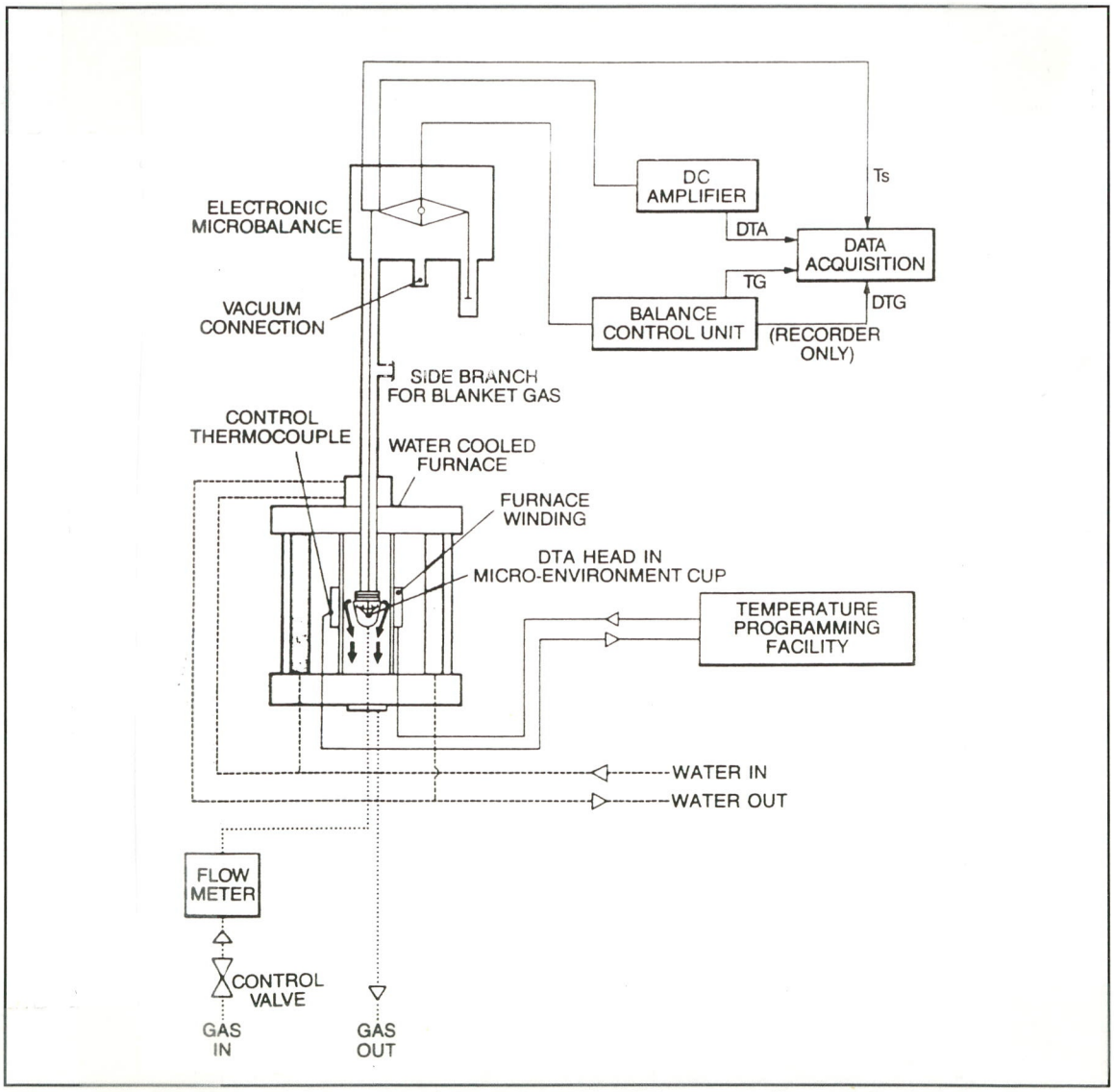

Figure 4.1 *PL Thermal Sciences Ltd TG-DTA STA 1500 system (Stanton Redcroft Ltd)*

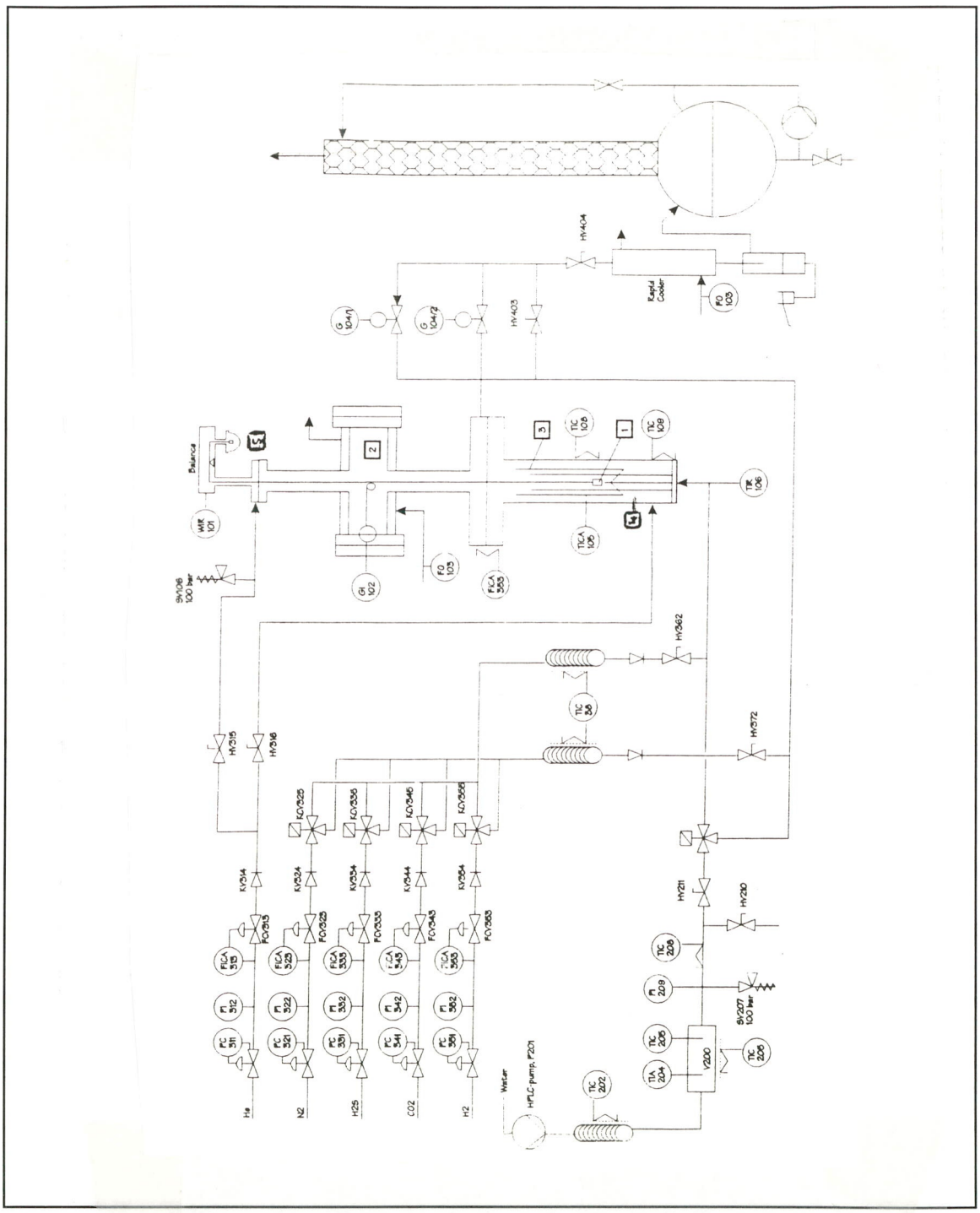

Figure 4.2 *High-pressure TGA system by Deutsche-Montan Technologie für Rohstoff, Energie und Umwelt*

Chapter 5

Results

As mentioned in chapter 2, the use of zeolite as an adsorbent for CO_2 removal in an IGCC power plant depends mainly on the thermal stability and the adsorption capacity as function of pressure and temperature. These properties were determined with the use of X-ray Diffraction (XRD) and Thermogravimetric Analyses (TGA). This chapter presents the results of these analyses.

In section 5.1, the preparation of the alkaline earth metal samples is discussed. The results of the ion-exchange process are examined on the basis of X-ray Energy-Dispersive Spectrometry (EDS or EDX) analyses and XRD analyses. With EDS, the chemical composition of the samples was determined and compared with the sodium and hydrogen zeolites used as starting material. XRD was used to see whether the zeolite structure was still intact after the ion-exchange.

In section 5.2, the thermal stability of the samples is discussed. This is mainly done on the basis of XRD spectra taken before and after heating the sample to the initial adsorption temperature. This initial temperature is needed for (a) the dehydration/activation and (b) the regeneration of the sample. Usually, an initial temperature of 800 °C was used. In addition, the stability is tested by TGA analyses. The loss of adsorption capacity seen during TGA analyses with increasing initial temperatures is interpreted as a sign of structural decline.

In section 5.3, the adsorption capacity is given as function of the temperature and the CO_2 pressure. TGA curves are given that show the adsorption for 1.0, 7.5, and 30 bar CO_2 in the temperature range of 25 °C to 800 °C. The capacity of the alkaline earth metal samples is compared with that of the sodium or hydrogen form used as starting material in the preparation. In addition, the TGA curves have been used to calculate the heat of adsorption for those zeolite samples that showed the best capacities. The calculated values are compared with the adsorption heats that are reported by other studies.

In section 5.4, the results of the analyses for the preparation, the stability, and the adsorption capacity are combined and compared with the information reported in the literature. Further, the results are compared with the objectives formulated in chapter 2 and an evaluation is given on the possibility of a high-temperature Temperature Swing Adsorption (TSA) process.

In section 5.5, the conclusions summarize the main results. A table with the best zeolite adsorbents for the high-temperature TSA process, and for the moderate-temperature TSA process are given. Some limitations of the measurements are mentioned and rendered into a few recommendations for further research. The consequences of the results for the process design of the IGCC power plant, as treated in chapter 6, are discussed.

5.1 Ion-exchange

5.1.1 EDS analyses

To confirm the procedure used for the ion-exchange, EDS-spectra have been made for a selection of samples:

Zeolite A:	Mg-A, Ca-A, Sr-A, Ba-A, and as reference Na-A
Zeolite X:	Ca-X, and as reference Na-X
Mordenite:	Ca-Mordenite, and as reference H-Mor
Zeolite β:	Ca-β, and as reference Na-β

Zeolite A:

Figures 5.1-5.4 show the characteristic energies of the elements that are present in each of the samples. When comparing figure 5.1 with the other figures, it is clear that after ion-exchange the Na peak of the starting material has disappeared and been replaced by one or more peaks of the alkaline earth metal.

For calcium, the EDS figure is not depicted here, due to a problem with the recording equipment, but the results of the analyses showed no presence of sodium.

For magnesium, a small rest peak of Na is still visible in figure 5.2. The low preference of Zeolite A toward magnesium in comparison with sodium, makes it difficult to reach complete exchange. With its high preference, calcium, which is always present in small amounts, is taken up instead.

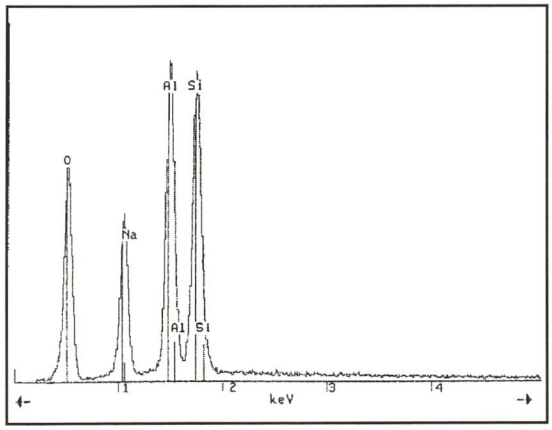

Figure 5.1 *EDS-spectrum Na-Zeolite A*

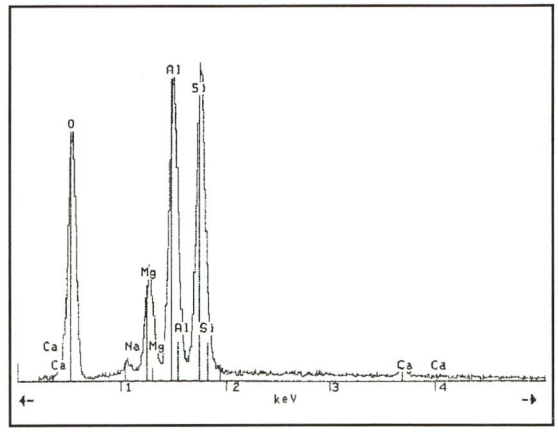

Figure 5.2 *EDS-spectrum Mg-Zeolite A*

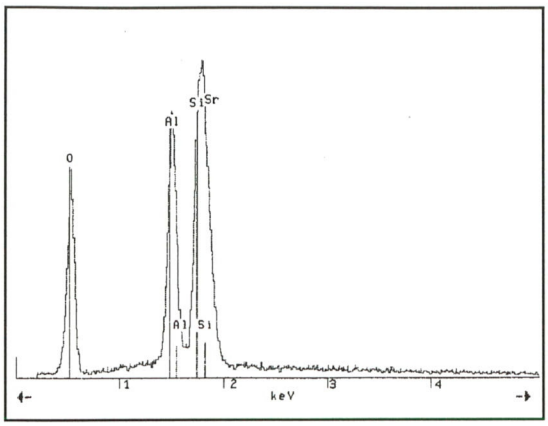

Figure 5.3 *EDS-spectrum Sr-Zeolite A*

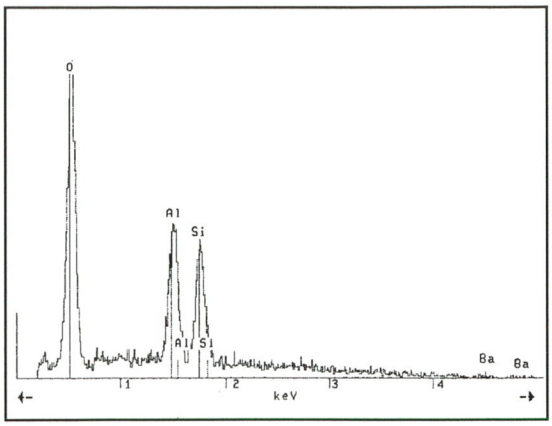

Figure 5.4 *EDS-spectrum Ba-Zeolite A*

For strontium, the ion exchange should result in a Sr peak at 1.8 keV. This peak can, however, not been seen as it coincides with the large peak of Si. The absence of the Na peak is, therefore, taken as sufficient prove.

For barium, two peaks are expected to appear at 4.5 and 4.8 keV. However, no peaks are seen in this region. As will be shown later, the XRD analysis proves that the Zeolite A in this barium sample has become amorphous during the ion exchange, so that no barium could be taken up. From the literature, it is known that Ba ion-exchanged Zeolite A has a tendency to be instable. Several authors have reported a disintegration of the structure at temperatures between 50 and 100 °C. [Barrer (1964, 1978), Breck (1974)]

Zeolite X:

For Zeolite X, a comparison of figures 5.5 and 5.6 shows that after ion-exchange the Na peak has disappeared and been replaced by the several peaks caused by calcium.

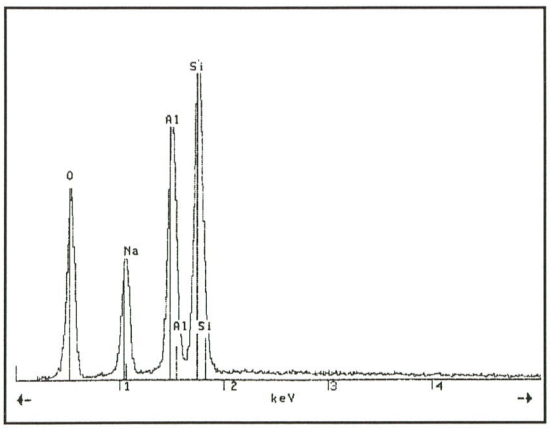

Figure 5.5 *EDS-spectrum Na-Zeolite X*

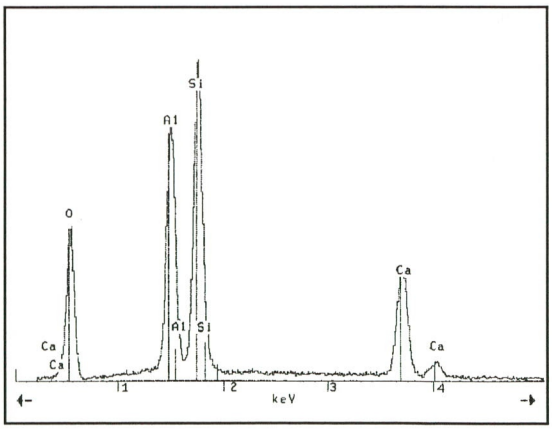

Figure 5.6 *EDS-spectrum Ca-Zeolite X*

Mordenite:

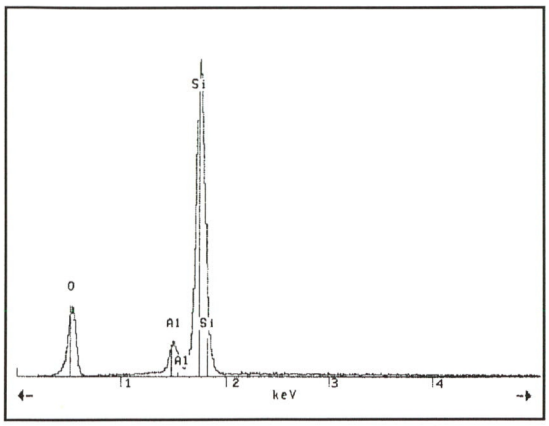

Figure 5.7 *EDS-spectrum H-Mordenite*

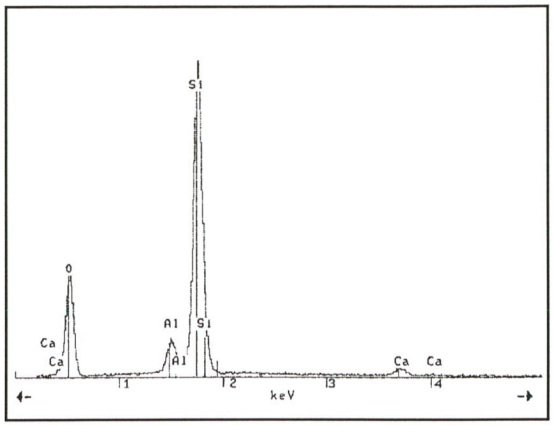

Figure 5.8 *EDS-spectrum Ca-Mordenite*

For Mordenite, the comparison is somewhat different, as H-Mordenite has no cation peak that can be seen with EDS. The calcium peaks in figure 5.8 can, therefore, not be compared with the reference H-Mordenite. Although the peaks are not very distinct, they have the height that could be expected for a Si/Al ratio of 10.

Zeolite Beta:

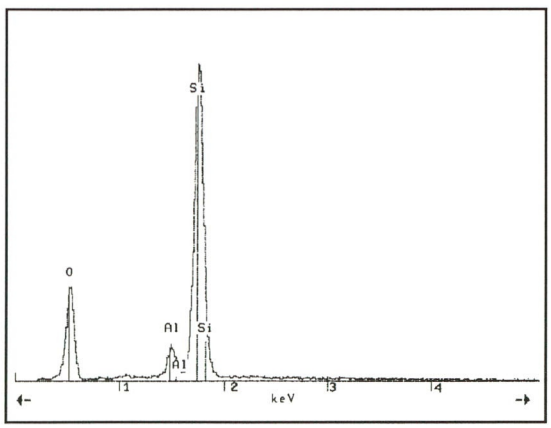

Figure 5.9 *EDS-spectrum Na-Zeolite* β

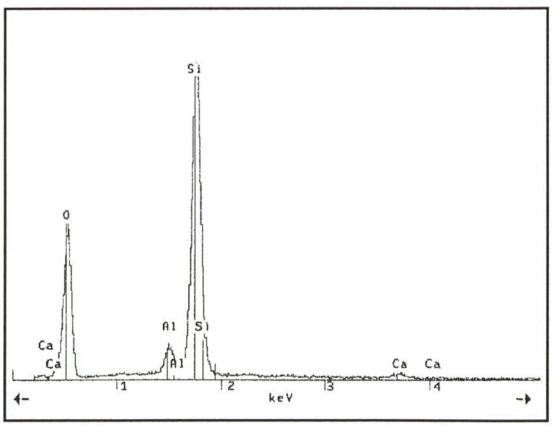

Figure 5.10 *EDS-spectrum Ca-Zeolite* β

For Zeolite β, the high Si/Al ratio makes it difficult to tell exactly how well the ion-exchange has been, but the Ca peaks in figure 5.10 make it clear that exchange has taken place.

5.1.2 XRD analyses

The samples of Zeolite A, X and Mordenite have all been analyzed with XRD after ion-exchange to see whether the zeolite framework was still intact.

Zeolite A:

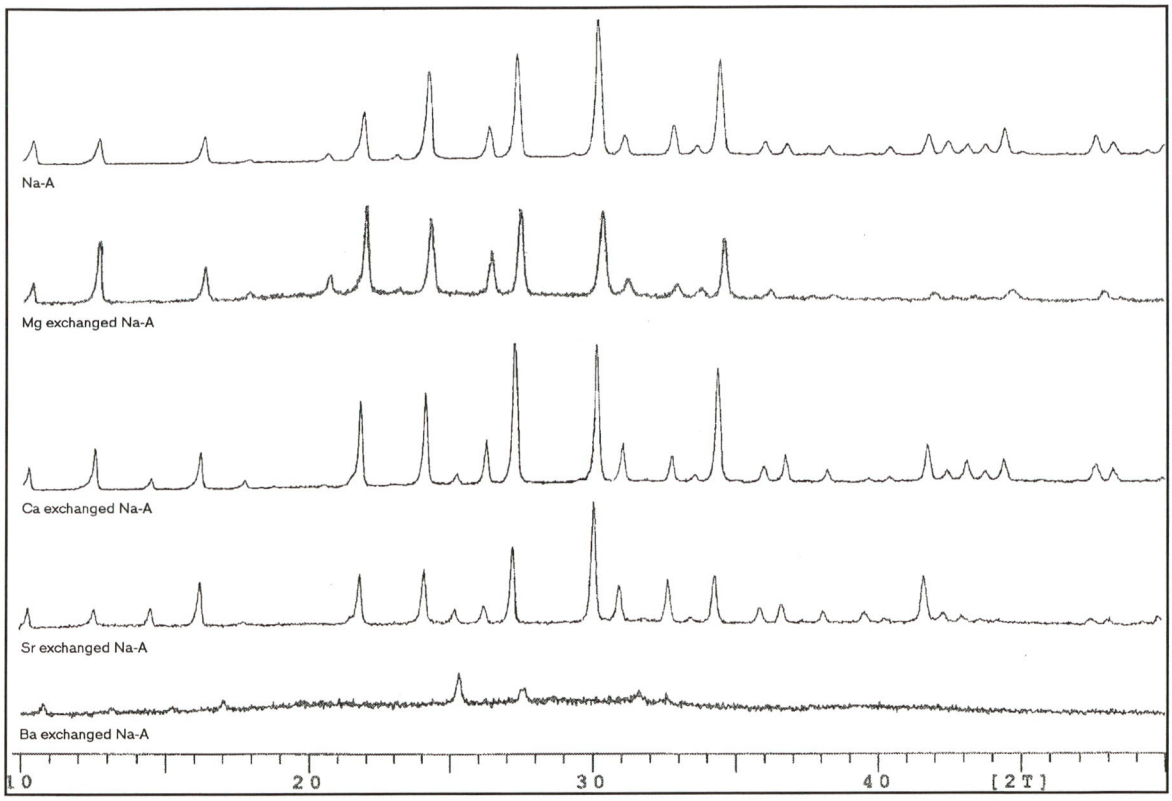

Figure 5.11 *XRD analysis of Zeolite A samples after ion-exchange (Cu $K\alpha_1$ = 1.54 Å)*

I/I_o strongest lines	*Na*		*Mg*		*Ca*		*Sr*		*Ba*	
	2θ	*d (Å)*	*2θ*	*d (Å)*	*2θ*	*d (Å)*	*2θ*	*d (Å)*	*2θ*	*d (Å)*
1st	30.19	2.960	21.96	4.045	27.23	3.275	30.07	2.970	25.38	3.507
2nd	27.35	3.260	27.45	3.247	30.05	2.974	27.24	3.272	27.65	3.224
3th	34.42	2.605	30.32	2.946	34.30	2.614	24.09	3.692	10.83	8.166
4th	24.24	3.672	24.29	3.661	24.09	3.694	21.79	4.075	17.06	5.195
5th	21.93	4.053	12.67	6.981	21.79	4.079	34.32	2.611		

Table 5.1 *Zeolite A: comparison of XRD results with reference data*

I/I_o strongest lines	*Na-A*				*Na-N-A*	*Na-P-A*	*Ca-A*	
	d (Å) this study	*IZA-SC*	*Breck 1)*	*Szostak*	*Breck 2)*	*Breck 3)*	*d (Å) this study*	*Breck 1)*
1st	2.960 *)	12.278	12.29	3.384	12.08	12.2	3.275 *)	12.24
2nd	3.260	8.681	8.71	17.7	3.65	2.96	2.974	8.66
3th	2.605	8.491	2.987	4.33	8.55	8.60	2.614	3.276
4th	3.672	7.088	3.714	6.22	4.03	3.69	3.694	4.084
5th	4.053	5.491	3.293	1.843	2.93	3.28	4.079	3.696
6th		3.702	4.107	8.67	3.36	7.07		7.08
7th		3.281	7.11	7.25		4.08		2.972
8th		2.978				2.62		2.614

Na-N-A: Zeolite A that was made with Na and TMA cations
Na-P-A: Zeolite A that contains some phosphate.
*) crystallographic dimensions: d-values larger than 8.83 Å ($2\theta = 10$) were not included in this study.
1) R.M. Milton, US patent 2.882.243 (1959); Breck D.W.; ..., *J. Amer. Chem. Soc.*, **78**, 5963 (1956)
2) Barrer R.M.; ..., US patent 3.308.922 (1967)
3) Flanigen E.M.; ..., *Molecular Sieves Zeolites*, vol **101**, American Chemical Society, Washington D.C. , p 76, 1971

[Breck (1974), Szostak (1992), IZA-SC (1996, 1997)]

In table 5.1, the XRD results of this study are compared with data from other studies in the literature. As in this study d-values larger than 8.83 Å have not been included, the comparison has to be done for less stronger lines. This might be the reason that a perfect match hasnot been found. For Na-A, the best correspondence is seen for the data by Milton and by Breck. [Breck (1974)] The data by the IZA-SC are also reasonable, but those of Szostak are far beside.

Looking at the data in table 5.1, there is a small chance that the material provided by Crosfield contains some TMA or phosphate. The data sheet that accompanied the material mentions, however, a composition free of both components. [Crosfield (1996)]

As shown in figure 5.11, ion-exchange with barium has let to an amorphous material. In all other cases, the framework was preserved.

Zeolite X:

The XRD analysis of Zeolite X is given in figure 5.12. A comparison of the ion-exchanged zeolites with the original sodium form shows that the framework structure is well preserved. In the case of strontium, a slight increase in the baseline is seen for the 2 θ-values between 15 and 30 degrees. There are no indications in the literature suggesting that the strontium exchanged form of Zeolite X is unstable. In fact, several authors report to have made it successfully. [Barrer (1964, 1978)]

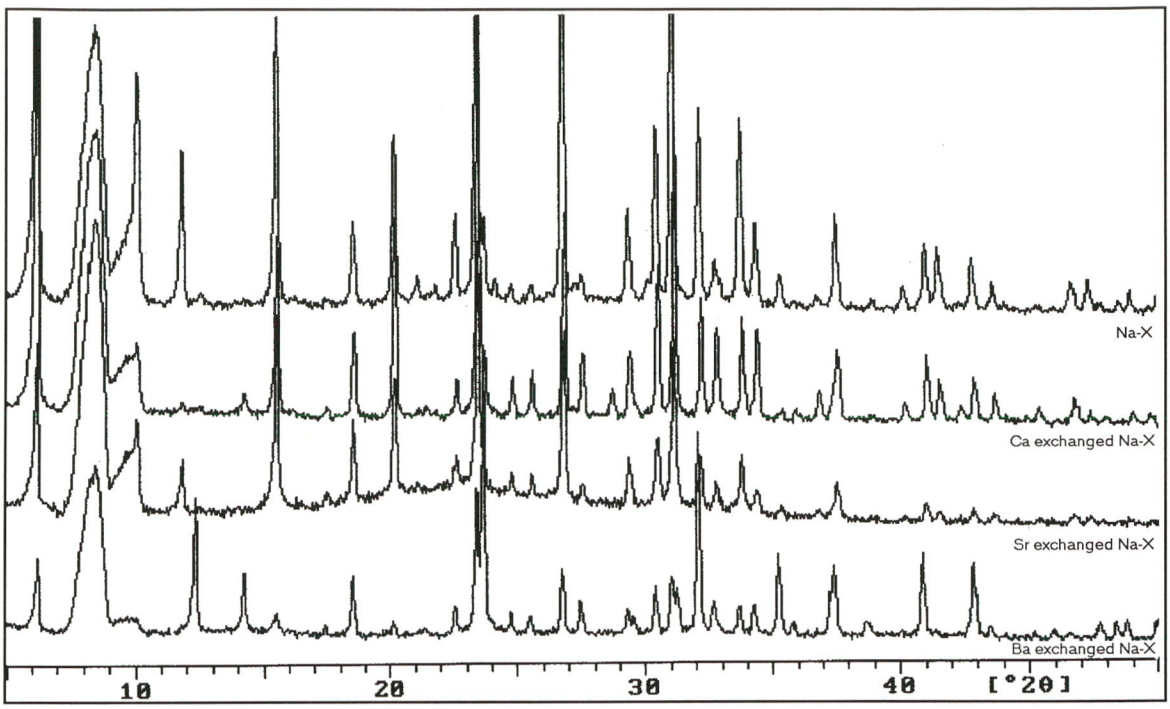

Figure 5.12 *XRD analysis of Zeolite X samples after ion-exchange (Cu $K\alpha_1$ = 1.54 Å)*

I/I_o strongest lines	*Na*		*Ca*		*Sr*		*Ba*	
	2θ	*d (Å)*	*2θ*	*d (Å)*	*2θ*	*d (Å)*	*2θ*	*d (Å)*
1st	6.20	14.244	6.20	14.255	23.46	3.790	23.67	3.757
2nd	23.42	3.795	23.47	3.787	8.69	10.173	32.07	2.789
3th	31.09	2.875	8.25	10.708	15.54	5.699	8.50	10.400
4th	26.78	3.326	8.59	10.291	26.82	3.321	23.38	3.802
5th	15.53	5.703	31.16	2.868	31.14	2.870	12.33	7.173

A explanation could be that in this hydrated zeolite the cations have different hydratation shells and are therefore located on different sites. This would cause a certain amount of stress in the framework which results in different bond lengths and angles.

In table 5.2, the d-values of this study are compared with those of other studies. For both Na-X and Ca-X, the data reported by Breck (which are the same values as are given by Szostak) correspond well with the data given here. The data by the IZA-SC show a different XRD pattern. A reason for this discrepancy could be that the data given by the IZA-SC are based on computer calculations of the framework and not on experimental data.

Table 5.2 *Zeolite X: comparison of XRD results with reference data*

I/I_o strongest lines	*Na-X*				*Ca-X*		
	d (Å) this study	*IZA-SC*	*Breck 1)*	*Szostak*	*d (Å) this study*	*Breck 1)*	*Szostak*
1st	14.244	14.491	14.465		14.255	14.371	
2nd	3.795	8.874	3.800		3.787	3.800	
3th	2.875	5.758	2.885		10.708	5.709	
4th	3.326	7.246	8.845		10.291	3.328	
5th	5.703	3.828	5.731		2.868	4.405	

1) R.M. Milton, US patent 2.882.244 (1959); Breck D.W.; ..., *Molecular Sieves*, Society of Chemical Industry, London, p 47, 1968

[Breck (1974), Szostak (1992), IZA-SC (1996, 1997)]

Mordenite:

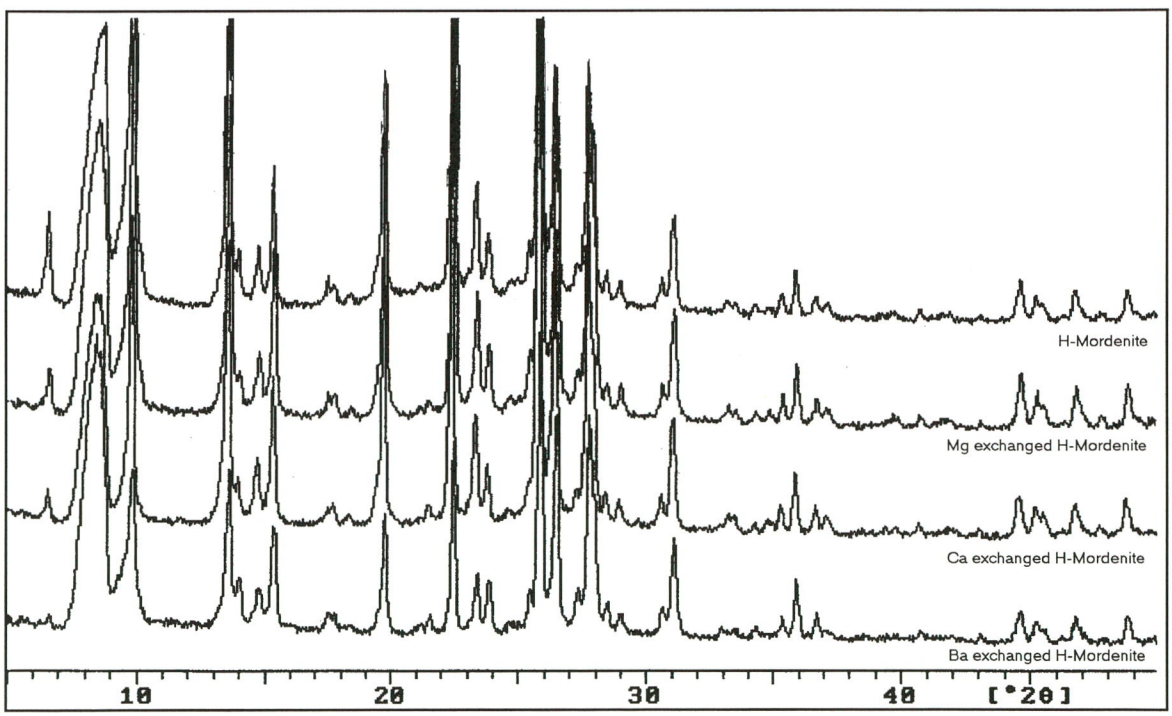

Figure 5.13 *XRD analysis of Mordenite samples after ion-exchange* ($Cu\ K\alpha_1 = 1.54$ *Å)*

I/I_0 *strongest lines*	*H*		*Mg*		*Ca*		*Ba*	
	2θ	*d* (Å)	2θ	*d* (Å)	2θ	*d* (Å)	2θ	*d* (Å)
1st	25.79	3.452	25.83	3.447	25.77	3.454	25.85	3.444
2nd	9.78	9.041	22.46	3.955	22.40	3.967	26.48	3.363
3th	22.41	3.964	9.83	8.995	27.71	3.217	27.76	3.211
4th	13.54	6.534	27.74	3.213	9.78	9.041	22.47	3.954
5th	27.70	3.218	13.59	6.513	26.42	3.371	8.76	10.086

The XRD-analysis in figure 5.13 shows that the zeolite structure of the Mordenite samples is preserved during the ion-exchange.

Ion-exchange: summary

With exception of barium and Zeolite A, the ion-exchange has been succesfull for all the samples (Zeolite A: Na, Mg, Ca, Sr, and Ba; Zeolite X, β: Na, and Ca; Mordenite: H, and Ca) that were examined.

The EDS analyses show that original ion (sodium or hydrogen) is replaced to a high degree by the alkaline earth metal ion. Only in the case of Mg in Zeolite A, the original sodium ion is still detected.

The XRD spectra of the ion- exchanged samples show that the zeolite structure is well preserved during the exchange.

For barium and Zeolite A, it is concluded that the sample becomes amorphous as is confirmed by both the EDS and the XRD analyses. Thsi behavior has been reported by several authors in the literature.

5.2 Stability

5.2.1 XRD analyses

The stability was tested by making XRD recording of Zeolite A, X, and Mordenite samples before and after heating to the initial adsorption temperature of 800 °C in a 7.5 bara CO_2 atmosphere.

Zeolite A:

The changes in peak height and the broadening seen in figure 5.14 are clearly suggesting that thermal degradation occur. Nevertheless, the zeolite framework does not collapse completely.

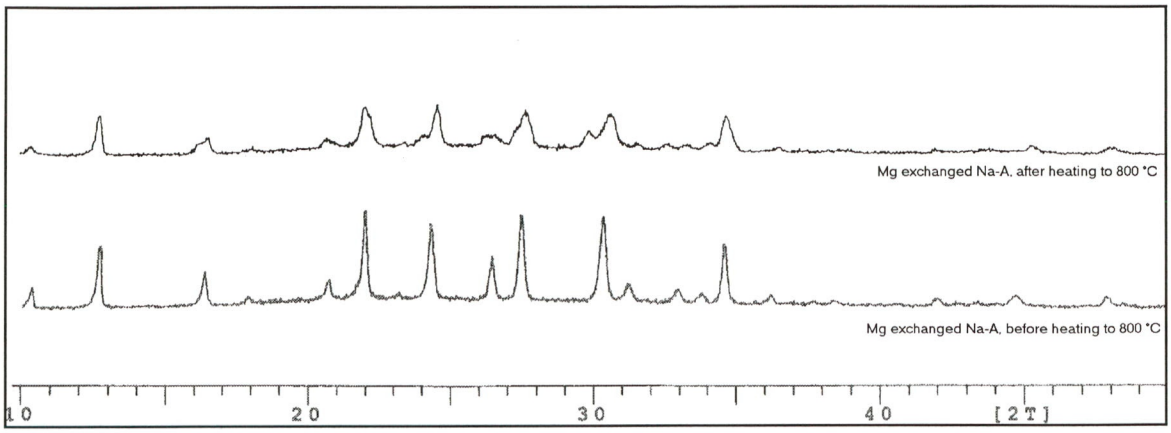

Figure 5.14 *Thermal stability of Mg exchanged Zeolite A (Cu Kα$_1$ = 1.54 Å)*

Ca exchanged Zeolite A shows no signs of thermal degradation after heating. Rearrangements of cations and small changes in the framework during the dehydration are probably the cause for the origination and the disappearance of some small peaks.

For strontium, the change in the baseline suggest that some thermal degradation has occured during heating. It should however be mentioned that both recordings were made on different equipment because the original equipment was replaced, so that a systematic fault cannot be excluded completely.

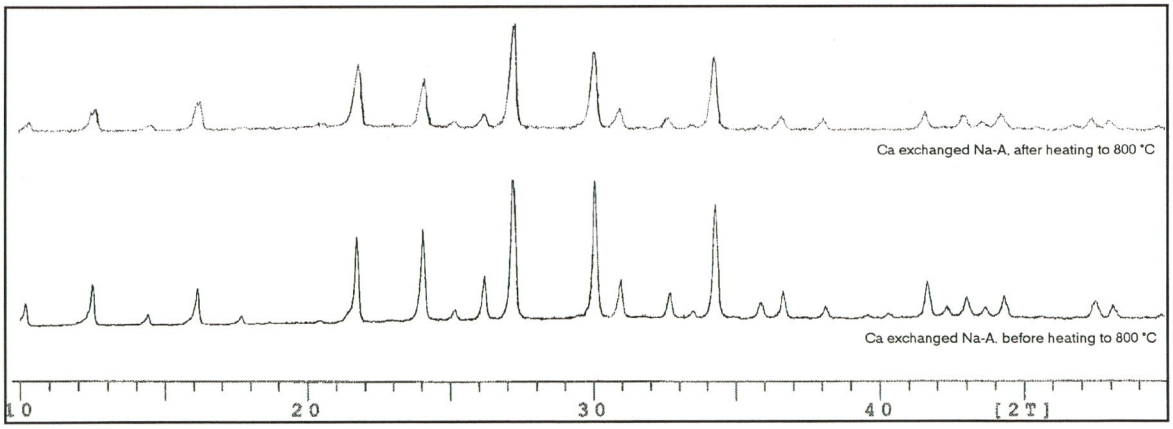

Figure 5.15 *Thermal stability of Ca exchanged Zeolite A (Cu Kα$_1$ = 1.54 Å)*

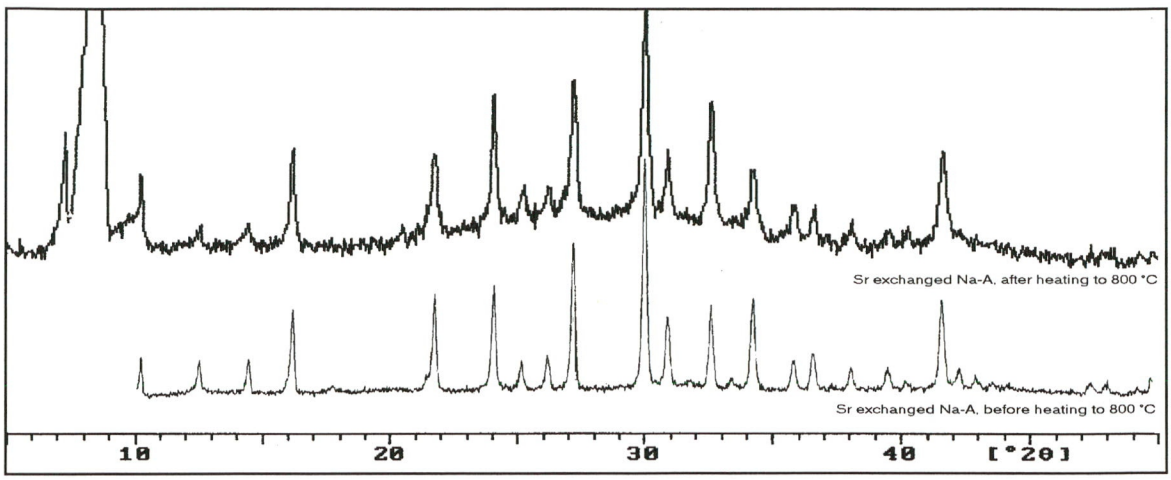

Figure 5.16 *Thermal stability of Sr exchanged Zeolite A (Cu $K\alpha_1$ = 1.54 Å)*

Zeolite X:

The Ca exchanged Zeolite X clearly shows signs of thermal instability after heating to 800 °C.

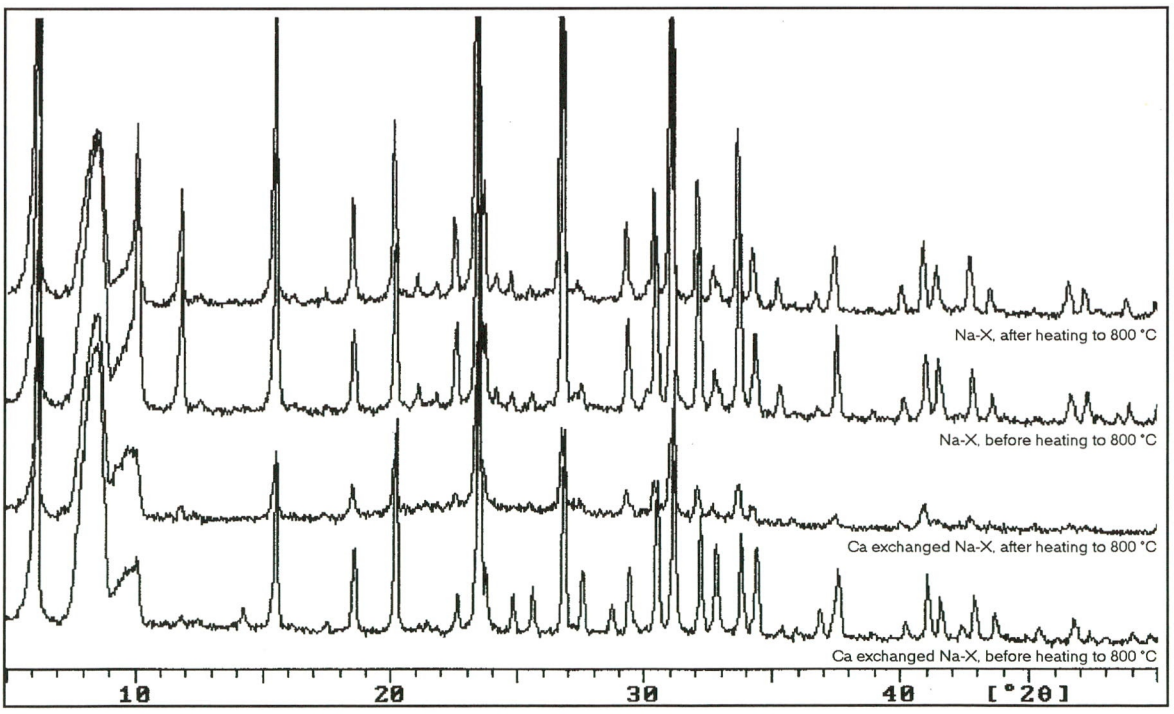

Figure 5.17 *Thermal stability of Ca Zeolite X and Na Zeolite X (Cu $K\alpha_1$ = 1.54 Å)*

Mordenite :

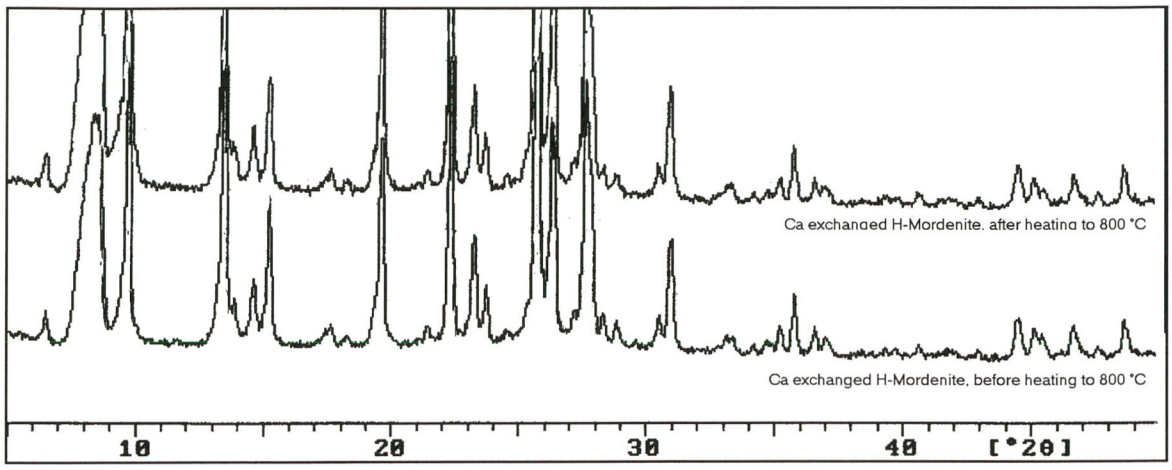

Figure 5.18 *Thermal stability of Ca exchanged Mordenite (Cu $K\alpha_1$ = 1.54 Å)*

For Mordenite, several authors have reported a stability of 1000 °C or more. In figure 5.18, the XRD spectrum of Ca-Mordenite taken at 800 °C shows, therefore, no signs of structural decline.

5.2.2 Thermogravimetric analyses

Zeolite A:

The initial preparation of the zeolites was done at several temperatures in order to test the stability against dehydration and the consequences for the adsorption behavior. As mentioned previously in chapter 3, the thermal stability of Zeolite A is approximately 800 °C. For Ca-Zeolite A, a higher stability is reported, while for sodium the stability is less.

In figure 5.19 and 5.20, the adsorption capacity of Na-Zeolite A for 1 atm CO_2 is shown after initial dehydration at 600 and 800 °C. In these figures, a 25 % weight loss is seen as a result of the dehydration process, which is necessary to clear the pores and to allow CO_2 to enter. Between 500 and 800 °C, no significant change in weight is observed. With the decrease of temperature the adsorption of CO_2 results in a gain in weight.

In figure 5.20, the higher initial temperature of 800 °C causes the capacity to decrease by approximately 0.05 mg/mg. For the 7.5 bara CO_2 experiment in figure 5.21, the decrease is much higher. In this experiment, the period at the temperature of 800 °C was not 1 but 5 minutes.

In conclusion, Na-Zeolite A becomes unstable between 700 and 800 °C, depending on the heating rate used in the measurement. TGA experiments with 7.5 bara steam, instead of CO_2, suggest that the hydrothermal stability of Na-Zeolite A ends between 450 and 600 °C.

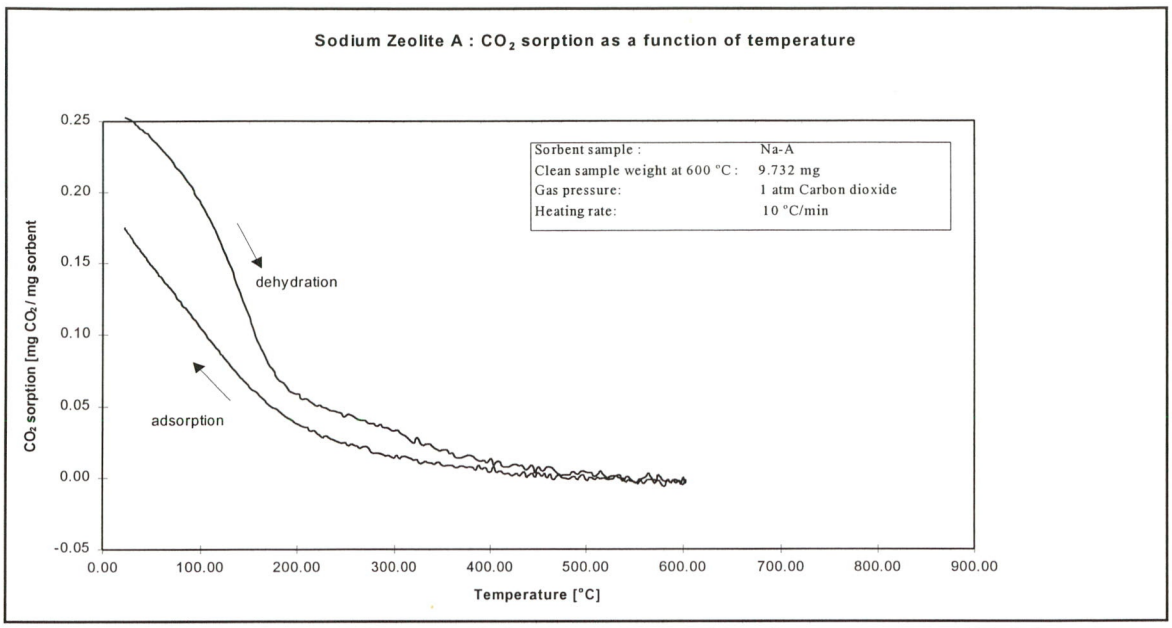

Figure 5.19 *Na Zeolite A: adsorption behavior at 1 atm CO_2 after initation at 600 °C*

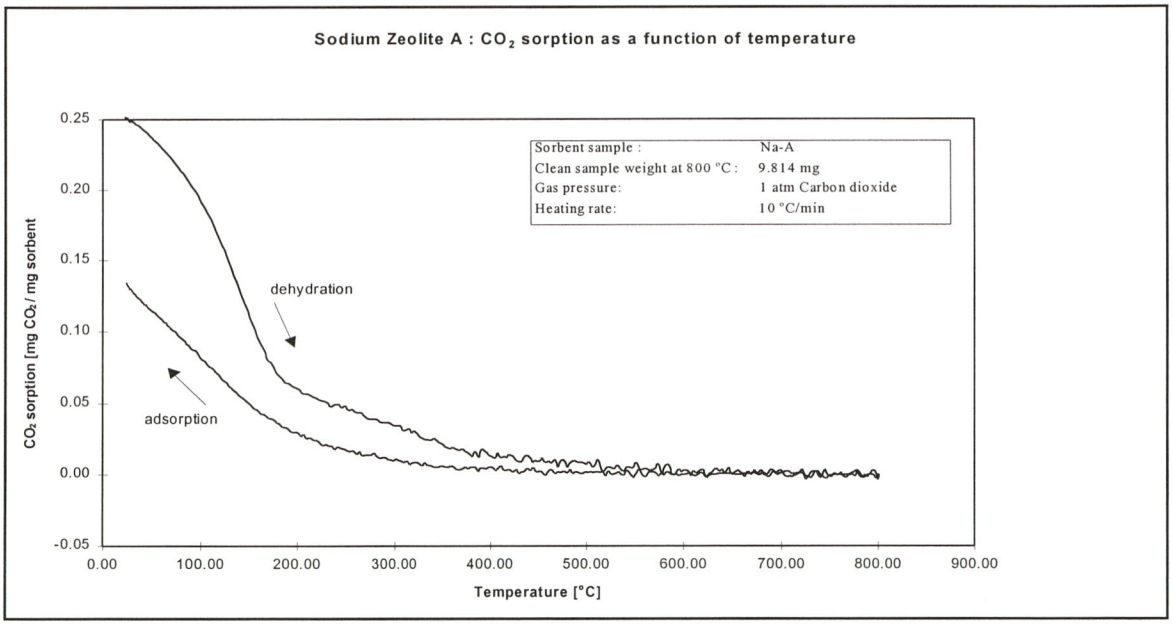

Figure 5.20 *Na Zeolite A: adsorption behavior at 1 atm CO_2 after initiation at 800 °C*

For magnesium and calcium, a comparison between the adsorption after initiation at 600 and 800 °C shows no signs of thermal instability. (Section 5.3: figures 5.29 and 5.30)

For strontium, the same comparison suggest also sufficient stability. However, when compared with the adsorption at 7.5 bara CO_2 an inconsistency occurs: the higher pressure

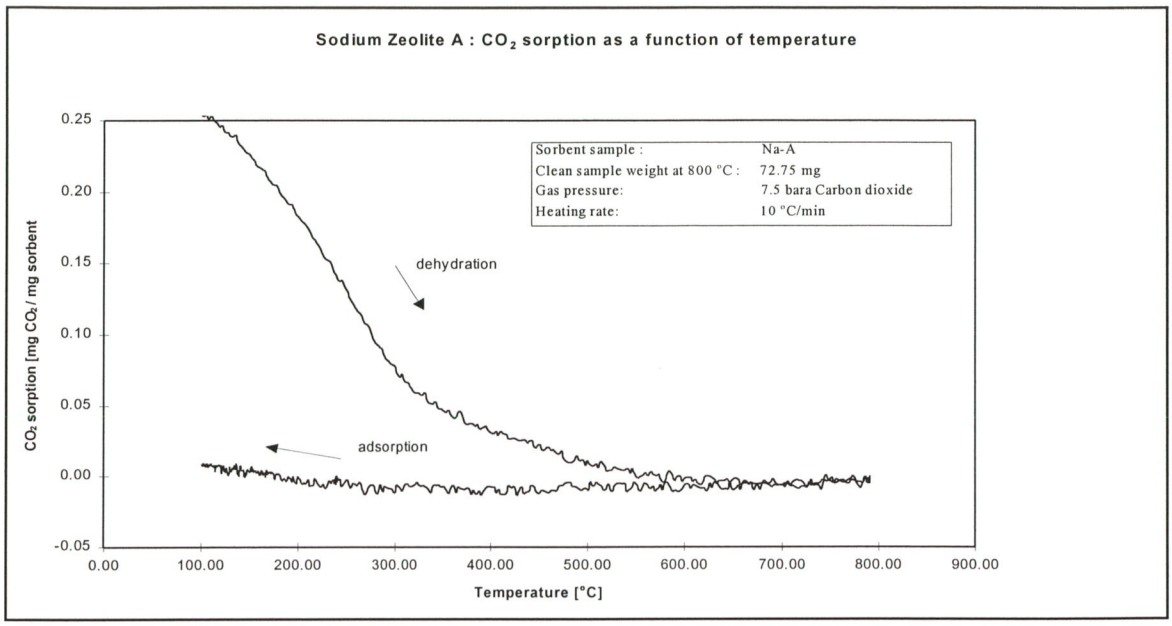

Figure 5.21 *Na Zeolite A: adsorption at 7.5 bara CO_2 after initiation at 800 °C*

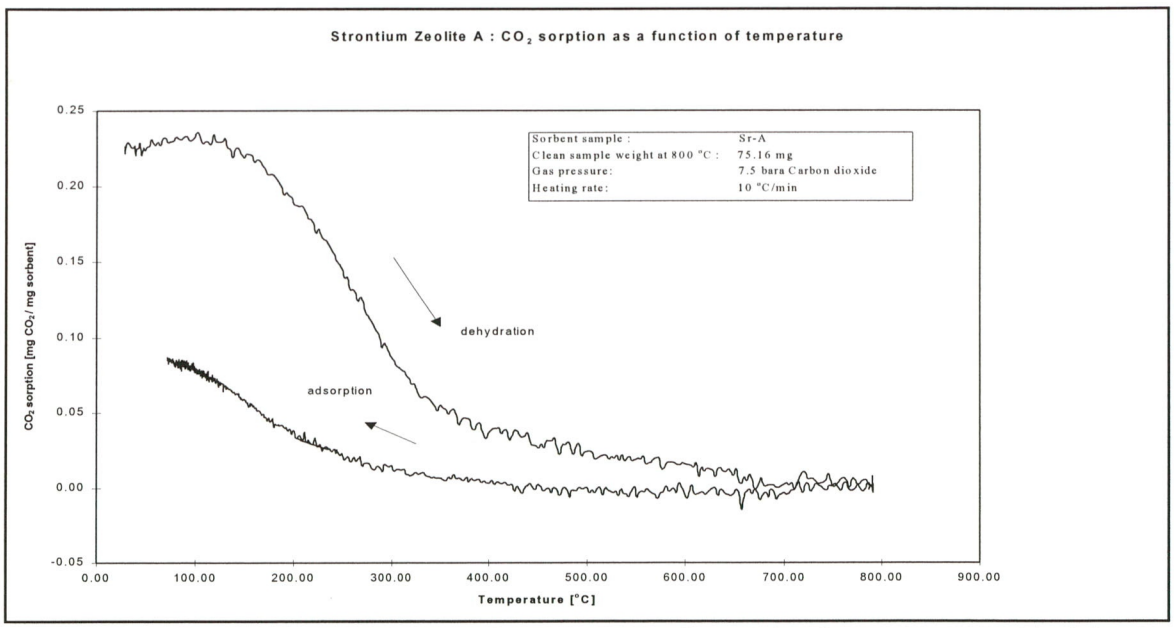

Figure 5.22 *Sr exchanged Zeolite A: adsorption at 7.5 bara CO_2 after initiation at 800 °C*

leaves the adsorption curve nearly unchanged. (Section 5.3: figure 5.34) Normally, the higher pressure would result in a higher capacity. Here, the increase of the period at 800 °C from 1 minute or five minutes in comparison with the atmospheric measurement is probably just enough to cause the loss in structure that is also seen in the XRD experiment. To test this explaination,

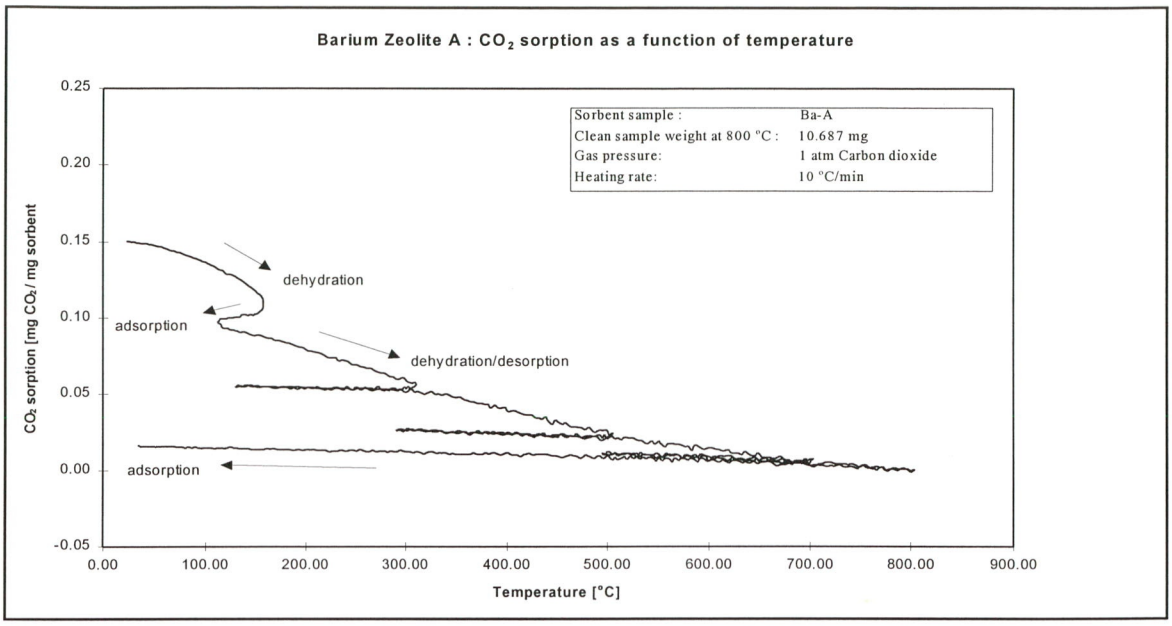

Figure 5.23 *Ba exchanged Zeolite A: adsorption at 1 atm CO_2 after initiation at several temperatures*

the high- pressure TGA experiment should, however, be repeated in order to exclude any coincidental errors in the measurements. Unfortunately, a confirmation at this stage is impossible due to technical problems with the TGA equipment.

For the barium samples, the experiments show a total lack of adsorption capacity. Even after an initiation at 150 °C, the material shows no signs of CO_2 adsorption as can be seen in figure 5.23. This confirms the amorphous character of the sample seen with the EDS and the XRD experiments.

Zeolite X:

For Na-Zeolite X, the adsorption curves show no change when the initial temperature is changed from 600 to 800 °C. Both temperatures give the same adsorption capacity of 0.21 mg/mg at 25 °C and 1 atm CO_2 pressure.

For calcium, the literature mentions a lower stability than for sodium. In the XRD experiments, some signs of structural decline are seen after heating to 800 °C. Nevertheless, in the TGA measurements that are given in figure 5.24 and 5.25, calcium shows no signs of decline. The curves for both initial temperatures are the same.

For strontium and barium, the capacity is strongly reduced by the higher initial temperature. After initiation at 600 °C, both samples show a capacity of 0.12 mg/mg at 25 °C and 1 atm CO_2 pressure. After initation at 800 °C, this capacity is reduced to 0.04 mg/mg for strontium and 0.07 mg/mg for barium. (Section 5.3: figures 5.35 and 5.36)

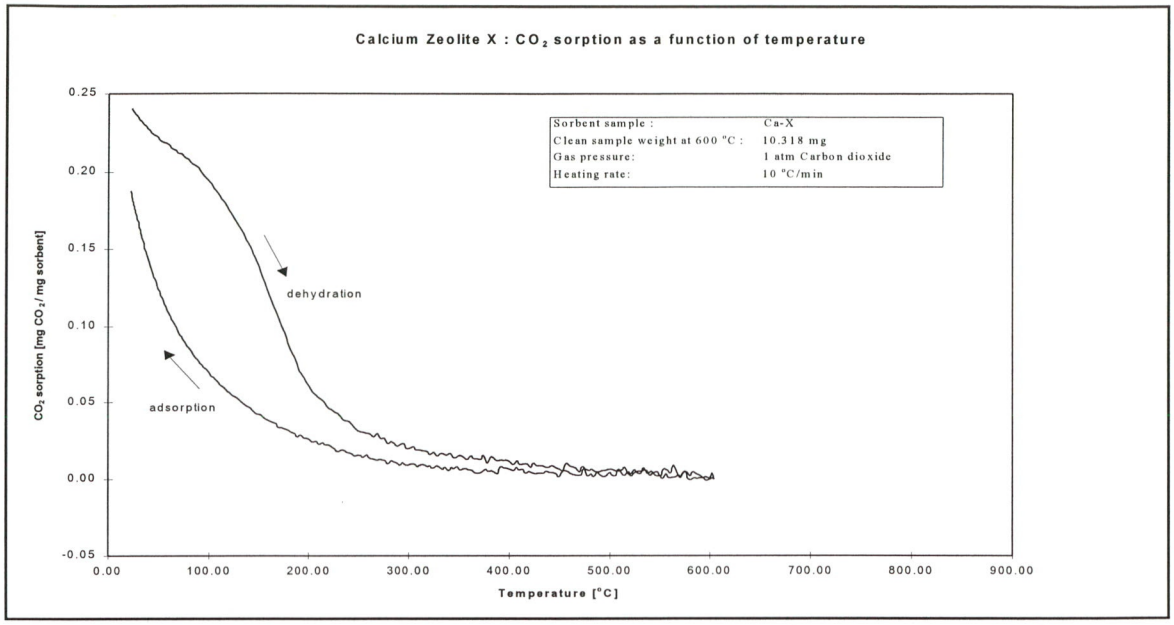

Figure 5.24 *Ca exchanged Zeolite X: adsorption at 1 atm CO_2 after initiation at 600 °C*

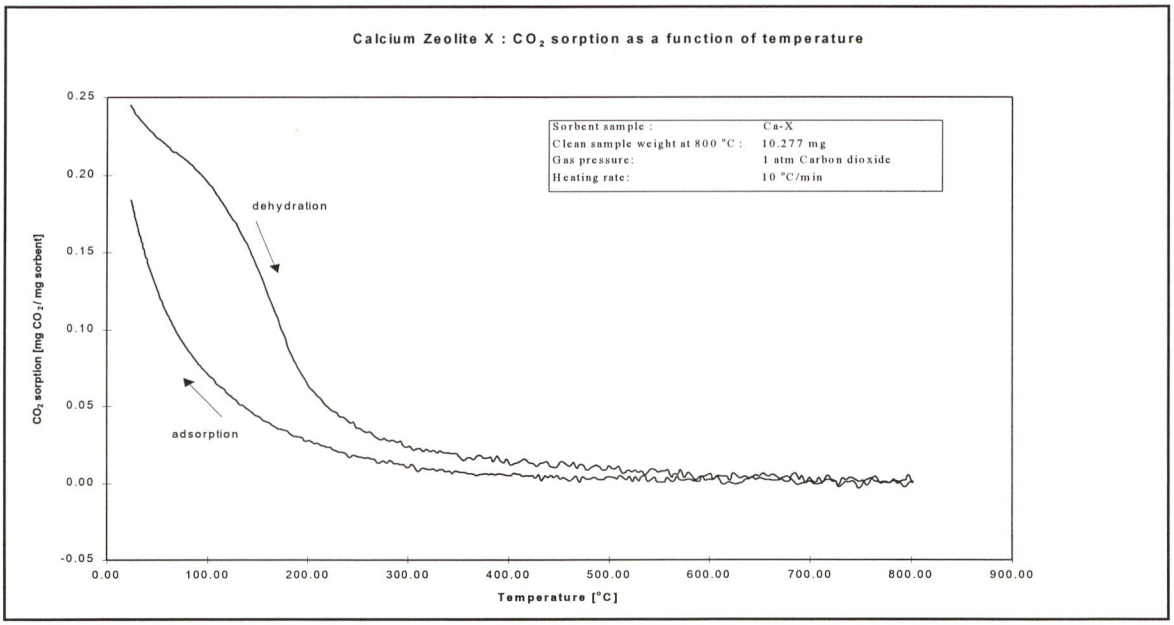

Figure 5.25 *Ca exchanged Zeolite X: adsorption at 1 atm CO_2 after initiation at 800 °C*

Zeolite P:

Figure 5.26 shows the typical results of an adsorption experiment with Zeolite P. In this case, the original material, Na-Zeolite P. The sample is alternately heated for dehydration and cooled

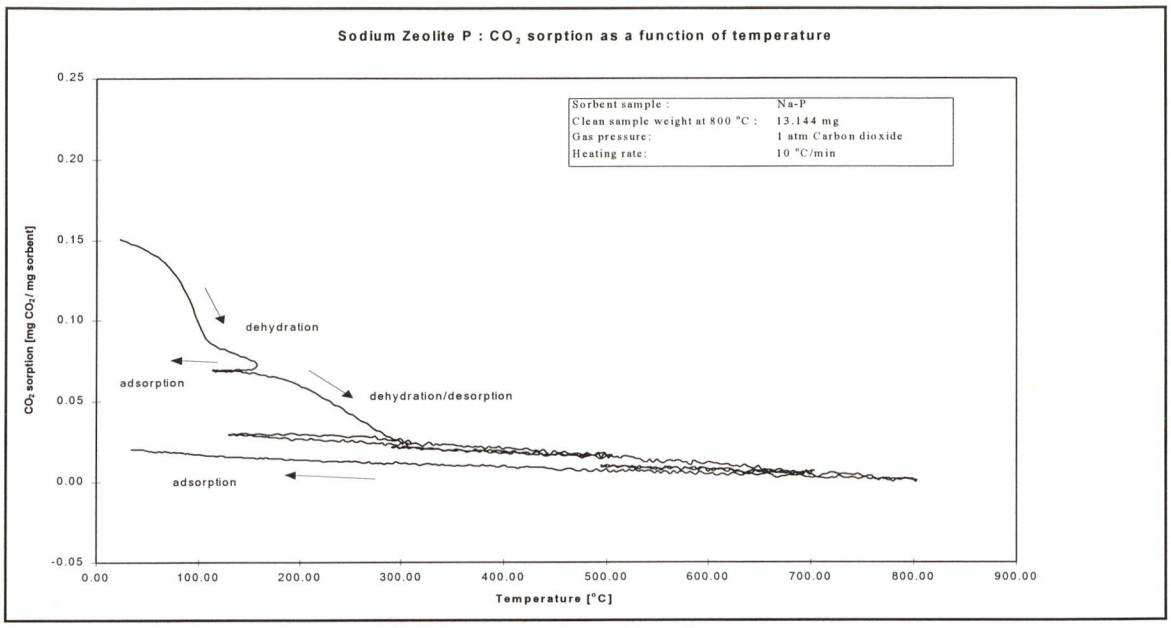

Figure 5.26 *Na Zeolite P: adsorption at 1 atm CO_2 after initiation at several temperatures*

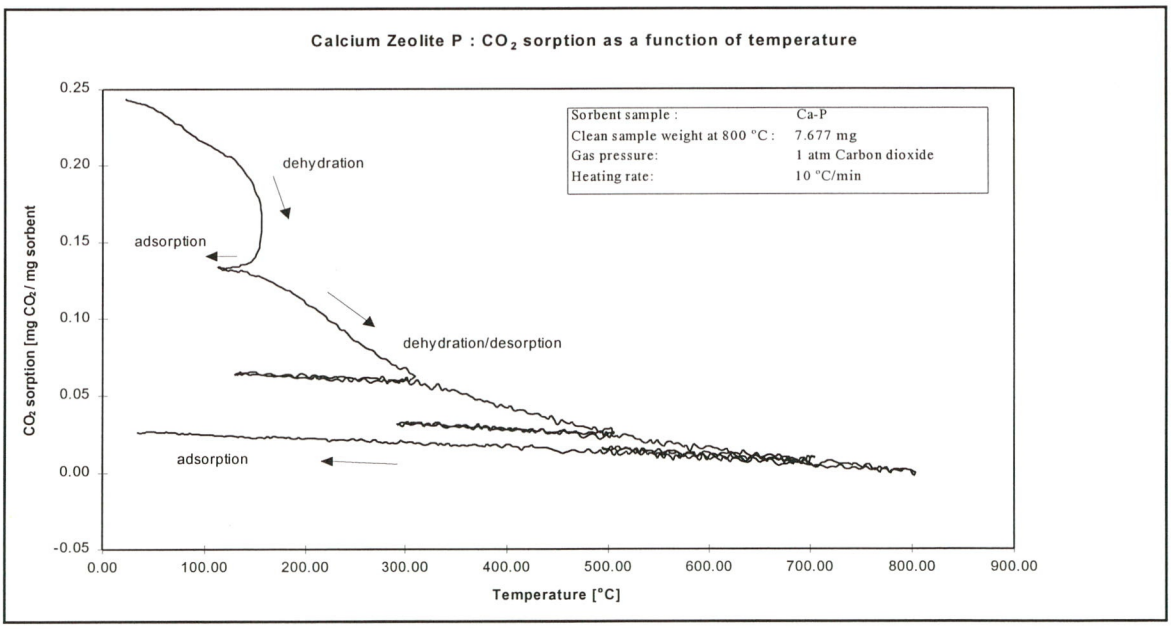

Figure 5.27 *Ca exchanged Zeolite P: adsorption at 1 atm CO_2 after initiation at several temperatures*

to test the adsorption capacity. Although, some weight gain is seen during adsorption, the capacity is so low that it is not interesting. The capacity resembles the capacity of other zeolites in group 1 who all have a very low capacity.

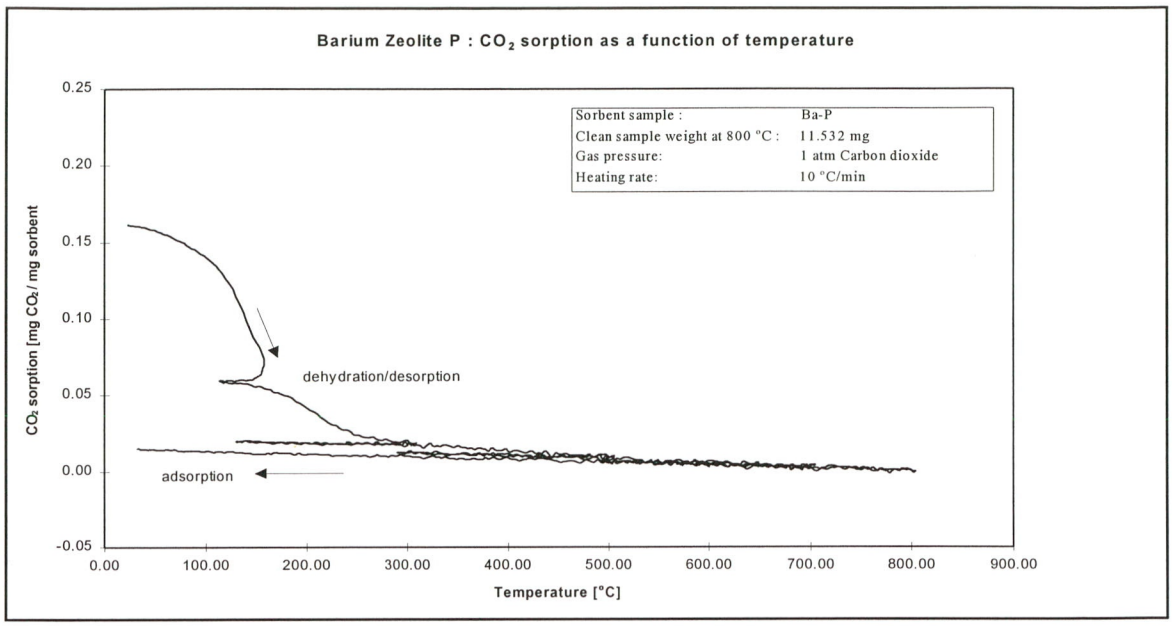

Figure 5.28 *Ba exchanged Zeolite P: adsorption at 1 atm CO_2 after initiation at several temperatures*

In the literature it is reported that Zeolite P might show a change in framework structure at moderate temperatures resulting in a reduction of the pore volume by 20 %. It is, however, suggested that this behavior depends on the actual conditions during the experiment and on the cations present. [Breck (1974), Dyer (1988)]

From figure 5.26, it can be seen that such a change in structure clearly takes place, already at temperatures as low as 150 °C. The presence of CO_2 is not enough to compensate the structural instability that is caused by the loss of water. The structural transformation is not reversed by the possible interaction with CO_2. A plausible cause could be that the new structure inaccessible for CO_2.

In figures 5.27 and 5.28, the results for the ion-exchanged samples are given. The presence neither of calcium nor of barium is improving the stability against structural transition. Both experiments show the same low adsorption capacity as seen for sodium.

Stability : summary

For Zeolite A, the TGA curves of the sodium and the strontium form initiated at 800 °C show a loss in adsorption capacity indicating insufficient stability. Some structural decline is confirmed by the XRD analysis of strontium . Calcium and magnesium proved to be stable at 800 °C.

For Zeolite X, the initial adsorption temperature of 800 °C caused a reduction of the capacity for strontium and barium. In the case of natrium and calcium, the capacity is unaffected. Yet, the XRD spectrum of calcium shows the first signs of structural decline.

For Zeolite P, all forms lose their original structure and their adsorption capacity at low temperatures. For Mordenite and Zeolite β, no instabilities were seen after initiation at 800 °C.

5.3 Adsorption

Zeolite A:

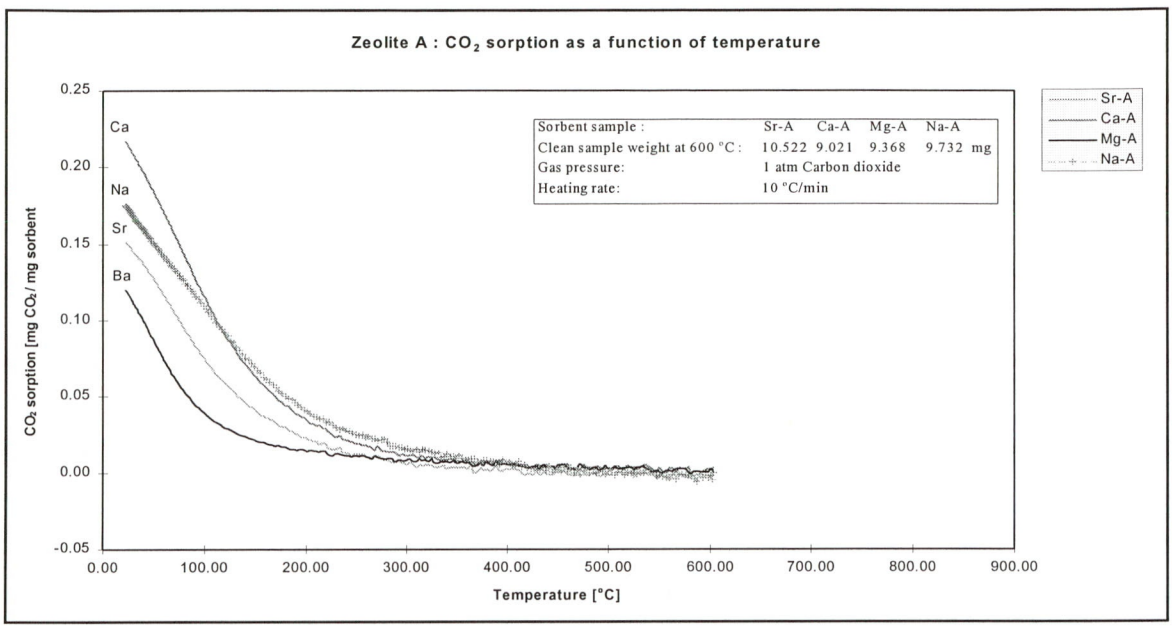

Figure 5.29 *Zeolite A: adsorption at 1 atm CO_2 for different cations after initiation at 600 °C*

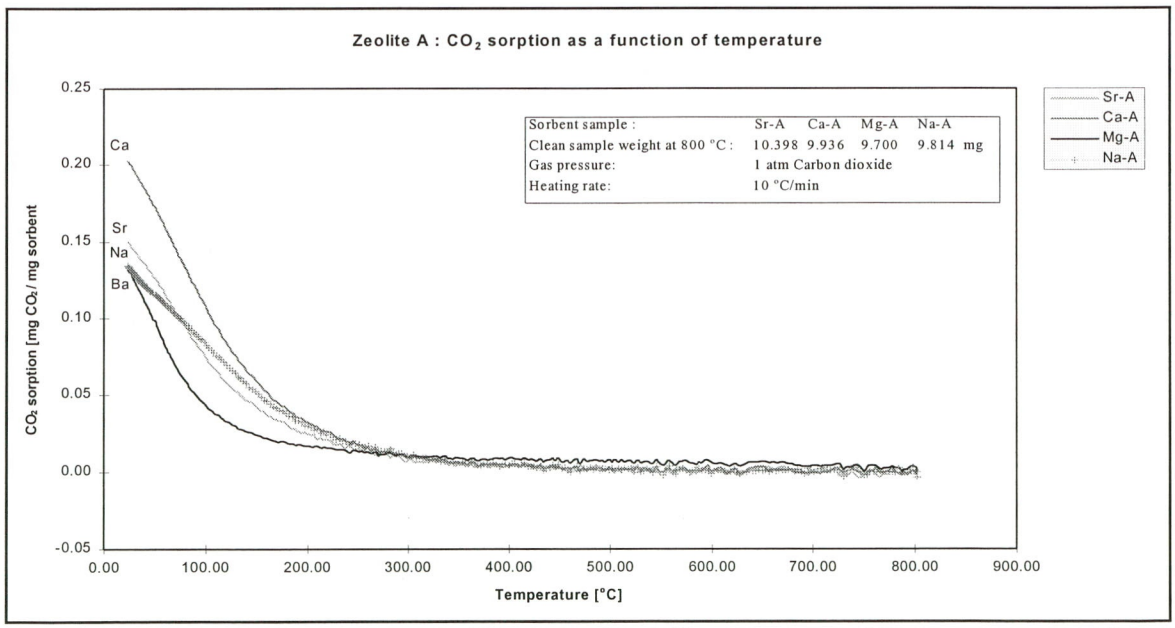

Figure 5.30 *Zeolite A: adsorption at 1 atm CO_2 for different cations after initiation at 800 °C*

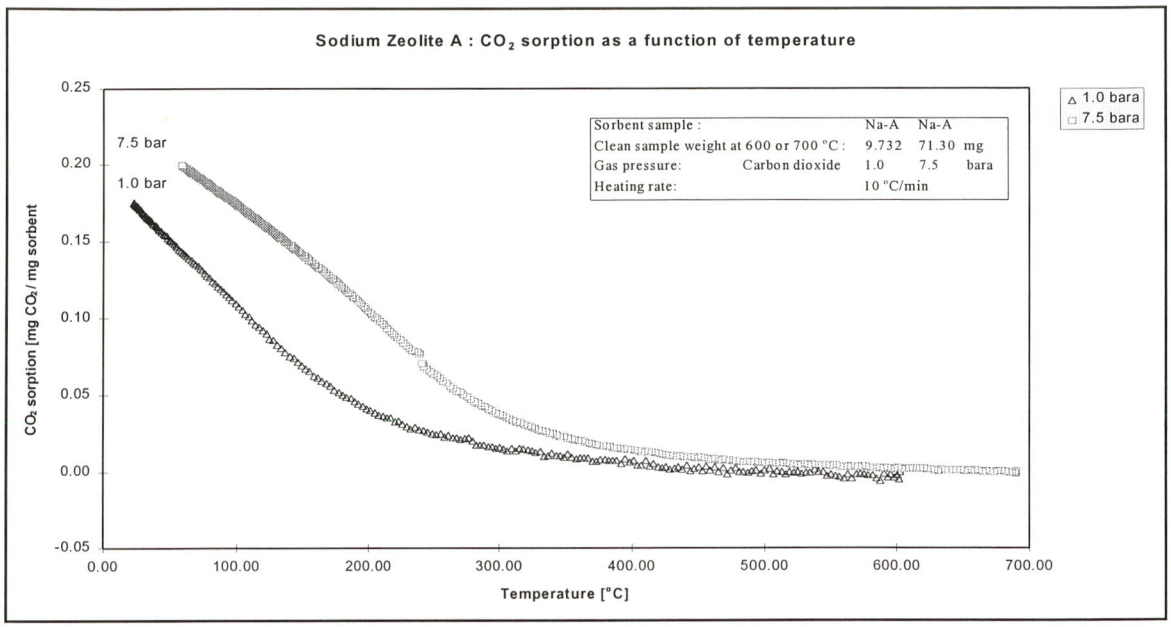

Figure 5.31 *Na Zeolite A: adsorption for 1.0 and 7.5 bara CO_2 after initiation at 600-700 °C*

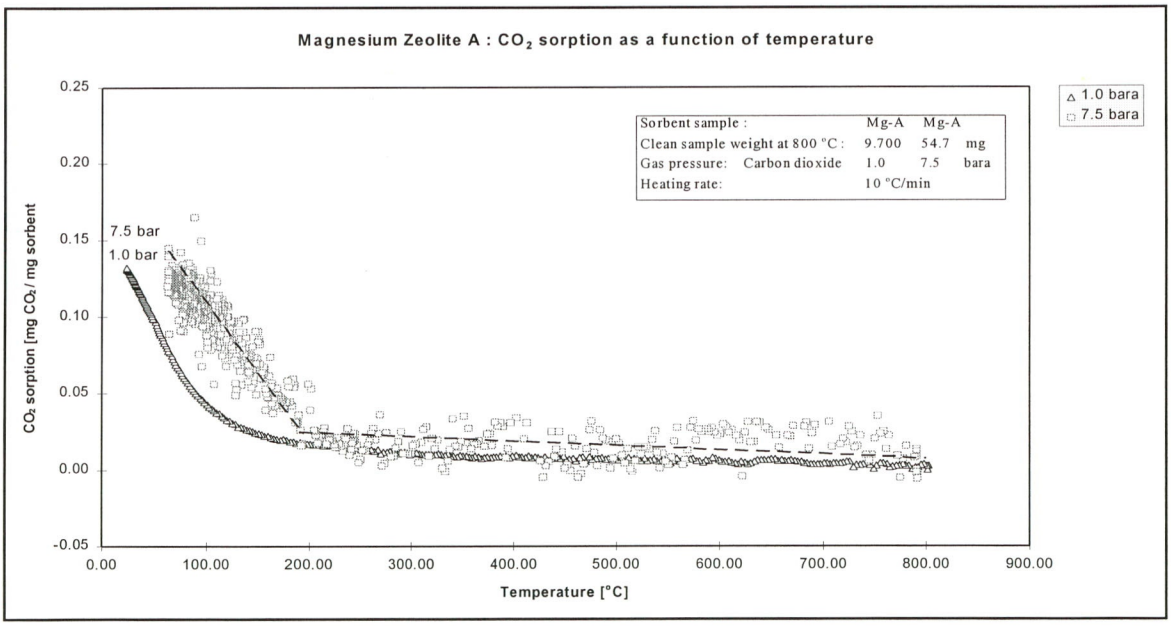

Figure 5.32 *Mg exchanged Zeolite A: adsorption for 1.0 and 7.5 bara CO_2 after initiation at 800 °C*

Figures 5.29 and 5.30 show the adsorption curves for different cations after initiation at 600 and 800 °C. The highest capacity is seen for Ca exchanged Zeolite A. The figures 5.31-5.34 show the influence of an increase in partial CO_2 pressure on the adsorption for different cations.

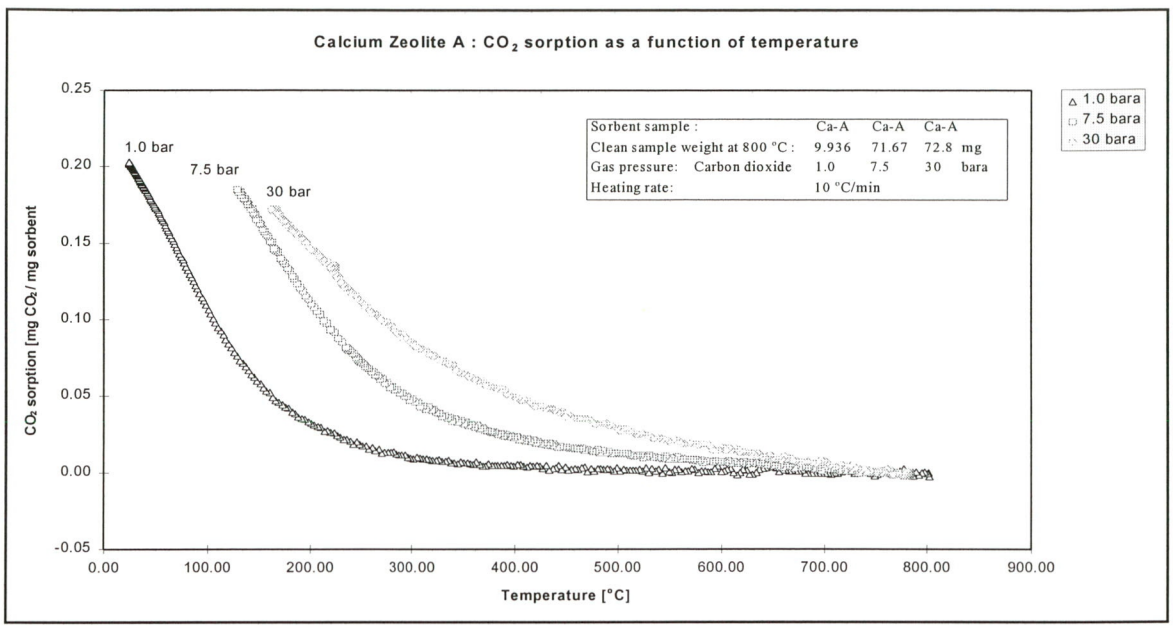

Figure 5.33 *Ca exchanged Zeolite A: adsorption behavior for 1.0, 7.5, and 30 bara CO_2 after initiation at 800 °C*

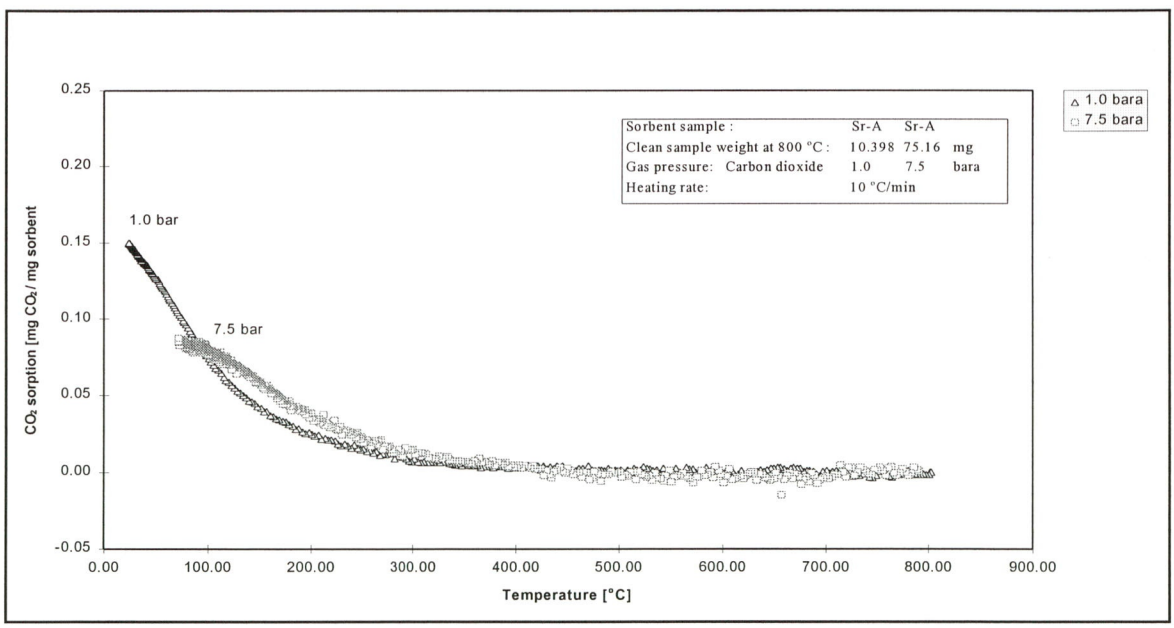

Figure 5.34 *Sr exchanged Zeolite A: adsorption for 1.0 and 7.5 bara CO_2 after initiation at 800 °C*

Taking its low stability into account, the initial temperature for Na-Zeolite A in the 7.5 bara CO_2 experiment was set at 700 °C instead of the 800 °C as used for the other cations. All

experiments with Na-Zeolite A initiated at 800 °C let to a complete loss of capacity.

Using the Clausius-Clapeyron relation (3.11), the heat of adsorption can be calculated from the adsorption curves in figure 5.31. In table 5.3 the results of these calculations are given as function of the CO_2 loading. The values of 58-42 kJ/mole calculated for a loading of 0-0.05 mg CO_2/mg sorbent are similar to those mentioned in the literature. [Breck (1974), Szotak (1992)]

Table 5.3 *Zeolite A: heat of adsorption ($\phi_{isosteric}$)*

Na-Zeolite A

loading (mg CO_2/mg sorbent)	*heat of adsorption in fig. 5.31 (kJ/mole)*	*reference data*	*(kJ/mole)*
0.025	58	46 ($\theta = 0.1$)	39 ($\theta = 0.4$)
0.050	42	51 ($\theta = 0.1$)	
0.100	32	54 ($\theta = 0.1$)	
0.150	25	43 ($\theta \approx 0.0$)	
0.175	24	46 ($\theta \approx 0.0$)	
		50 ($\theta \approx 0.0$)	

Mg-Zeolite A

loading (mg CO_2/mg sorbent)	*heat of adsorption in fig. 5.32 (kJ/mole)*	*reference data*	*(kJ/mole)*
0.025	53		
0.050	37		
0.100	40		
0.125	39		

Ca-Zeolite A

loading (mg CO_2/mg sorbent)	*heat of adsorption in fig. 5.33 (kJ/mole)*	*reference data*	*(kJ/mole)*
0.025	33 *) 39 **)	52 ($\theta = 0.1$)	33 ($\theta = 0.6$)
0.050	32 37	37 ($\theta \approx 0.0$)	
0.100	30 37	37 ($\theta \approx 0.0$)	
0.150	26 36	37 ($\theta \approx 0.0$)	
0.175	24 35	39 ($\theta \approx 0.0$)	

*) calculated from 1.0 and 7.5 bara data
**) calculated from 1.0 and 30 bara data

[Barrer (1978), Breck (1974), Dyer (1988), Haq (1986-1, 2), Kim (1994), Szotak (1992)]

The high pressure measurement for magnesium shows some noise in the recorded signal. This is probably caused by the dynamics of the pressure control used for the TGA equipment. Although the experiment was repeated several times, all resulting in similar adsorption curves, the noise could not be controlled or reduced.

For calcium, adsorption was measured both at 7.5 and 30 bara CO_2. The 7.5 bar measurement was performed several times. During one of these experiments, a sample was taken twice through a cycle of desorption and adsorption while afterwards still showing the same capacity.

In table 5.3, two $\phi_{isosteric}$ series for calcium are given which have been calculated using either the 7.5 bar or the 30 bar data in combination with the 1.0 bar data. Both series resemble the values mentioned in the literature reasonably well. As fas as the large difference with the 52 kJ/mole, reported as initial heat of adsorption by Breck [(1974)], is concerned, it should be mentioned that in this range the calculation is highly sensible to errors as a result of the flat slope in the curves. Comparing both $\phi_{isosteric}$ series, it becomes clear that the accuracy of the high-pressure TGA measurements and the calculated heats of adsorption is not extremely high. The use of a different method to determine the heats of adsorption should, therefore, be considered.

The results of the 7.5 bar experiment with strontium in figure 5.34 have already been discussed in section 5.2.2. Between 50-150 °C, the adsorption curves of 1.0 bara and of 7.5 bara almost coincide, which is very unlikely to appear with increasing pressure. In addition, the smoothing of the 7.5 bara curve in this range is striking.

Between 150-800 °C, the distance between the curves looks in itself all right, but with the low adsorption loading it is difficult to determine whether or not the capacity is affected by a lack of structural stability.

Zeolite X:

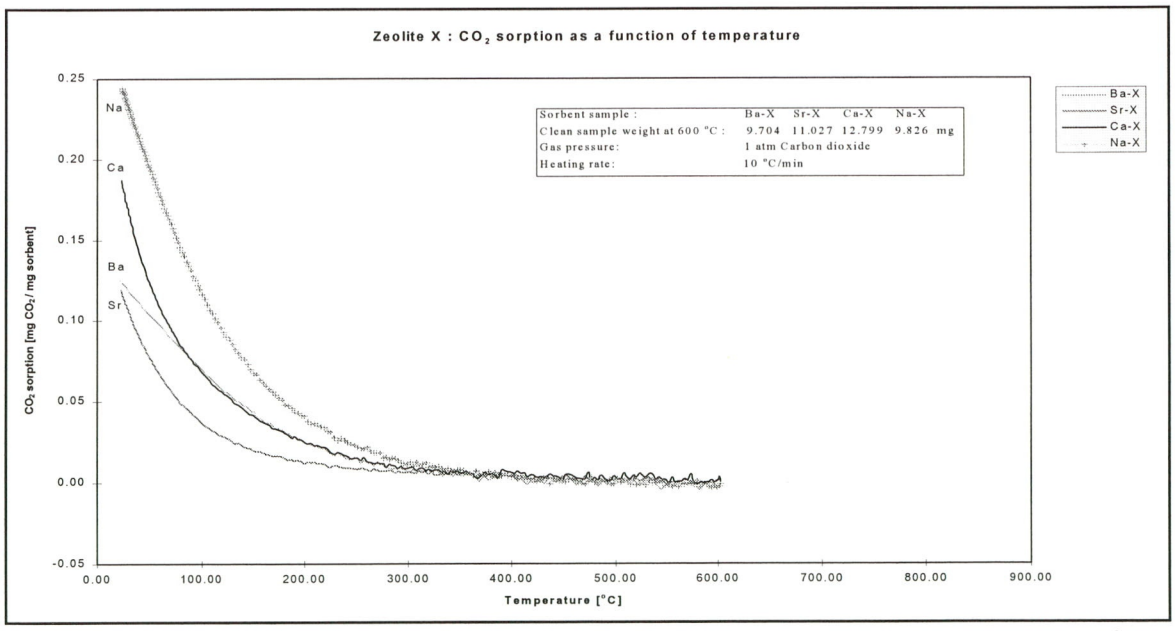

Figure 5.35 *Zeolite X: adsorption at 1 atm CO_2 for different cations after initiation at 600 °C*

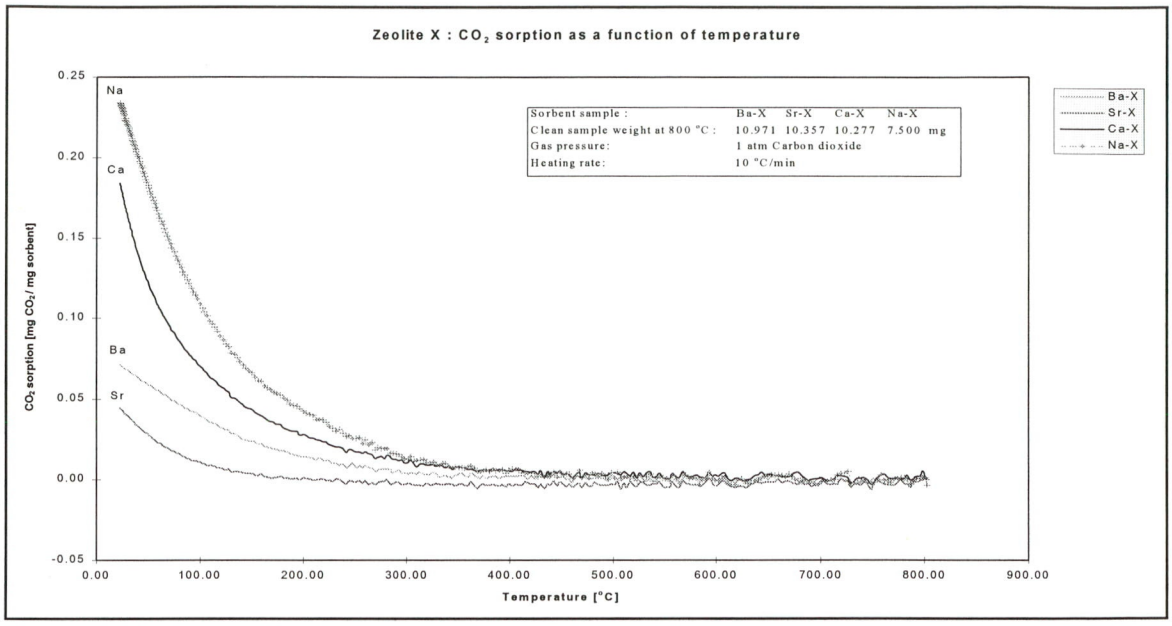

Figure 5.36 *Zeolite X: adsorption at 1 atm CO_2 for different cations after initiation at 800 °C*

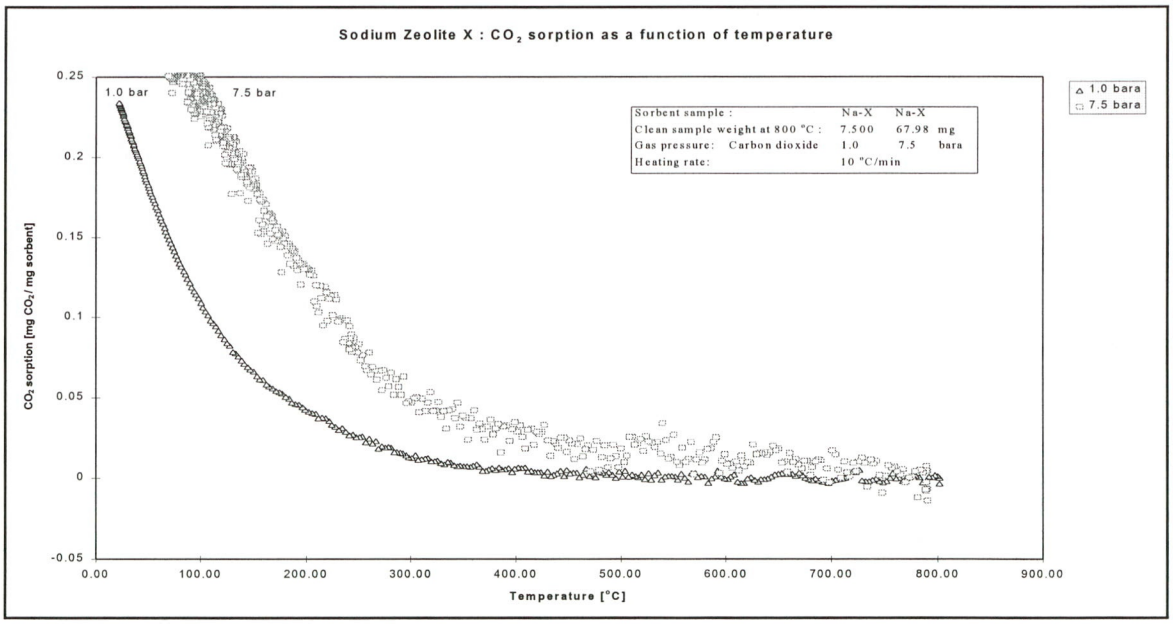

Figure 5.37 *Na Zeolite X: adsorption for 1.0 and 7.5 bara CO_2 after initiation at 800 °C*

Figures 5.35 and 5.36 give the adsorption curves of Zeolite X samples with different cations after dehydration at 600 or 800 °C. The best result is shown by the Na-Zeolite X sample, while the Ca-Zeolite X has a capacity equal to Na-Zeolite A.

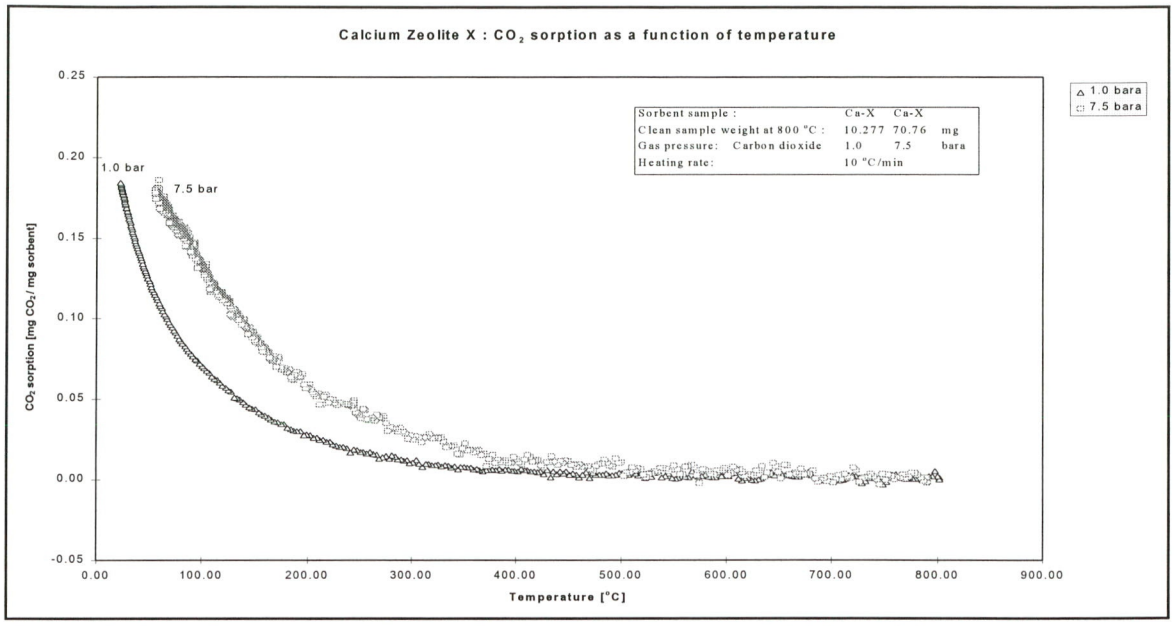

Figure 5.38 *Ca exchanged Zeolite X: adsorption for 1.0 and 7.5 bara CO_2 after initiation at 800 °C*

In figures 5.37 and 5.38, the adsorption behavior of Na-Zeolite X and Ca-Zeolite X is seen for 1.0 and 7.5 bara CO_2 pressure. Both experiments used an initial temperature of 800 °C which did not let to any signs of structural decomposition.

In table 5.4, the heats of adsorption for both samples are compared with values mentioned in the literature. Although the values for sodium are somewhat lower than expected when compared with the ones reported by Breck [(1974)] or by Gerhartz [(1988-B3)], they differ only slightly from the value mentioned by Kim [(1994)] and Chue [(1995)].

It is possible that the differences are caused by a different Si/Al ratio for the samples and the

Table 5.4 *Zeolite X: heat of adsorption ($\phi_{isosteric}$)*

Na-Zeolite X

loading (mg CO_2/mg sorbent)	*heat of adsorption in fig. 5.37 (kJ/mole)*	*reference data*	*(kJ/mole)*
0.025	35	51 ($\theta \approx 0.0$)	44 ($\theta = 0.2$)
0.050	38		36 ($\theta = 0.8$)
0.100	27	36 (0.04 mg/mg)	36 (0.12 mg/mg)
0.150	24		33 (0.22 mg/mg)
0.200	24	46 ($\theta \approx 0.0$)	
0.225	24		

Ca-Zeolite X

loading (mg CO_2/mg sorbent)	*heat of adsorption in fig. 5.38 (kJ/mole)*	*reference data*	*(kJ/mole)*
0.025	44	48 ($\theta = 0.1$)	46 ($\theta = 0.2$)
0.050	41		37 ($\theta = 0.8$)
0.100	33	48 (0.04 mg/mg)	33 (0.10 mg/mg)
0.150	38		
0.175	49		

[Barrer (1964, 1978), Breck (1974), Chue (1995), Dyer (1988), Gerhartz (1988-B3), Kim (1994), Szostak (1992)]

references. Insufficient information makes it difficult to check this hypothesis, but the values here resemble the 31-34 kJ/mole given for Na-Zeolite Y in table 3.13 and 3.15.

For calcium, the values match those given by the references quit well. The 49 kJ/mole for 0.175 mg CO_2/mg clean sorbent is, however, too high and is also not in line with the normal pattern of an adsorption curve. Normally, the heat of adsorption becomes less with high loadings. As on why it becomes higher in this case, a coincidental error in the measurement is most likely explanation.

Mordenite:

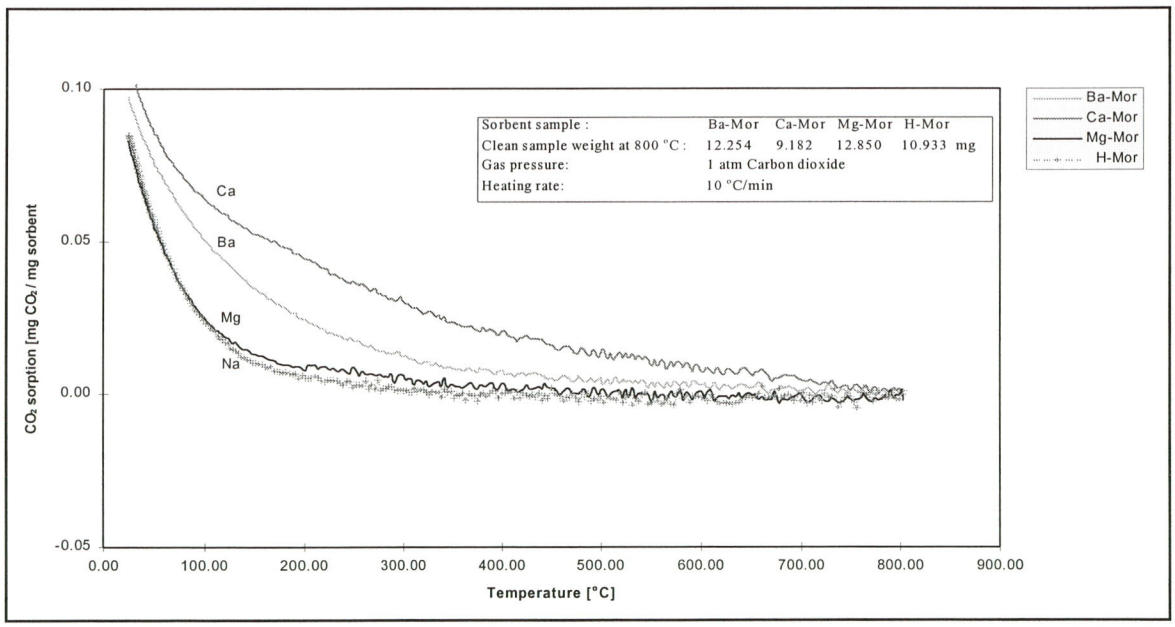

Figure 5.39 *Mordenite: adsorption at 1 atm CO_2 for different cations after initiation at 800 °C*

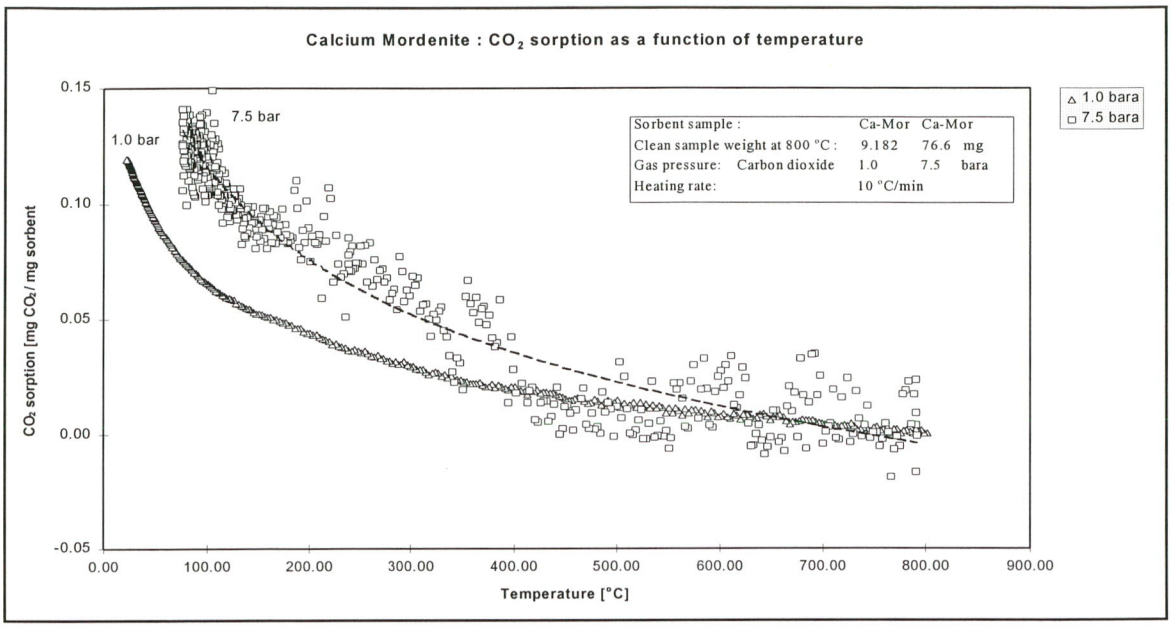

Figure 5.40 *Ca exchanged Mordenite: adsorption for 1.0 and 7.5 bara CO_2 after initiation at 800 °C*

Figure 5.39 shows that the capacity of Mordenite at moderate elevated temperatures is improved by the ion-exchange with Ca and Ba ions. With 10-12 mg/mg, the maximum capacity is however not as high as for Zeolite A and X.

Surprisingly, the adsorption curve of magnesium coincides with the curve of H-Mordenite. Based on the adsorption data of other gases which are shown in table 5.5, the magnesium curve would be expected to lie above the curve of calcium. The fact that the curve shows no difference with H-Mordenite suggests that the ion-exchange of H-Mordenite with magnesium ions has not been successful.

Table 5.5 *Mordenite: initial heat of adsorption ($\theta = 0.02$) for several gases (kJ/mole gas)*

cation *adsorbate*	*Ar*	*O_2*	*N_2*	*NO*	*CO*	*CO_2*
H	18	18	23-25	23	29	43-50
Na	18	19	28	28	34	61-65
Mg	24	31	54	42-63	66	-
Ca	26	27	41	38-42	50	-
Ba	23	23	31	33	39	-

[Barrer (1978), Furuyama (1982, 1984-1 and -2)]

For Ca-Mordenite, the effects of pressure on the adsorption are given in figure 5.40. The high-pressure adsorption experiment shows much noise in the recorded signal. Although a trendline can be seen, it is difficult to determine exactly the minimum value needed for the meaningful comparison with the atmospheric adsorption experiment. The results are, therefore, not very useful and the experiment should be repeated. Unfortunately, this is impossible at the moment due to technical problems with the equipment.

Table 5.6 *Mordenite: heat of adsorption ($\phi_{isosteric}$)*

Ca-Mordenite

loading (mg CO_2/mg sorbent)	*heat of adsorption in fig. 5.40 (kJ/mole)*	*reference data*	*(kJ/mole)*
0.025	56	*H-Mor:*	
0.040	35	43 (0.0 mg/mg)	32 (0.08 mg/mg)
0.050	31	46 ($\theta \approx 0.0$)	
0.100	26	50 ($\theta \approx 0.0$)	
0.120	26	*Na-Mor:*	
		61 (0.0 mg/mg)	45 (0.08 mg/mg)
		65 ($\theta \approx 0.0$)	

[Barrer (1978), Breck (1974), Ma (1972), Szostak (1992)]

The heat of adsorption which is calculated with these data is somewhat lower than expected. Nevertheless, given the bad recording and the inaccuracy seen for the determination of the initial heat of adsorption, the 56 kJ/mole is an acceptable value.

Although no references have been found for the calcium, H-Mordenite and Na-Mordenite have an initial $\phi_{isosteric}$ of 40-65 kJ/mole. When looking at the adsorption of other gases as shown in table 5.5, it can be expected that Ca-Mordenite has a $\phi_{isosteric}$ higher than Na-Mordenite. Using a concept introduced by Barrer [Barrer (1978), Breck (1974)] in which initial heats are plotted against the polarizability of the adsorbate, it is possible to get an impression of the initial heat for CO_2 by extrapolation. The initial $\phi_{isosteric}$ for Ca-Mordenite is, therefore, estimated to be 70-80 kJ/mole.

Zeolite Beta:

In figure 5.41, the adsorption curves of Zeolite Beta with different cations are compared. The best results are seen for Ca-Zeolite Beta. At moderate temperatures, this sample clearly shows a higher capacity. The magnesium and the sodium samples differ only a bit of the original material H-Zeolite Beta.

With 10 mg/mg, the maximum capacity is similar to that of Mordenite but only half of the capacity seen for Zeolite A and X.

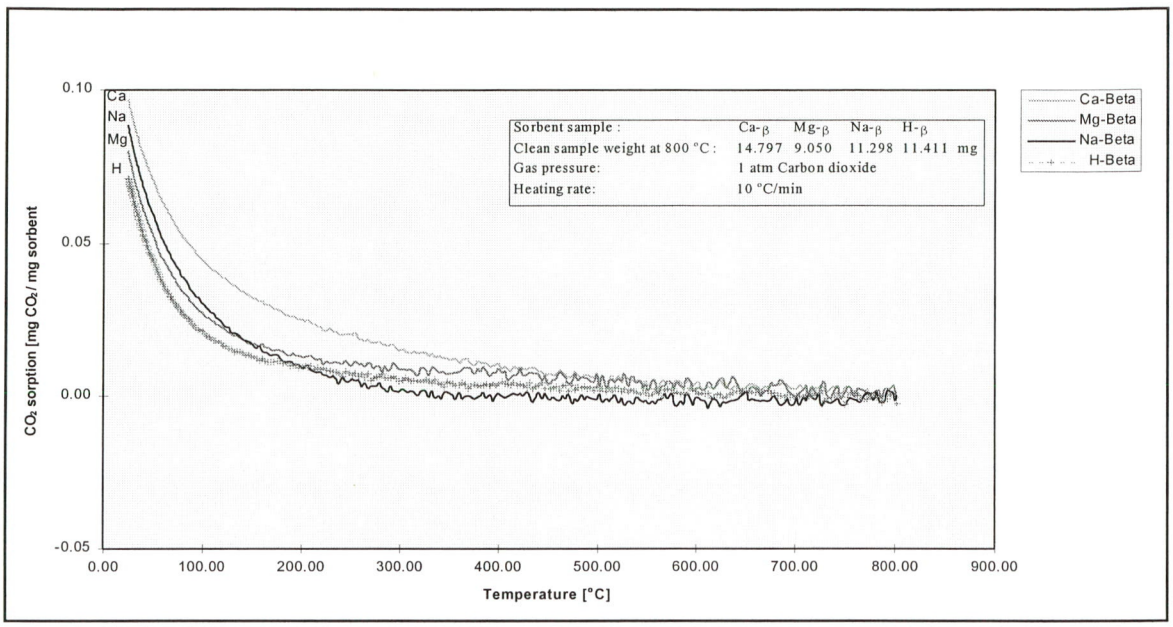

Figure 5.41 *Zeolite β: adsorption at 1 atm CO_2 for different cations after initiation at 800 °C*

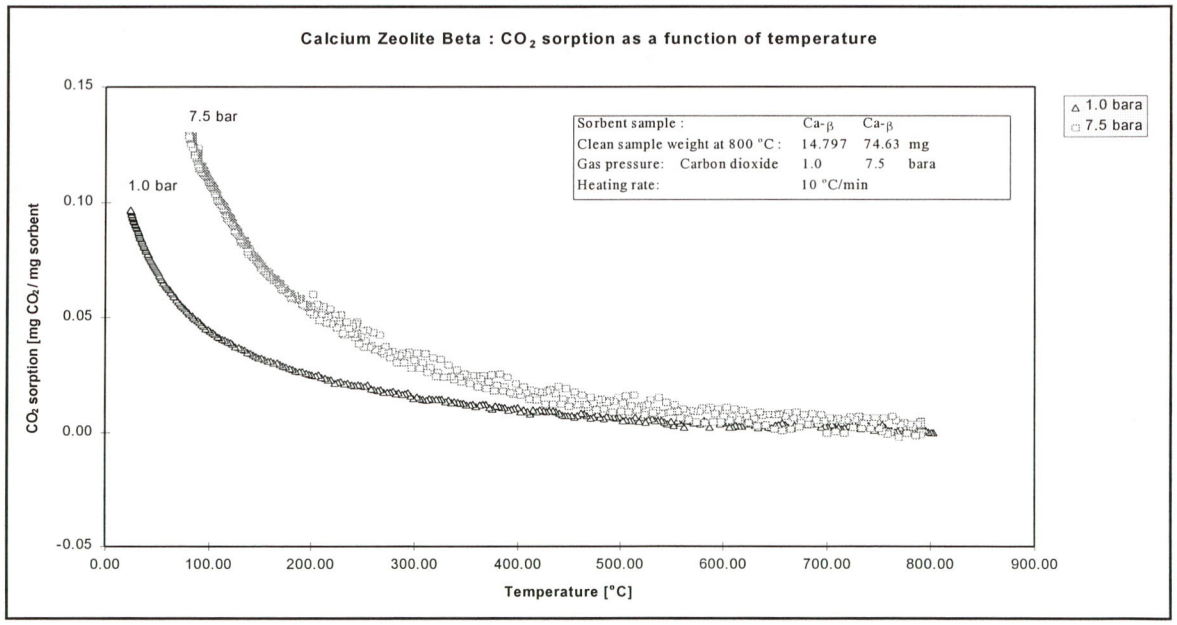

Figure 5.42 *Ca exchanged Zoelite β: adsorption for 1.0 and 7.5 bara CO_2 after initiation at 800 °C*

For Ca-Zeolite Beta, the adsorption is also measured at 7.5 bara CO_2. The results of this experiment are plotted together with the 1.0 bara data in figure 5.42. The heat of adsorption is

given in table 5.7. Little is known about Zeolite Beta, so no references are available to check the calculated values. The 36 kJ/mole found as heat of adsorption for 0.025 mg loading is, however, a reasonable value.

Table 5.7 *Zeolite Beta: heat of adsorption ($\phi_{isosteric}$)*

Ca Zeolite Beta

loading (mg CO_2/mg sorbent)	*heat of adsorption in fig. 5.42 (kJ/mole)*	*reference data (kJ/mole)*
0.025	36	no references
0.040	25	
0.050	23	
0.070	22	
0.090	21	

5.4 Discussion

Zeolite A:

The thermal stability of the Zeolite A samples is limited to 700-800 °C and decreases in the sequence:

$$thermal\ stability:\ \ Ca\text{-}A > Mg\text{-}A > Sr\text{-}A > Na\text{-}A > Ba\text{-}A$$

The Ba-Zeolite A sample became already amorphous during the ion-exchange as is confirmed by EDS, XRD, and TGA measurements. The instability of Na-Zeolite A was seen in all TGA measurements that had an initial temperature of 800 °C. Further confirmation by XRD was thought to be dispensable. For Sr-Zeolite A, the invariability of the TGA curve in response to pressure and the baseline changes in the XRD signal were seen as indications of its instability. Magnesium showed only some peak broadening in the XRD without affection of its adsorption capacity. Ca-Zeolite A was the only sample that did not show any signs of instability at 800 °C.

The thermogravimetric adsorption measurements show that the capacity for Zeolite A decreases in the sequence:

$$adsorption\ capacity:\ \ Ca\text{-}A > Na\text{-}A > Sr\text{-}A > Mg\text{-}A$$

The highest adsorption is seen for Ca-Zeolite A. The capacity at 25 °C and 1.01 bar CO_2 reaches 0.22 mg/mg clean sorbent, which agrees well with the 0.24 mg/mg at 25 °C and 0.93 bar CO_2 mentioned by Breck. [(1974)]

With its adsorption heat of ~ 37 kJ/mole, the capacity at 325-350 °C is, however, reduced to 0.01-0.02 mg/mg. An increase in CO_2 pressure from 1.0 bar to 7.5 bar results only in a capacity of 0.03-0.04 mg/mg. These values are too low to be interesting for a high-temperature adsorption process in an IGCC power plant. Such a Temperature Swing Adsorption (TSA) process should be operated between 325 and 500-800 °C, if it is to use the high temperature exergy without consuming energy in such a way that the plant efficiency is negatively influenced.

For a moderate-temperature TGA process that only aims at reducing the compression work, Ca-Zeolite A provides an option that is worth considering. In addition, Na-Zeolite A shows also sufficient capacity and should not be excluded, although Ca-Zeolite A is clearly preferred for its higher stability and capacity.

Zeolite X:

The different measurement show that the thermal stability of Zeolite X reaches approximately to 800 °C depending on the cation present:

$$thermal\ stability:\ Na\text{-}X,\ Ca\text{-}X > Sr\text{-}X,\ Ba\text{-}X$$

The TGA experiments with different initial temperatures proved that the adsorption of the strontium and barium samples was negatively influenced at 800 °C. For calcium, an XRD recording of a sample initiated at 800 °C showed a loss in intensity and some peak changes, but this did not result in a reduced adsorption capacity.

The adsorption measurements using TGA show that the capacity for Zeolite A decreases in the sequence:

$$adsorption\ capacity:\ Na\text{-}X > Ca\text{-}X > Ba\text{-}X > Sr\text{-}X$$

The best adsorption is seen for Na-Zeolite X, which has a capacity of 0.24 mg/mg at 25 °C and 1.01 bar CO_2. This value is similar to the 0.26 mg/mg at 25 °C and 0.93 bar CO_2 reported by Breck. [(1974)] and the 0.21 mg/mg at 15 °C and 1.01 bar by Kim. [(1994)]

The order in the sequence as was found here differs from those reported elsewhere in the literature:

$$Breck\ \ adsorption\ capacity:\ Ca\text{-}X > Na\text{-}X$$

Breck [(1974)]: 25 °C, 0.93 bar, initial temperature 350-400 °C

Barrer adsorption capacity: $Na-X > Sr-X$, $Ba-X > Ca-X$

Barrer [(1964)]: 30 °C, 0.07 bar, initial temperature 350°C

The sequence reported by Barrer was measured between 0-0.07 bar CO_2 and extrapolation of the curves suggest that the curve for calcium will cross those of strontium and of barium between 0.07-1.0 bar. Whether the sodium curve is crossed by calcium is less clear.

Breck reports an adsorption capacity of 0.29 mg/mg for Ca-Zeolite X, which is considerably higher than the 0.18 mg/mg found in this study. The origin of this difference is not directly clear. If it is caused by the different initial temperature, this would indicate that Ca-Zeolite X loses its stability between 400 and 600 °C. In that case, it seems however unlikely that adsorption is still seen after initiation at 800 °C.

For a high-temperature TSA process, the adsorption capacity above 350 °C and the heat of adsorption are too low. For a moderate-temperature process, both Na-zeolite X and Ca-Zeolite X show sufficient capacity.

Mordenite:

Although it is questionable whether the preparation of the magnesium sample has been successful, all Mordenite samples could endure the initial temperature of 800 °C.

The adsorption capacity as measured with TGA is given by the following sequence:

adsorption capacity: $Ca-Mor > Ba-Mor > H-Mor$

For Ca-Mordenite, the capacity at 25 °C and 1.01 bar CO_2 is 0.12 mg/mg, and 0.03-0.04 at 325-350 °C. Although higher than the Zeolites A and X, the capacity is still too low to be interesting for a high-temperature TSA process.

Magnesium is, however, thought to have a heat of adsorption of 75-85 kJ/mole, which is higher than the objective of 70 kJ/mole. Magnesium could, therefore, have a capacity that might be high enough for a high-temperature TSA process.

For a TSA process at moderate temperatures, the capacity of Mordenite is too low in comparison with the other zeolites to be interesting.

Zeolite P and Zeolite Beta:

As shown in the TGA experiments, all samples of Zeolite P lost their capacity at low temperatures and are therefore unsuitable for a TSA process.

The Zeolite Beta samples showed no signs of instability after initiation at 800 °C. XRD and other spectroscopic analysis will have to give more exact information on the composition and the

stability before profound conclusions can be drawn.

So far, the TGA experiments suggest that the adsorption capacity follows the sequence:

$$adsorption\ capacity:\quad Ca\text{-}\beta > Mg\text{-}\beta,\ Na\text{-}\beta,\ H\text{-}\beta$$

The best result is seen for Ca-Zeolite Beta, but its capacity of 10 mg/mg and its heat of adsorption of 36 kJ/mole are too low for either a high-temperature TSA or a moderate-temperature TSA.

5.5 Conclusions

As can be seen from table 5.8, Na-Zeolite X is preferred for the moderate-temperature TSA process, but Ca-Zeolite A and Na-Zeolite A could also be used.

Table 5.8 *Summary of the main results*

Moderate-temperature TSA process: adsorption 125 °C and desorption 500-800° C

	pressure (bara CO_2)	temperature (°C)	preference: * Na-Zeolite X > Ca-Zeolite A > Na-Zeolite A > Ca-Zeolite X			
adsorption capacity (mg CO_2/mg sorbent)	1.0	25	0.24	0.22	0.18	0.18
	1.0	125	0.10	0.09	0.09	0.06
	7.5***	125	0.21	0.19	0.15	0.12
heat of adsorption at 0.025 mg/mg (kJ/mole)			35 (36-51)**	39 (37-52)**	58 (39-54)**	44 (48-48)**

*) thermal stability: Na-Zeolite X, Ca-Zeolite A > Ca-Zeolite X > Na-Zeolite A
**) values from references in the literature.
***) the partial pressure of CO_2 during adsorption in a IGCC power plant

High-temperature TSA process: adsorption 325 °C and desorption 500-800 °C

	pressure (bara CO_2)	temperature (°C)	preference: * Mg-Mordenite	> Ca-Mordenite
adsorption capacity (mg CO_2/mg sorbent)	1.0	325	.... (> 0.03)	0.03
	7.5	325	.... (> 0.05)	0.05
heat of adsorption at 0.025 mg/mg (kJ/mole)			.... (~75-85)**	~56 *** (~70-80)**

*) thermal stability: Mg-Mordenite ≈ Ca-Mordenite
**) estimated values based on data for other gases from references in the literature.
***) the value measured in this study is not very exact and probably too low.

In a study into Pressure Swing Adsorption (PSA) processes for CO_2 in air separation by Inui et al. [(1988)], the same zeolites are mentioned as good choices, but as the best choice Chabazite is mentioned.

For a high-temperature TSA process, the best adsorption capacity at 325 °C is expected for Mg-Mordenite. Unfortunately, the results on magnesium given in this study are questionable and therefore of no use. Based on the similarity between the data for other gases, it is however estimated that capacity should higher than 0.05 mg/mg at 325 °C and 7.5 bar CO_2.

Summarizing, it can be said that several zeolites have been found that could act as an adsorbent for a moderate-temperature TSA process, but no concrete absorbents are available for a high-temperature TSA process.

This raises the question whether the operation of a moderate-temperature TSA process in an IGCC power plant could be feasible and advantageous in comparison with conventional techniques. The moderate-temperature process represents more or less the worse case. If later, an adsorbent would be found for the high-temperature process, the comparison with conventional techniques would simply be improved in favor of the zeolite TSA process. It was, therefore, decided that the moderate-temperature TSA process would be worked out in a process design.

Such a process involves a multi-component adsorption while here only a single-component adsorption was tested. It is reasonable to expect that the adsorption capacity for CO_2 will be reduced by the other the components (i.e., H_2O and H_2). Further experiments will have to provide these multi-component data. For the time being, it is therefore assumed that the CO_2-capacity is not affected by other components.

Because of its availability in sufficient quantities for further, larger scale experiments, Na-Zeolite A was selected as adsorbent. In the process design, it is therefore assumed that the adsorbent has a capacity of 0.15 mg/mg and an average heat of adsorption of 42 kJ/mole.

Chapter 6

Conclusions

In comparison with conventional techniques of removing CO_2 in IGCC power plants, the use of a TSA process with zeolite adsorbents can be advantageous in two way:

a) The regeneration at high pressure (~ 20 bar) can reduce the amount of work needed for the compression to 110 bar by approximately 75 %.

b) The adsorption at high temperature (~ 325 °C) makes it possible to use the adsorption heat for the generation of electricity, thereby reducing the loss in plant efficiency due to the CO_2 removal to only a few %-points (< 8 %-points).

Both, the regeneration at high pressure and the adsorption at high temperature require that the zeolite adsorbent has good thermal stability and a sufficient capacity.

Several zeolites have a stability that allows regeneration at temperatures between 500 °C and 800 °C that are needed for complete desorption at 20 bar. The reduction of the compression work can, therefore, be realized easily by using a TSA process operating with adsorption at a moderate temperature (~125 °C).

To operate a TSA process with adsorption at high temperature (~325 °C), the zeolite should have an adsorption heat of 70 kJ/mole CO_2 or more. For the few zeolites of which an adsorption heat is mentioned in the literature, the reported value is less than 70 kJ/mole. By carefully selecting the zeolite type and its modifications, it might however be possible to find an adsorbent that meets the criterium.

The selection of the zeolite type and its modifications cannot be made on the basis of the theory on zeolite. The theory describes a great many parameters that influence the adsorption behavior and the stability. Unfortunately, most of these parameters are mutual dependent, by that preventing the optimization of the adsorption properties needed for the selection.

Consequently, the selection has to be based on the limited amount of experimental data concerning CO_2 adsorption that have been published. The highest adsorption capacities are mentioned for Zeolite A, Zeolite X, and Chabazite. Their heat of adsorption is, however, only 40-60 kJ/mole. For Mordenite, a heat of adsorption of 60-70 kJ/mole is reported.

Considering the specific demands of an IGCC power plant and the objectives of this study, five zeolite types have been selected: Zeolite A, Zeolite X, Zeolite P, Mordenite, and Zeolite β. The stability and the adsorption behavior of these zeolites, in particular of the alkaline earth metal forms, have been studied with the use of EDS, XRD and TGA. The results are summarized in table 6.1.

Table 6.1 *The main results of the zeolite characterization*

Zeolite type	*CO_2 adsorption (25 °C and 1 bara)*	*Thermal stability between 500 °C and 800 °C*
Zeolite A	Ca-A > Na-A > Sr-A > Mg-A	Ca-A > Mg-A > Sr-A > Na-A; Ba-A was unstable
Zeolite X	Na-X > Ca-X > Ba-X > Sr-X	Na-X, Ca-X > Sr-X, Ba-X
Zeolite P	no adsorption due to instability	all samples became unstable at low temperatures
Mordenite	Ca-Mor > Ba-Mor > H-Mor, (Mg-Mor)*	all samples were stable up to at least 800 °C **
Zeolite β	Ca-β > Mg-β, Na-β, H-β	all samples were stable up to at least 800 °C **

*) unreliable: there are indications that the ion-exchange of the Mg-Mor sample has been unsuccessful
**) meaning that no indications were found that instability occurred.

Based on these results, the feasibility of a TSA process with one of these zeolite adsorbents can be evaluated. For most of the samples, the adsorption capacity at 325 °C is too low to be interesting for a high-temperature TSA process. Mordenite is the only zeolite type that offers some perspective. The capacity measured for Ca-Mordenite is still somewhat low, but Mg-Mordenite is expected to be a good option. Although a confirmation could not be given by the measurements in this study, as there were indications that the ion-exchange of the Mg-Mordenite sample has been unsuccessful, data in the literature suggest that Mg-Mordenite has a higher capacity than Ca-Mordenite.

Table 6.2 *Temperature Swing Adsorption (TSA) process*

TSA process:

	pressure (bara CO_2)	temperature (°C)	moderate temperature TSA Na-X	Ca-A	Na-A	Ca-X	high temperature TSA Mg-Mor	Ca-Mor
adsorption (mg/mg)	1.0	25	0.24	0.22	0.18	0.18	... (>0.12)	0.12
	7.5 ***	125	0.21	0.19	0.15	0.12	... (>0.10)	0.10
	7.5 ***	325	0.05	0.04	0.03	0.03	... (>0.05)	0.05
heat of adsorption at 0.025 mg/mg (kJ/mole) **			35 (36-51)	39 (37-52)	58 (39-54)	44 (48-48)	... (75-85)*	56 (70-80)*

*) estimated values based on data for other gases from references in the literature
**) the values given between brackets: data from references in the literature.
***) the partial pressure of CO_2 during adsorption in an IGCC power plant

Because the use of Mg-mordenite as an absorbent for the high-temperature TSA process is still uncertain, the process design has been based on a moderate temperature TSA process. A zeolite

with a capacity of 0.15 mg CO_2/ mg sorbent at 125 °C, 7.5 bar CO_2 pressure, and an adsorption heat of 42 kJ/mole is used in these calculations.

Chapter 7

References

Adams J.M.; Rees L.V.C., *J. Solid State Chem.*, **62**, 184-190 (1986)

Alderliesten P.T.; Brunia A.; Enoch G.D.; Jansen D.; Janssen F.J.; Klein Teesink H.; Melman A.G.; Raas J.L.; Schmal D.; Tummers J.F.; Verschoor M.J.E.; Woudstra N., *Systeemstudie hoge temperatuur gasreining bij KV-STEG-installaties*, Novem report 90-310/8725-21421/500, 1990

Alders J.G.M., *Energy Conver. Mgmt.*, **33** (5-8), 283-286 (1992)

Aspen Technology Inc, *Handbooks of Aspen Plus™ release 9/9.2*, 1994
(in particular the handbook on *Modeling Processes with solids*)

Baird C., *Environmental Chemistry*, Freeman and Co., New York, 1995

Baker M.D.; Godber J.; Helwig K.; Ozin G.A., *J. Phys. Chem.*, **92** (21), 6017-6024 (1988)

Barrer R.M.; Meier W.M., *Trans. Faraday. Soc.*, **54**, 1074-1085 (1958)

Barrer R.M.; Gibbons R.M., *Trans. Faraday. Soc.*, A **59,** 948-961 (1964)

Barrer R.M., *Zeolites and Clay Minerals as Sorbents and Molecular Sieves*, Academic Press, London, 1978

Barrer R.M., *Pure & Appl. Chem.*, **51**, 1091-1100 (1979)

Barthomeuf D., *Materials Chemistry and Physics*, **18**, 553-575 (1988)

Breck D.W., *Zeolite Molecular Sieves*, Wiley, New York, 1974

Bekkum van H.; Flanigen E.M.; Jansen J.C., *Introduction to Zeolite Science and Practice*, Elsevier, Amsterdam, 1991

Burgt van der M.J.; Boutkan V.K., *Energie- en Milieuspectrum*, **4/5**, 26-28 (1993)

Branan C.R. (ed.), *Rules of Thumb for Chemical Engineers*, Gulf Publishing Company, Houston, 1994

Carty R.H.; et al., *The MAGSORB process for bulk separation of carbon dioxide*, DEA contract no. DE-AC21-90MC26364 reports 1990 and 1991

Choudhary V.R.; Mayadevi S., *Sep. Sci. and Technol.*, **28** (13&14), 2197-2209 (1993)

Chue K.T.; Kim J.N.; Yoo Y.J.; Cho S.H.; Yang R.T., *Ind. Eng. Chem. Res.*, **34**, 591-598 (1995)

Cox P.A.,*The Elements on Earth; Inorganic Chemistry in the Environment*, Oxford Univ. Press, Oxford, 1995

Coulson J.M.; Richardson J.F.; Backhurst J.R.; Harker J.H., *Coulson and Richardson's Chemical Engineering*, 4th ed., vol.2, Pergamon Press, Oxford, 1991

Crosfield, *Manufacturing Chemist*, 65 (11), 45-47 (1994)

Crosfield B.V., *Material Safety Data Sheet* on *Zeocros CA-150* and on *Zeocros CG-180*, 1996

Dorfner K. (ed.), *Ion Exchanger*, de Gruyter, Berlin, 1991

Dyer A., *An Introduction to Zeolite Molecular Sieves*, Wiley, New York, 1988

Eberly (Jr) P.E., *J. Phys. Chem.*, **66**, 812-816 (1962)

Edwards R.B.; Graham P., *Manufacture of alkali metal aluminosilicates of zeolite P-type*, PCT Int. Patent Appl. WO 95 12.546, 1995

Elvers B. (ed.); Hawkins S. (ed.), *Ullmann's Encyclopedia of Industrial Chemistry*, 5th ed., A 12, VCH Verlagsgesellschaft, Weinheim, pp. 213-306, 1989

Elvers B. (ed.); Hawkins S. (ed.), *Ullmann's Encyclopedia of Industrial Chemistry*, 5th ed., A 13, VCH Verlagsgesellschaft, Weinheim, pp. 379-382, 1989

Elvers B. (ed.); Hawkins S. (ed.), *Ullmann's Encyclopedia of Industrial Chemistry*, 5th ed., A 28, VCH Verlagsgesellschaft, Weinheim, pp. 475-504, 1996

Franklin K.R.; Townsend R.P., *J. Chem. Soc. Faraday Trans I*, **84** (8), 2755-2770, (1988)

Furuyama S.; Sato K., *J. Phys. Chem.*, **86** (13), 2499-2503 (1982)

Furuyama S.; Nagato M., *J. Phys. Chem.*, **88** (9), 1735-1740 (1984)

Furuyama S.; Miyazaki M.; Inoue H., *J. Phys. Chem.*, **88** (9), 1741-1744 (1984)

Gerhartz W. (ed.), *Ullmann's Encyclopedia of Industrial Chemistry*, 5th ed., B3, VCH Verlagsgesellschaft, Weinheim, pp. 4.46-4.47 8.1-8.36 9.1-9.52 20.36-20.39, 1988

Grayson M. (ed.), *Kirk Othmer Encyclopedia of Chemical Technology*, 3th ed., V2, Wiley, New York, pp. 492-493, 1978

Grayson M. (ed.), *Kirk Othmer Encyclopedia of Chemical Technology*, 3th ed., V4, Wiley, New York, pp. 734-735, 1978

Grayson M. (ed.), *Kirk Othmer Encyclopedia of Chemical Technology*, 3th ed., V17, Wiley, New York, pp. 928-925, 1983

Grayson M. (ed.), *Kirk Othmer Encyclopedia of Chemical Technology*, 3th ed., V22, Wiley, New York, pp. 267-291, 1983

Han C.; Harrison D.P., *Chem. Eng. Sci.*, **49** (24B), 5875-83 (1994)

Haq N.; Ruthven D.M., *J. Colloid Interface Sci.*, **112** (1), 154-163 (1986)

Haq N.; Ruthven D.M., *J. Colloid Interface Sci.*, **112** (1), 164-169 (1986)

Harjula R.; Dyer A.; Pearson S.D.; Townsend R.P., *J. Chem. Soc. Faraday Trans I*, **88** (11), 1591-1597 (1992)

Hathaway P.E.; Davis M.E., *J of Catalysis*, **119** (2), 497-507 (1989)

Heesink A.B.M.; Temmink H.M.G., *Process for removing carbon dioxide regeratively from gas stream*, patent US 5.520.894, 1996

Hendriks C.A.; Blok B.; Turkenburg W.C., *Technology and cost of recovering and storing carbon dioxide from an integrated gasifier, combined cycle plant*, Ministry of VROM, publikatiereeks Lucht nr. 92, 1990

Hendriks C., *Carbon Dioxide Removal from Coal-Fired Power Plants*, PhD thesis Utrecht University, 1994

Hilten van O., *Energie- en milieuspectrum*,12, 26-29 (1994)

Inui T.; Okugawa Y.; Yasuda M., *Ind. Eng. Chem. Res.*, **27**, 1103-1109 (1988)

IZA-SC (The International Zeolite Association, the Structure Commision of), *Zeolites*, **16**, 323-802 (1996)

IZA-SC (The International Zeolite Association, the Structure Commision of), at her internet site: www.iza-sc.ethz.ch\IZA-SC, 1997

Jack A.R.; Audus H.; Reimer P.W.F., *Energy Conver. Mgmt.*, **33** (5-8), 813-818 (1992)

Jasra R.V.; Bhat S.G.T., *Sep. Sci. Technol.*, **23** (10&11), 945-989 (1988)

Joy D.C.(ed.); Romig (Jr) A.D.; Goldstein J.I., *Principles of analytical electron microscopy*, Plunum Press, New York, pp. 123-153, 1986

Kessel van L.B.M.; Heesink A.B.M., *Verkort haalbaarheidsonderzoek naar de regeneratieve CO_2-verwijdering/-winning by KV-STEG*, TNO (IMET) report 93-087, 1993

Kessel van L.B.M.; Heesink A.B.M.;Haan de J.A.; Nijmeijer J., *Vervolgonderzoek naar de haalbaarheid van regeneratieve CO_2-verwijdering bij KV-STEG*, TNO (IMET) report 94-199, 1994

Kessler B.; Eysmondt von J.; Merten H., *Chem.-Ing.-Tech.*, **64** (12), 1075-1083 (1992)

Kim J.N.; Chue K.T.; Kim K.I.; Cho S.H.; kim J.D., *J. of Chem. Eng. of Japan*, 27 (1), 45-51 (1994)

Ma Y.H.; Mancel C., *AIChE J.*, **18** (6), 1148-1153 (1972)

Meier W.M.; Olsen D.H., *Atlas of Zeolite Structure Types*, 2nd ed., IZA/Butterworths, London, 1987

Meier W.M.; Olson D.H.; Baerlocher Ch., *Atlas of Zeolite Structure Types*, 4th ed., IZA/Elsevier, Amsterdam, 1996

Meyers R.A. (ed.), *Handbook of Synfuels Technology*, McGraw-Hill, New York, 1984
(in particular: Vogt E.V.; Weller P.J., Burgt van der M.J., *The Shell Coal Gasification Process*, pp. 3.27-3.45)

Ministry of Economic Affairs (The Netherlands), *Technieuws Tokyo*, **29** (1), 2-5 (1991)

Ministry of VROM (= Housing, Physical Planning and Environment) (The Netherlands), *Nationaal Milieubeleidsplan 2 ; milieu als maatstaf*, TK 1993-1994 nr.23.560 1-2, SDU uitgeverij, Den Haag, 1993

Mortier W.J., *Composition of Extra Framework Sites in Zeolites*, IZA/Butterworth-Heinemann, Oxford, 1982

Mot E.; et al., *Procestechnologie*, **2** (11), 43-47 (1992)

Oudhuis A.B.J., *Inventarisation of techniques for CO_2 removal from fuel gas or reformer gas*, Netherlands Energy Research Foundation ECN-report C-92-043, 1992

Ree van R., *Carbon Dioxide: Problem matter or inexpensive raw material ? An inventory of technologies for the usage and disposal of CO_2*, Netherlands Energy Research Foundation ECN-report I-93-037, 1993

RIVM, *Nationale Miliuverkenning 2, 1990-2010*, Samson HD Tjeen Willink bv, Alphen a/d Rijn, 1991

Saeijs J.C.P.L., Van Kessel L.B.M., Heesink A.B.M. and Temmink H.M.G., *IGCC Power Plant: CO_2 removal with high temperature adsorbents; Part I: Literature survey,* TNO-report R97/363a, 1997

Santen van R.A.; Ooms G.; Ouden den J.J.; Beest van B.W.; Post M.F.M., *Computational Studies of Zeolite Framework Stability*, ACS Symp. Ser. 398 (Zeolite Synth.), pp. 617-33, 1989

Santen van R.A.; Beest van B.W.H.; Man de A.J.M., *On Lattice Dynamics, Stability and Acidity of Zeolites*, in *Guidelines for Mastering the Porperties of Molecular Sieves*, Barthomeuf D. (ed.), Plenum Press, New York, pp.201-224, 1990

Sawa M.; Niwa M.; Murakami Y., *Zeolites*, **10**, 532-538 (1990)

Sawa M.; Kato K.; Hirota K.; Niwa M.; Murakami Y., *Applied Catalysis*, **64**, 297-308 (1990)

Sherry H.S., *J. Phys. Chem.*, **72** (12), 4086-4094 (1968)

Sherry H.S., *J. Phys. Chem.*, **70** (4), 1332-1334 (1966)

Silaban A.; Harrison D.P., *Chem. Eng. Comm.*, **137**, 177-190 (1995)

Stam B., *PT Elektrornica-elektrotechniek*, 4, 52-53 (1989)

Steinberg M., *Energy Conver. Mgmt.*, **33** (5-8), 311-315 (1992)

Szostak R., *Handbook of Molecular Sieves*, Van Nostrand Reinhold, New York, 1992

TNO Milieu, Energie en Procesinnovatie/divisie Reststoffen, *Improvement of the profitability of an IGCC power plant by producing hydrogen as a commercial side product*, research proposal ED/074 Annex 1 (EGKS), 1995

Topper J.M.; Cross P.J.L.; Goldthrope S.H., *Fuel*, **73** (7), 1056-63 (1994)

Treacy M.M.J.; Higgins J.B.; Ballmoos von R., *Collection of simulated XRD power patherns for zeolites*, 3th ed., IZA/Elsevier, Amsterdam, 1996

VDI-Gesellschaft Energietechnik, *Energiehaushalten und CO_2-Minderung : Einsparpotentiale im Sector Stromversorgung*, Tagung Würzburg 25. und 26. März 1992, VDI Berichte 941, VDI-Verlag, Düsseldorf, 1992

Weast R.C. (ed.), *CRC Handbook of Chemistry and Physics*, 60th ed. 3th print, CRC Press, Boca Raton, 1981

Wendlandt W.W., *Thermal Analysis*, 3th ed. Wiley, New York, 1986

Wijnen P.W.J.G.; Beelen T.P.M.;Haan de J.W.; Rummers C.P.J.; Ven van de L.J.M.; Santen van R.A., *J. Non-Cryst. Solids*, **109**, 85-94 (1989)

Wijnen P.W.J.G., *A Spectroscopic Study of Silica Gel Formation from Aqueous Silicate Solutions*, PhD thesis Eindhoven University of Technology, Wibro dissertatiedrukkerij, Helmond, 1990

Williams B.C.; McMullan J.T.; Campbell P., *Fuel*, **73** (7), 1068-73 (1994)

Wunderlich B., *Thermal Analysis*, Academic Press, Boston, 1990

Chapter 8

Authentication

Name and address of the principal

ECSC
attn. Mr J.K. Wilkinson
Rue de la Loi
Bruxelles

Name of the (co)-operators

Ir. J.C.P.L. Saeijs	-Twente University
Ir. L.B.M. van Kessel	-TNO-MEP
Dr. Ir. A.B.M. Heesink	-Twente University
Ir. H.M.G. Temmink	-TNO-MEP
Prof. Dr. Ir. H. Verweij	-Twente University

Names and establishments to which part of the research was put out to contract:

Twente University

Date upon which, or period in which, the research took place

February 1997 - October 1998

Signature

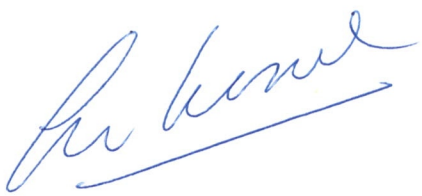

Ir. L.B.M. van Kessel

Project leader

Approved by

Ing. S. van Loo

Head of the department
of Thermal Conversion
Technology